COMPUTATIONAL INVESTIGATION OF SENSITIVITY OF THE CROSSFLOW INSTABILITY TO TWO-DIMENSIONAL SURFACE IMPERFECTIONS

A Dissertation

by

MATTHEW WARE TUFTS

Submitted to the Office of Graduate and Professional Studies of
Texas A&M University
in partial fulfillment of the requirements for the degree of

DOCTOR OF PHILOSOPHY

Chair of Committee,	Helen L. Reed
Committee Members,	William S. Saric
	Diego Donzis
	Hamn-Ching Chen
Head of Department,	Rodney Bowersox

December 2015

Major Subject: Aerospace Engineering

ABSTRACT

The interaction between two-dimensional steps and gaps with stationary crossflow vortices on a swept laminar wing has been investigated using computational methods. Using flow conditions as experienced in complementary experiments using the SWIFTER and SWIFTEST airfoils as found in flight and as installed in the KSWT facility, the growth of stationary crossflow disturbances were calculated using direct simulation.

Forward-facing steps were found to amplify stationary crossflow waves significantly once a threshold step height had been exceeded. This value was found to correlate well with experimentally observed movement of the transition front forward. A correlation based on a physical explanation of the mechanisms involved was proposed, and also was found to correlate well with the SWIFTER and SWIFTEST experimental observations.

Backward-facing steps were found not to amplify stationary waves for step heights tested in the computational regime. Local stability analyses of the flowfield surrounding the backward-facing steps reveal the existence of a traveling mode similar to traveling crossflow vortices. A mechanism whereby this leads to transition to turbulence was hypothesized.

DEDICATION

This work is dedicated to my wife Annie.

ACKNOWLEDGEMENTS

I feel very fortunate to have been part of the research groups I interacted with during my time at Texas A&M. I know that without the help, support, advice, collaboration, and examples of the people I worked with that I could not have made it this far. I hope that my contributions have proved valuable.

I would first of all like to thank my advisor, Dr. Helen Reed, for providing me with years of encouragement, advice, and friendship. Thank you for giving me the opportunity to integrate my passion for flight into my work, and allowing me to explore new avenues and to take on various side projects.

I would also like to thank Dr. Wiliam Saric for his advice and guidance. Thank you to the other members of my graduate commitee, Dr. Diego Donzis and Dr. Hamn-Ching Chen for their helpful criticisms and insights.

I greatly appreciate the discussions and interactions with my fellow graduate students. Mike Belisle, Brian Crawford, Alex Craig, Jacob Cooper, Tom Duncan, Megan Heard, Jerrod Hofferth, Lauren Hunt, Travis Kocian, Alex Moyes, Nick Oliviero, Eddie Perez, Matt Roberts, Aaron Tucker, David West, Tom Williams, and Matt Woodruff. Beyond being simply co-workers I cherish your friendship and am grateful for your support both in and out of the laboratory.

I would like to thank in a special way both David West and Lee Denham who put forth the extra effort to get me involved in O-2 flights as an active participant. The experience of flying has fulfilled a dream of mine, and has given me memories (and logbook entries) I will cherish for the rest of my life.

To my Family, Annie Tufts, Lauren Tufts, Dolores Tufts, Barry Tufts, Emily Legault, Peggy Legault and John Legault, thank you for your love and support.

I would also like to thank those teachers who throughout the years encouraged or inspired me in a special way. Thank you to Frances Pustejovsky, Scott Richardson, Mihir Sen, Meng Wang, and John Hurtado.

NOMENCLATURE

D	Hydraulic Diameter : $D = 2h$ for rectangular channels.
Q_∞	Freestream Total Velocity
Q_e	Local Edge Total Velocity
Re'	Unit Reynolds Number
Re_D	Reynolds Number based on Hydraulic Diameter : $Re_D = \frac{\frac{2}{3}U_{max}D}{\nu} \equiv \frac{\frac{4}{3}U_{max}h}{\nu}$
Re_h	Reynolds Number based on Step Height and U_{max} : $Re_h = \frac{U_{max}h}{\nu}$
Re_{ke}	Reynolds Number based on Step Height and Edge Conditions : $Re_{ke} = \frac{U_e k}{\nu_e}$
Re_{kk}	Reynolds Number based on Step Height for Length and Flow Conditions : $Re_{kk} = \frac{U_k k}{\nu_k}$
U'_e	Local Edge Velocity Component Aligned with Inviscid Streamline
U_∞	Freestream Velocity Component Normal to Step
U_e	Local Edge Velocity Component Normal to Step
U_k	Velocity Component Normal to Step, Measured at Height k in Undisturbed Boundary Layer Profile
U_{max}	Maximum Velocity for Given Profile (Used for 2-D Velocity Profiles)
η	Blasius Length Scale
μ	Dynamic Viscosity

ν Kinematic Viscosity : $\nu = \frac{\mu}{\rho}$

ν_∞ Freestream Kinematic Velocity

ν_e Local Edge Kinematic Velocity

ν_k Kinematic Velocity, Measured at Height k in Undisturbed Boundary Layer Profile

h Height of Inlet Channel

k Step Height

DOC Direct Operating Costs

DRE Discrete Roughness Elements

FEA Finite-Element Analysis

FFT Fast-Fourier Transform

GCI Grid Convergence Index

HLFC Hybrid Laminar-Flow Control

IATA International Air Transport Association

IR Infrared

KKO Kaiktsis, Karniadakis, and Orszag (authors)

KSWT Klebanoff-Saric Wind Tunnel

NGC Northrop Grumman Corporation

POH Pilot's Operating Handbook

SWIFT Swept-Wing In-Flight Testing
(Model with No Excrescence)

SWIFTER Swept-Wing In-Flight Testing Excrescence Research
(Model with 15% x/c Excrescence)

SWIFTEST Swept-Wing In-Flight Testing Excrescence Stability Theory
(Model with 1% x/c Excrescence)

TAMU Texas A&M University

TRL Technology Readiness Level

UDF User-Defined Function

USAF United States Air Force

X Coordinate Aligned Normal to Step Excrescence (Downstream)

X' Coordinate Aligned with Local Inviscid Streamline

Y Coordinate Aligned Normal to Local Wall (Outward)

Z Coordinate Resultant of X $\times$ Y (Parallel to Step Excrescence)

Z' Coordinate Resultant of X' $\times$ Y (Normal to Streamline Direction)

TABLE OF CONTENTS

Page

LIST OF FIGURES

FIGURE Page

LIST OF TABLES

TABLE Page

I. INTRODUCTION AND BACKGROUND

I.1 Motivation

The International Air Transport Association (IATA) [1] estimated that fuel expenses made up approximately 29% of the system-wide expenses for global commercial airlines, totaling 204 billion dollars for the 2014 fiscal year. While future total expenses are expected to fall slightly, largely due to the recent dip in fuel prices, total fuel consumption in gallons, as well as CO_2 emissions are expected to increase in the coming years.

A 1991 study by Arcara et al. [2] found that Hybrid Laminar-Flow Control (HFLC) implemented on a nominal twin-engined commercial transport design could reduce the Direct Operating Costs (DOC) of that aircraft by 5.8% when operating under a fuel cost of 65 cents per gallon. For fuel costs of 2 dollars per gallon, they found HFLC could reduce the DOC by up to 8.8%.

According to a report released by the United States Department of Transportation Bureau of Transportation Statistics, [3] the domestic airline fleet paid an average of $2.93 per gallon year to date through November 2014. It is therefore apparent that practical implementation of laminar-flow technologies to the airline fleet has the potential to save on the order of tens of billions of dollars per year just in fuel costs if integrated across the global airline fleet.

I.2 Mechanisms of Transition to Turbulence

It is believed that in the majority of instances transition to turbulence in subsonic low-freestream-disturbance environments at aircraft-relevant Reynolds numbers (e.g. subsonic atmospheric flight) is caused by linear, modal growth of infinitesimal disturbances to the boundary layer. [4, 5]

There are four linear modal growth mechanisms that have been identified for subsonic boundary layers:

1. Attachment-Line Instability

2. Centrifugal/Görtler Instabilities

3. Viscous Streamwise (Tollmien-Schlichting) Instabilities

4. Crossflow Instabilities

In addition to this linear modal growth, other paths to transition must be addressed for LFC designs.

5. Leading-Edge Contamination

6. Transient Growth

Control of the attachment-line instability and Görtler instability can be achieved through remaining under a maximum leading edge radius [5, 6] and by avoiding concave curvature in the airfoil shape, [5] respectively. Following the relative ease of controlling these two instabilities on an airfoil with no imperfections, a correspondingly small amount of emphasis will be placed on them in the current work.

The streamwise, viscous instability present in boundary layers, typically known as Tollmien-Schlichting waves arises from the combined presence of viscosity and basic-state vorticity. Experience has shown that when the boundary-layer profile becomes fuller (e.g. the effect as would be experienced by decreasing viscosity) that the T-S instability will experience lower growth rates. Accordingly, for a passive design (requiring no input energy), designing the airfoil to have a favorable-pressure gradient is a common approach. Other feasible methods for low-speed and transonic

flows include wall cooling (for gas flows, wall heating for liquids) and weak suction at the wall.

The remaining challenge then, is typically to stabilize the crossflow instability without unduly destabilizing the T-S wave. All this must be done while simultaneously fulfilling the structural and vehicle-system requirements. Because on a swept surface with a pressure gradient a wall-bounded shear layer has velocity in the direction normal to the freestream direction (the crossflow direction), and this velocity profile must disappear both at the wall and at infinity, it is necessary that an inflection point exist somewhere in the boundary layer, as can be seen in Figure I.1. It is known from Rayleigh [7] that this profile is inviscidly unstable. In low freestream-disturbance conditions, this instability of the crossflow profile manifests in stationary co-rotating vortices and traveling co-rotating vortices.

An interesting result, and one that is potentially important to this problem, of the crossflow vortices being stationary is that the meanflow tends to become distorted by these vortices. This may have non-intuitive non-linear effects upon the boundary layer, an example of which is transition control by periodic discrete roughness elements (DRE) to be discussed later.

Leading-edge contamination describes the process by which a swept wing, if attached by the root to a turbulent boundary layer (e.g. the fuselage of an aircraft), will have the turbulence present on the body's boundary layer travel from the main body (fuselage) down the leading edge of the wing and "contaminate" the boundary layer of the wing. This contamination leads directly to the swept-wing boundary layer becoming turbulent, without the need for any sort of modal or non-modal growth of infinitesimal disturbances.

In the tradition of Morkovin's paths to transition, [8] seen in Figure I.2, one must also consider the changes to the processes that occur with increasing disturbance

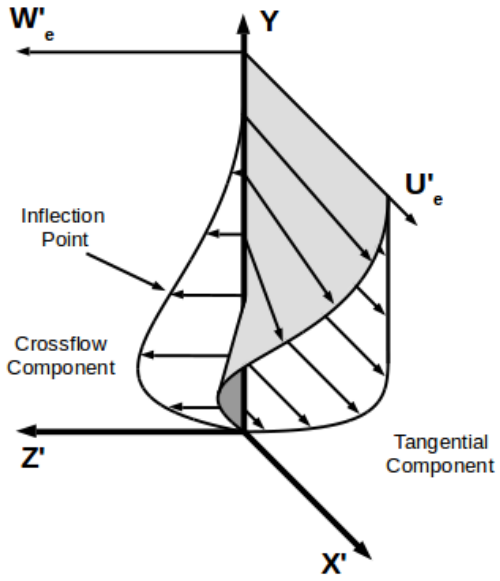

(a) Velocity Profiles

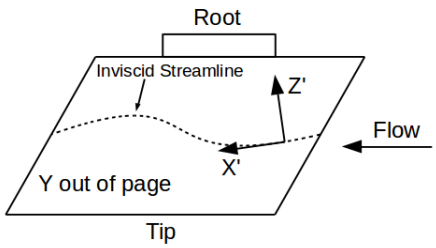

(b) Coordinate System

Figure I.1: Swept-Wing Velocity Profiles (Using SWIFT Coordinate System)

levels. The increase in disturbance levels tends to most prominently correlate with an increase in freestream turbulence, but also disturbance leves also increase with an elevation in surface roughness. However, it should be noted that the complete role of surface roughness in inducing disturbances (an aspect of receptivity) is an open area of research, but as a general trend increased turbulence or increased surface roughness moves one to the right of Morkovin's chart.

One possible effect of increased roughness or turbulence levels is what is known as transient growth. Transient growth refers to the algebraic (as opposed to exponential) growth of the sum of non-orthogonal decaying modes. Imagine one has two modes, both of which are individually decaying. The resulting disturbance arising from the sum of these two modes can increase in amplitude despite decay of all individual components. The mechanism for this lies in the non-orthogonality of the modes, noting that the interference between these may be either constructive or de-

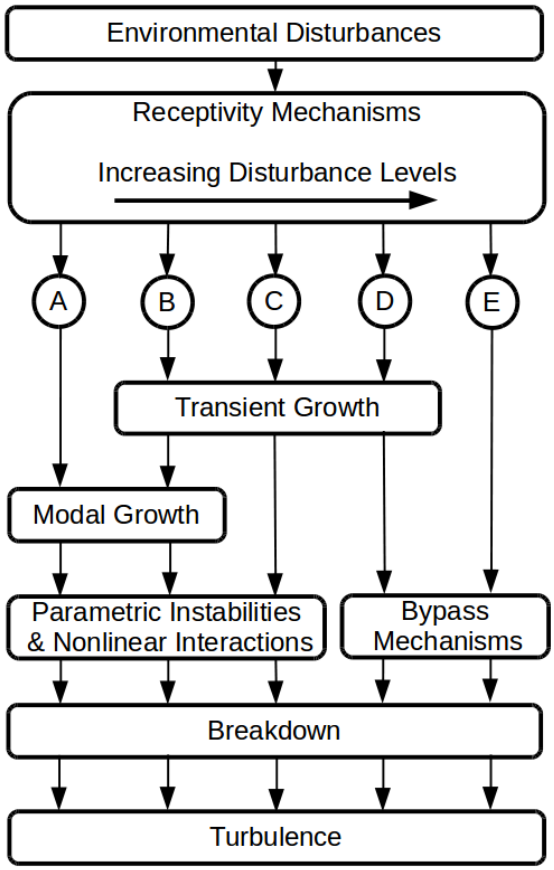

Figure I.2: Morkovin's Paths to Turbulence

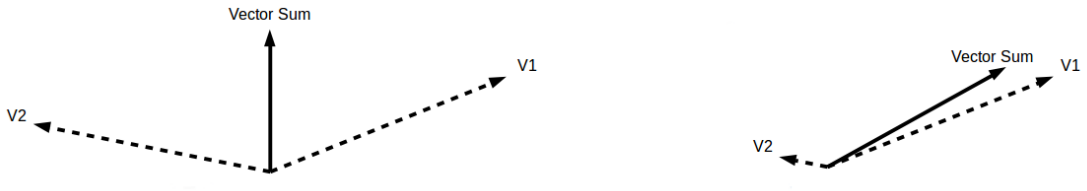

(a) $t = 0$ (b) $t = \Delta t$

Figure I.3: Cartoon Illustrating Simple "Transient Growth"

structive. The most intuitive illustration of this situation is to imagine the decaying modes as two non-orthogonal vectors, seen in Figure I.3. At time $t = 0$ the "horizontal" component of these vectors largely cancel one another out, however at $t = \Delta t$ despite both $V1$ and $V2$ decreasing in size, the sum total vector has now become larger. This is but a very simple example however, the field of transient growth is a large and complex one. References such as Reshotko [9] are a good jumping off point.

I.3 Methods of Transition Control

As the mechanisms of transition have been further understood and explored, likewise the methods for controlling these mechanisms have become better understood. As Arnal and Archumbaud [10] point out, while there are many proposed methods for control of transition, today's mature methods (arguably also the most feasible) rely on modification of the mean flow. The punchline is instead of "fighting" the instabilities themselves, one should modify the environment in which they are developing to be less favorable. A crude analogy would be to prevent the spread of bacteria, instead of applying antibiotics and actively combating the organisms, one should instead remove moisture from the Petri dish.

All of the modal mechanisms for transition when taken in isolation have a known

method of controlling or eliminating their growth. However, the current challenge lies not in the fundamental problem of controlling an individual mode, but in controlling the collection of modes present, while not violating the constraints "external" to the problem of boundary-layer stability (e.g. C_l requirements, structural constraints, low-observability constraints).

In most cases, with some notable exceptions, [11] the desire to travel at high subsonic or supersonic speeds has led designers to include wing sweep in their designs. The inclusion of wing sweep, along with the presence of a streamwise pressure gradient excites the crossflow instability as previously discussed. Controlling the Tollmien-Schlichting wave and crossflow wave simultaneously in a reliable fashion is still an open area of research, and arguably the crux of reliably maintaining laminar-flow runs on transport-class aircraft today.

Boundary-layer suction as implemented by Pfenninger [12] provides an excellent example of the "real world" challenges present in this problem. Boundary-layer suction and sensible geometric design of the wing proved to be effective in controlling all known modal instabilities and producing long runs of laminar flow. Despite these successes, boundary-layer suction as a laminar flow control solution received high levels of pushback due to the perceived complications of moving parts (e.g. the mechanisms to pull vacuum) and surface maintenance (e.g. clearing and cleaning of a perforated surface).

As a result, alternative methods of control with lower Technology Readiness Levels (TRLs) have been explored, including Discrete Roughness Element (DRE) technology. DREs exploit the ability of stationary crossflow to non-linearly modify the meanflow over a wing, by selectively "seeding" wavelengths of crossflow vortices not likely to cause transition of their own accord, and by their presence and distortion of the flow prevent the formulation of waves with larger growth potential. [13, 14]

DREs are a promising alternative, but until further studies regarding receptivity of the crossflow vortices are completed DREs are not feasible for "commercial" applications. [15]

I.4 Imperfections and Excrescences

However, even if one assumes a priori that a working method of transition control can be built in a controlled laboratory environment, one must still account for the imperfections built into (e.g. machining tolerances, systematic waviness, panel seams) or externally applied to (e.g. bug strikes, paint weathering, icing) the wing in question. Excrescences, the catch all term for these deviations from the laboratory design, must be accounted for before laminar flow designs can be implemented into commercial applications. Famously, the P-51 during WWII was built using a laminar flow wing design, but did not have the performance gains expected. The discrepancy has since been attributed to the combination of wartime manufacturing imperfections, as well as the harsh environmental conditions the combat aircraft endure. [16]

The inclusion of wing sweep complicates setting a tolerance or criterion for surface excrescences, due to the presence of the crossflow instability. While some work has been done to quantify the effect of design excrescences on "other" geometries, little has been done looking at swept wings. The inclusion of the crossflow vortex makes this in effect a new problem, since the crossflow profile is itself unstable. This is in contrast to a two-dimensional laminar flow wing, which due to the lack of wing sweep and presence of a favorable pressure gradient has stabilized all primary modes. The interaction between the existing instability (crossflow inflectional profile) and the newly created instability from the step (shear layer inflectional profile) is yet unexplored.

I.5 Problem Statement

A need therefore exists to determine a criterion for manufacturing tolerances applicable to two-dimensional steps in the presence of crossflow-dominated transition phenomena. This work intends to determine if a suitable manufacturing tolerance can be found by modeling both forward-facing and backdward-facing two-dimensional step excrescences in a realistic swept-wing flowfield. This task will be accomplished by directly modeling both the step excrescence and related modal growth and also validating the results using experimental data gathered as a part of the complementary SWIFTER and SWIFTEST campaigns. The increased physical understanding found by these computations is expected to allow more accurate, and therefore less conservative and restrictive, tolerances to be implemented into swept-wing laminar-flow designs.

II. LITERATURE REVIEW

II.1 A Note on Reynolds Numbers

There are two issues pertaining to reference quantities worth noting when dealing with excrescences. The first is that there are frequently differences in the definition of Reynolds number across literature sources, and one must take care to note these. Historically in excrescence work, the convention has been to choose the step height as the length scale, while using boundary-layer edge quantities (or centerline quantities for channel flows) for velocity and viscosity. The definitions given within this paper are intended to be internally consistent, but may differ from the definitions given in literature sources.

There are two obvious velocity references that may be chosen, the total velocity at the edge of the boundary layer Q_e, or the boundary-layer edge velocity normal to the excrescence U_e. As the community moves into swept wing studies, there should at least be a discussion as to the proper reference velocity. Note that for many previous studies the distinction between these two quantities has not been necessary. For an

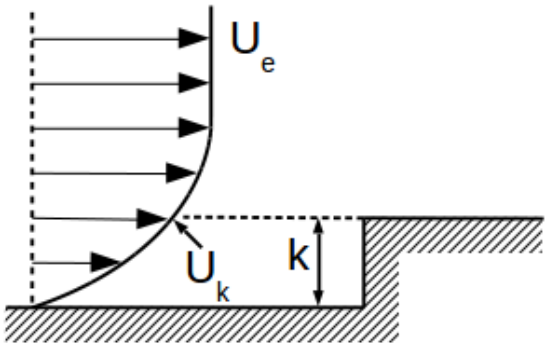

Figure II.1: Definition of Velocities

unswept 2-D excrescence problem the difference in choosing total edge conditions or conditions normal to the excrescence is clearly immaterial. In addition for any three-dimensional roughness, the definition of conditions normal to the excrescence is not meaningful. However, it seems logical that when considering a swept two-dimensional excrescence such as a step on a swept wing, one should use only the component U_e normal to the excrescence.

For this work, the 'standard' non-dimensional quantity will be called $Re_{ke} = \frac{U_e k}{\nu_e}$, however note that in literature this quantity is typically denoted as Re_k.

On a more fundamental level, the second issue is that it has yet to become clear that any of these quantities are good indicators of the behavior inherent in the problem.[1]

For three-dimensional discrete roughnesses (e.g. a rivet head) the relative parameter has been assumed to be what is called $Re_{kk} = \frac{U_k k}{\nu_k}$ using the speed at the height of the excrescence in the undisturbed boundary layer profile as seen in Figure II.1. This is somewhat logical for a forward-facing step, from an intuitive view. However, it is less clear how this parameter relates to the flow surrounding a backward-facing step. In addition the parameter Re_{kk} also tends to scale differently depending on the specifics of the excrescence. Specifically, when the excrescence is well inside the boundary-layer Re_{kk} scales as a power law of k due to the "double" effect of an increasing k and U_k. However, in the case of an excrescence outside the boundary layer Re_{kk} now scales linearly with k. This makes Re_{kk} a somewhat problematic choice as a reference quantity, particularly since this distinction cannot be determined when simply given an Re_{kk} value.

In some sense the use of Re_{kk} as the reference quantity implies that the transition mechanism at play is governed by an unknown neutral stability curve. In other

[1]H. Reed, W. Saric, G. Duncan, B. Crawford, Personal Communication

words, attempting to collapse roughness induced instabilities to a set value of Re_{kk} assumes that there is a threshold value above which some stable mechanism will become unstable. It has yet to be shown that the mechanisms causing transition to turbulence due to roughness are of this character. Furthermore, it seems likely that the mechanisms between 2-D and 3-D roughnesses; swept and unswept flows; forward-facing, backward-facing and gaps may all be different.

The proper quantity is then up for debate.

II.2 Unswept Channel Flow with Backward-Facing Steps

The interaction between crossflow vortices and step excrescences is a relatively new problem. Because this is a new area of research, we can look first to similar problems.

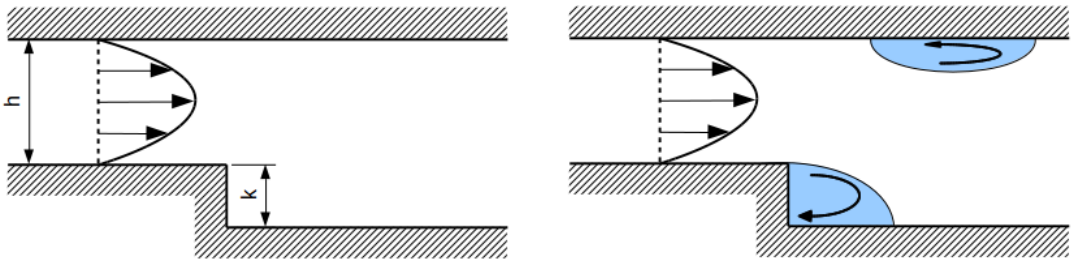

(a) Definitions of Dimensions (b) Recirculation Regions

Figure II.2: Channel Flow Diagrams

Using channel flows or using unswept flows as a comparison for the problem at hand should be done with the understanding that the direct applicability will be limited. In an attempt to provide the most relevant reference numbers, quantities for channel flows will be converted to a Reynolds Number based on Step Height and U_{max}, $Re_h = \frac{U_{max}h}{\nu}$ as used in the more recent papers e.g. Blackburn et al. [17]

Channel flows obviously have a different incoming velocity profile than a similar "open" flat plate experiment. As has been discussed previously the stability of fluid motions strongly depends on the mean flow properties, in fact most of the mature transition control schemes focus on modification of the mean flow. In addition, at sufficient Reynolds number the top wall typically will also produce one or more separation regions, similar to Figure II.2b It is also typical that a channel flow experiment will include side walls. These side walls can produce pronounced effects on the three-dimensionality of the flow, further distancing the results from an open flow boundary-layer problem.

Armaly et al. [18] define Reynolds number for their problem using $Re_D = \frac{\frac{2}{3}U_{max}D}{\nu}$, basing the length scale on hydraulic diameter, which is equivalent to 2 times the height of the channel ($D = 2h$) and basing the velocity on the average inlet velocity for a laminar fully-developed duct ($U_{avg} = \frac{2}{3}U_{max}$).

Armaly et al. report that the flow is completely laminar until an $Re_D = 1200$ ($Re_h = 900$). Between $1200 < Re_D < 6600$ ($900 < Re_h < 4950$) the flow is what is called "transitional" and if $Re_D > 6600$ ($Re_h > 4950$) the flow is fully turbulent.

Armaly et al. also reports that three-dimensionality sets in prior to onset of "transitional" flow at $Re_D = 400$ ($Re_h = 300$) This is worth noting because there appears to be confusion between the onset of three-dimensionality and the onset of turbulence, especially in nomenclature across the different sources.

Kaiktsis, Karniadakis, and Orszag, (KKO) [19] in their 1991 computational paper note that three dimensionality of this flow sets in prior to the onset of turbulence. This is true even when the inflow is nominally and effectively two-dimensional. KKO defines $Re_D = \frac{\frac{2}{3}U_{max}D}{\nu}$ in the same way as Armaly et al. KKO report that the flow becomes unsteady (but not yet turbulent) at $Re_D = 700$, ($Re_h = 525$) and becomes turbulent at around $Re_D = 5000$ ($Re_h = 3750$)

Gresho, et al. [20] however, published a computational paper specifically intended to challenge this assertion. Gresho et al. posits that the flow over a backward facing step is stable and steady until a Reynolds number $Re_D = 800$. ($Re_h = 600$) This is done via a lengthy and substantial numerical investigation, which explains care needed to do this study at even "low" Reynolds numbers.

Kaiktsis, Karniadakis, and Orszag then responded with a second computational paper in 1996 [21] which attempts to reconcile these discrepancies. In the 1996 paper KKO state that the flow over a backward facing step is absolutely stable up to a Reynolds number of $Re_D = 2500$ ($Re_h = 1875$). However, they believe that the flow is *convectively* unstable between the Reynolds numbers previously cited in their 1991 paper, $700 \leq Re_D \leq 2500$ ($525 \leq Re_h \leq 1875$). With "selective sustained external excitation" the flow will become time-dependent despite the flow being stable in the asymptotic sense to perturbations.

Up until this point in the literature, the authors reviewed dealt with the two-dimensional stability of the problem. This was done presumably because the nominal problem is a two-dimensional one, being that the base problem is two-dimensional. Barkley et al. [22] in a computational study added another wrinkle to the issue in that they began to study the effect of making the perturbations three dimensional. The Barkley et al. study found that the flow is absolutely stable to two-dimensional perturbations up to a Reynolds number of $Re_h = 1500$. However, the flow becomes absolutely unstable to *three-dimensional* perturbations at a smaller $Re_h = 748$.

A computational paper by Blackburn et al. [17] notes that the onset of convective instabilities begins at a Reynolds number well below the onset of absolute instabilities. Blackburn et al. posit that the transient response in this case could be a contributing factor to the relative disagreement between computation and experiments performed for this flow type. It is noted that the optimal three-dimensional

disturbances have a spanwise wavelengths on the order of ten step-heights, and that these modes have an energy growth of order $80 \cdot 10^3$ at $Re_h = 500$.

It should be noted that in general little to nothing is said regarding the freestream noise levels of the experiments in question. It is known that the freestream disturbance level can have a dramatic impact on transition phenomena observed. In particular with reference to Morkovin's path's to turbulence as seen in Figure I.2 transient growth phenomena are seen most frequently in relatively high disturbance environments. This cannot be construed as a "carte blanche" to completely dismiss transient growth however, since as previously mentioned, the receptivity problem is an open area of research. To put it another way, even though we would expect transient growth to appear only in higher disturbance environments, it is unclear what effect the step itself has on the receptivity of freestream disturbances. Thus even though in flight and in quiet test facilities there are low levels of freestream disturbances, the step itself may serve to amplify these disturbances to a level conducive to promoting transient growth.

II.3 Unswept Open Flows with Backward-Facing Steps

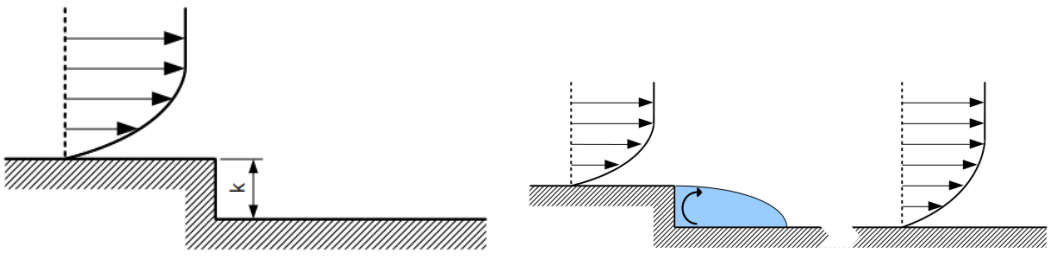

(a) Definitions of Dimensions (b) Recirculation Region

Figure II.3: Unswept Open Flow Diagrams

Beaudoin et al. [23] performed an experimental study within a channel, but believed the channel to be "tall" enough that the flow over the step was a boundary-layer type of flow, resulting in a flow similar to that seen in Figure II.3b. Beaudoin et al. were concerned with the origin of three dimensionality, as opposed to the onset of turbulence. However, during the course of their studies, they found evidence of a dominant centrifugal instability arising in the bulk flow downstream of the reattachment point as opposed to an instability arising inside the recirculation region.

Perraud et al. [24] experimentally found that in unswept boundary-layer cases, backward-facing steps tend to cause transition to move forward gradually with increasing step heights.[2] Perraud et al. were met with some success by attempting to quantify this effect computationally using PSE stability formulations, and producing a rough ΔN correlation as a function of Reynolds number.

A series of experiments by Drake et al. [25], Drake and Bender [26] and Drake et al. [27] report that for unswept, backward-facing steps, the presence of a favorable pressure gradient has the effect of increasing allowable step heights. This is particularly encouraging for laminar-flow applications, since the majority of well-designed laminar-flow airfoils tend to include a favorable pressure gradient in an attempt to stabilize the Tollmien-Schlichting instability. For these cases, it was found that the transition point moved gradually forward with increasing step height, as was seen in Perraud et al. [24]

[2]This paper was published by the Institut de l'Information Scientifique et Technique-CNRS. However due to changes in French law since publication, this paper is no longer easily available to non-French citizens at the time of writing. Many of the results, however, are apparently published elsewhere, notably Arnal et al. [6]

II.4 Unswept Open Flows with Forward-Facing Steps

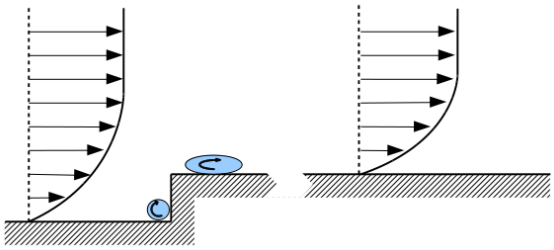

Figure II.4: Unswept Open Flow Recirculation Regions

For open flows, as seen in Figure II.4 the typical reference quantity is used is a Reynolds Number based on Step Height and Edge Conditions, $Re_{k\infty} = \frac{U_\infty k}{\nu_\infty}$.

The Holmes et al. [28] experiments found that the shape of a step excrescence can significantly affect the critical step height. Holmes et al. report that the critical $Re_{k\infty}$ increases by 50% from 1800 to 2700 when the shape of the excrescence is changed from square to rounded.

Perraud et al. [24] experimentally found for unswept cases with forward-facing steps, in contrast to backward-facing steps, cause a somewhat "binary" response in the transition location. Compared with the "baseline" transition location, a small step excrescence will have little or no effect upon the breakdown to turbulence. With increasing step size, one will see no changes in the transition location until some critical value of step height. At the critical step height, the transition front will move rapidly forward to the step location itself.

Both Perraud et al. [24] and Holmes et al. [28] found that the critical height, at which step excrescences start to affect the transition location is larger for the forward-facing step as compared to a backward-facing step.

Drake et al. [25], Drake and Bender [26] and Drake et al. [27] also experimentally examined unswept forward-facing steps as part of their studies. In Drake et al. [27] it is reported that contrary to the Perraud [24] study, that a somewhat gradual movement forward of the transition location was observed. This movement forward is less gradual than the corresponding backward-facing steps, but a substantial amount of "sub-critical" behavior appears to be present. In addition, like with the backward facing steps, a strong correlation between pressure gradient and the critical step heights was observed.

II.5 Unswept Open Flows with Swept Backward-Facing Steps

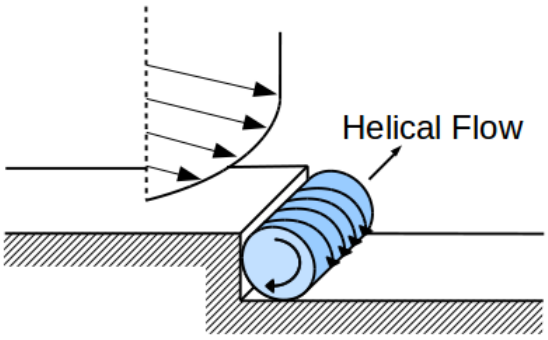

Figure II.5: Swept Flat-Plate Recirculation Helix

Holmes et al. [28] also experimented with sweeping the steps they investigated. It should be noted however that their experiments were done on an unswept wing, but with the excrescence placed at an angle to the leading edge. This is an important difference from a swept wing, since there is no crossflow velocity in the meanflow, and therefore no crossflow instabilities present, as seen in Figure II.5. Interestingly, Holmes et al. found that the swept steps tended to have a higher critical Reynolds

number than their unswept counterparts. They also found that modifying the step shape from a 'steep' ramp (approximately 45°) to an elongated ramp delayed the transition due to the step.

II.6 Unswept Open Flows with Swept Forward-Facing Steps

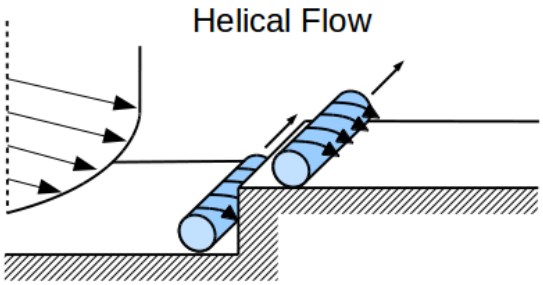

Figure II.6: Swept Flat-Plate Recirculation Helices

Holmes et al. [28], with the same caveats as to the backward-facing steps discussed in the last section, found that forward-facing steps, similar to Figure II.6 have a higher critical Reynolds number than the unswept counterpart. Holmes et al also showed that the shape of the forward-facing step can be changed from square to 45° ramped, and this delays transition caused by the step. This is a small indication that the shape of forward-facing steps matters.

II.7 Swept-Wing Flows with Backward-Facing Steps

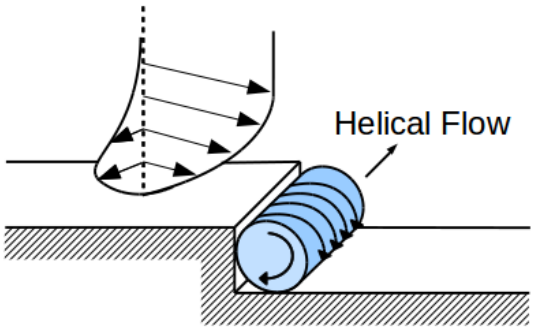

Figure II.7: Swept-Wing Recirculation Helix

Perraud et al. [24] showed experimentally that when the transition phenomena in a given flow are dominated by crossflow vortices, due to the presence of a crossflow velocity profile as seen in Figure II.7, the movement of the transition front is much like forward-facing steps in that it is what could be called “binary” in nature. The transition front will remain at the baseline position for small values of step height, however, at some critical step height the transition front moves forward rapidly to the step location. Perraud et al. found that by using the so-called ”envelope” method, taking the highest N-Factor at a given location, regardless of its wavelength, backward-facing steps increased the height of the N-Factor envelope by some constant factor at all chord locations past the step, and did not recover to the undisturbed value.

A computational paper by Balakumar et al. [29] showed that within a supersonic boundary layer, the effect of a step on crossflow instabilities is dependent on the wavelength of the disturbance. Balakumar et al. found that smaller wavelengths

were amplified more by interaction with a step excrescence than a larger wavelength. Furthermore, the reaction of the disturbances as computed by direct simulation do not always agree with the predictions of linear stability theory. This suggests that non-linear interactions may have a role to play in the breakdown to turbulence.

Eppink et al. [30] reported experimental investigations into backward-facing steps only. Using a swept flat plate in conjunction with a pressure body on the top wall of a subsonic wind tunnel, Eppink et al. showed that as stationary crossflow amplitudes increase the transition location moves forward on the model. This suggests that the stationary crossflow instability does play a role in the transition due to backward-facing step excrescences.

II.8 Swept-Wing Flows with Forward-Facing Steps

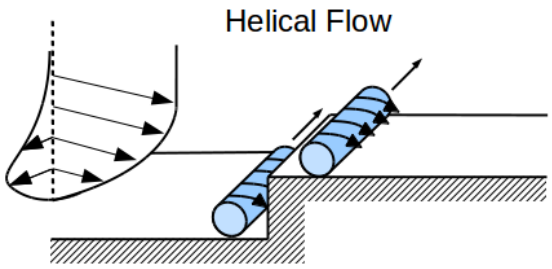

Figure II.8: Swept-Wing Recirculation Helices

Perraud et al [24] investigated forward-facing steps on swept and unswept wings. This class of flow has a flow field with two recirculation regions similar to Figure II.8. Like the unswept case, Perraud et al. found that a small forward-facing step excrescence will have little or no effect upon the breakdown to turbulence. Using the envelope N-Factor method, the study found that the height of the envelope in-

creased locally, but in contrast to backward-facing steps, recovers to the undisturbed value downstream. If one assumes a constant transition N-Factor, when observed experimentally this would appear as no change in the transition location until some critical value of step height. At the critical step height, the transition front will move rapidly forward to the step location itself.

Figure II.9: Cessna O-2A Aircraft with SWIFTER Model

II.9 Current Experiments

As part of a collaborative effort by the research teams at the Texas A&M Flight Research Laboratory and the Texas A&M Computational Stability and Transition Laboratory to investigate various aspects of transition to turbulence dominated by the stationary crossflow instability, in the mid-2000's an in-flight test model suited to these tasks was designed. This model was denoted the Swept-Wing In-Flight Testing model or SWIFT. The 30°-swept SWIFT model with a minimum pressure location at $\approx 75\%$ x/c on the test side (See Figure III.3) was specifically designed to isolate the stationary crossflow instability at a unit Reynolds number relevant to transport-class aircraft. Geometric and aerodynamic design features have eliminated three of the four common modal instability mechanisms in low-disturbance environments, as well as leading-edge contamination leaving only the desired crossflow vortices. Details of the original model can be found in Carpenter et al., [31] Carpenter, [32] and Rhodes et al. [33]

During in-flight experimental campaigns, infrared (IR) thermography of the model confirmed that the transition process on this geometry is dominated by the stationary crossflow instability as was the design intent. Furthermore, the model proved

capable of sustaining long runs of laminar flow back to the pressure minimum under transport relevant flight conditions (Re' = 5.5 10^6 /m) at relatively high angles of attack. As the angle of attack is lowered (made more negative) the favorable pressure gradient becomes increasingly strong, increasing the strength of crossflow vortices present. In general these lower angles of attack produce a transition location somewhere in the center of the model, allowing for testing of methods to increase the laminar run.

II.9.1 SWIFTER Experiments

The first flight experiment campaign carried out specifically to investigate the phenomena relevant to this paper (interaction of 2-D step excrescences and stationary crossflow) used the same Outer Mold Line (OML) as the SWIFT airfoil and accordingly had the same stability characteristics of the earlier airfoil described above, along with added provisions for including step excrescences at a location of 15% chord. This new model, in reference to the previous experiments, was named the Swept-Wing In-Flight Testing Excrescence Research (SWIFTER). Having the same shape as the earlier SWIFT model, SWIFTER is well suited to study stationary crossflow. SWIFTER was built with a number of improvements over SWIFT including the capability to internally articulate a step excrescence both forward-facing and backward-facing while in flight. The new model can be mounted on a Cessna O-2A aircraft as seen in Figure II.9 but was also designed to be capable of wind-tunnel tests in the Klebanoff-Saric Wind Tunnel (KSWT) at Texas A&M University. Details of the SWIFTER model and the experimental methods can be found in Duncan et al., [34] Duncan, [35] and Tufts et al. [36]

The SWIFTER experiments found behavior similar to the cases in Perraud et al. [24] for crossflow dominated cases. For small step sizes, there is no discernible

effect on the location of transition to turbulence, however, once a certain step size is reached the transition front moves quickly to the location of the step itself. This behavior seemed to hold for both forward-facing and backward-facing steps. The critical step height was found to be relatively insensitive to the angle of attack of the model, however, a strong dependence on the Reynolds number of the freestream was observed. It was also shown that the tolerance, in terms of dimensional step size, was roughly twice as large for a forward-facing step compared to a backward-facing step for any transport-relevant flow condition.

For reference Duncan [35] was able to empirically fit two curves to the data collected from the SWIFTER experiments. Note that because this is a graphical curve fit, and not an analytical equation, the units do not "cancel" and must be entered as indicated in the text.

$$k \text{ [microns]} = 2.116 \cdot 10^8 \cdot \left(Re' \left[\frac{1}{m} \right] \right)^{-0.857} \quad \text{(Forward-facing Steps)} \tag{II.1}$$

$$k \text{ [microns]} = 7.748 \cdot 10^{10} \cdot \left(Re' \left[\frac{1}{m} \right] \right)^{-1.298} \quad \text{(Backward-facing Steps)} \tag{II.2}$$

For reference, implementing the fits at a unit Reynolds number of 5.5 $10^6/m$ gives allowable steps of 354 microns forward-facing and 138 microns backward-facing. Note that there is uncertainty to this fit, as Duncan [35] characterizes the critical step heights as 350 ± 25 μm and 150 ± 25 μm respectively.

Another important revelation from the SWIFTER experiments came from examination of the infrared images themselves. For all cases examined, both forward-facing and backward-facing, the transition front remained time-invariant and spatially fixed to the model. In addition, the transition front showed the "sawtooth" pattern with turbulent wedges propagating along approximately 12° characteristic lines. An ex-

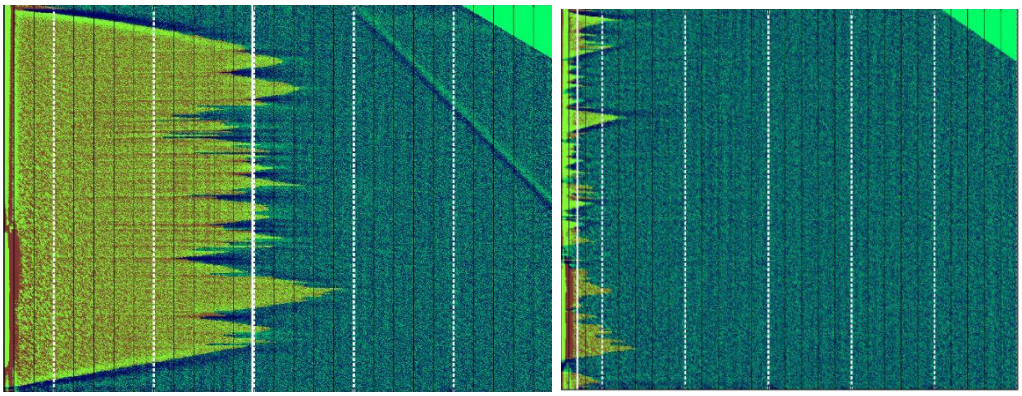

(a) Sub-Critical Step (b) Critical Step

Figure II.10: Sample IR Thermography Images
(Courtesy Glen Duncan & Brian Crawford, December 2014)

ample of both a subcritical step and a critical step seen under IR thermography can be seen in Figure II.10. This type of transition front is characteristic of flows dominated by the stationary crossflow instability. Because the transition front retained this character even when the step was "critical", meaning those steps causing transition to turbulence very close to the step location, the data strongly suggest that the breakdown to turbulence is related to the stationary crossflow instability. This should not be taken to suggest a priori that the stationary crossflow instability is solely responsible for the breakdown to turbulence, but rather that it must be modeled in computations in order to capture the relevant effects.

SWIFTER was tested at a number of angles of attack, and accordingly at a number of favorable pressure gradients. It was found during the course of the experiments that the angle of attack had a minimal effect on the critical step heights, appearing to be a much weaker effect than Reynolds number. This is in contrast to the Northrop Grumman Corporation (NGC) experiments, which showed a significant difference in behavior with and without a pressure gradient. These effects may be explained if the

transition mechanism has changed from T-S like waves in the NGC experiments, to stationary crossflow in the SWIFTER experiments. Because the NGC experiments were unswept, there is no chance for crossflow vortices to be the cause of transition, while the SWIFTER experiments are known to be dominated by stationary crossflow. It is known that T-S waves are stabilized by favorable pressure gradients, while crossflow waves are not which may help explain this difference between the two sets of experiments.

In addition to the in-flight testing, SWIFTER was also examined in the low-disturbance KSWT wind tunnel at Texas A&M. Along with IR thermography, the wind tunnel experiments were also able to provide detailed hotwire anemometry velocity profiles over the test article. Hotwire data showed that cases with subcritical forward-facing steps increased steady disturbances by a small amount and had essentially no effect on unsteady disturbance levels compared with baseline (no step) cases. Critical forward-facing steps showed a large increase in steady disturbances and a small increase in unsteady disturbances. Subcritical backward-facing steps also show a small increase in steady disturbances, but a significant (moderate) increase in unsteady disturbances. Critical backward-facing steps, however, again cause a small increase in steady disturbances, but a large increase in the levels of unsteady disturbances. This can be seen most clearly in Figures 173-175 of Duncan. [35]

While in the KSWT acoustic disturbances from a range of 10 Hz to 650 Hz were created by a wall speaker wall driven to 110 dB. There was no observed change in transition behavior, proving that the transition mechanisms in play for this model are not sensitive to acoustic disturbances. Furthermore, from experience this suggests 3-D transition mechanisms (crossflow) rather than 2-D mechanisms (T-S waves). In Duncan [35], it is noted that the inclusion of a large, near-critical forward-facing step did not affect these results.

It should be noted however, that in the KSWT, although the sweep angle is the same and the pressure gradient is similar to the in flight experiments, the lower Reynolds numbers for this flow decreases crossflow growth rates significantly. From the IR thermography campaign, it is known that the transition process for the model both in the KSWT and in the flight environment is dominated by the stationary crossflow instability. One may assume that the behavior in flight and in the KSWT with respect to transition behavior would be the same however the full effect of the lowered crossflow levels is not known at this time.

In addition the transitional behavior observed in the KSWT differed somewhat from that seen in-flight. During flight experiments, transition to turbulence was observed to be exclusively of the type expected for stationary crossflow, i.e. a sawtooth transition pattern somewhat uniform in span. For the KSWT, presumably due to the low levels of stationary crossflow growth, transition was observed as intermittent wedges appearing to jump forward to the step location. With increasing step heights, more wedges appear and with ever increasing frequency, until the entire model becomes turbulent at the step location.

II.9.2 SWIFTEST Experiments

The second experimental campaign was performed using a new leading-edge part manufactured for the SWIFTER model. With this new leading-edge installed, the model was referred to as the Swept-Wing In-Flight Testing Excrescence Stability Theory (SWIFTEST) model. In this configuration, the model was capable of being equipped with an excrescence at 1% chord, enabling the study of changing the location of steps. Details of this model and the experimental methods can be found in Crawford et al. [37] and Crawford. [38]

The SWIFTEST experiments returned slightly different results compared with

the SWIFTER experiments. The SWIFTER experiments report no significant response due to the steps prior to the snap forward of the transition front. SWIFTEST during in-flight tests reports that an observable increase in crossflow streaking and a small movement forward of the transition front results from small steps. However, it should be noted that for SWIFTEST the step excrescence was now located near the Branch I neutral point in flight, and forward of the Branch I neutral point in the KSWT. For an example of this behavior compare Figures 4.4 and 4.5 from Crawford. [38]

Unlike the SWIFTER experiments, the SWIFTEST campaign demonstrated an appreciable sensitivity to pressure gradient changes. It was shown that in the SWIFTEST experiment, as the pressure gradient becomes more favorable, the step height at which transition occurs immediately (i.e. at the location of the step itself) increases (becomes higher). In addition as the pressure gradient became more favorable, the degradation to the laminar fraction for a given step height was also reduced. This is to say that these data suggest that a favorable pressure gradient is stabilizing to the behavior dominating the steps at 1% x/c in terms of Re_{kk}. Where Re_{kk} is the Reynolds number based on step height for length and flow conditions at the height of the step in the undisturbed boundary layer $Re_{kk} = \frac{U_k k}{\nu_k}$. Accordingly, the SWIFTEST experiments were unable to collapse the onset of critical behavior to a single value of Re_{kk}.

Additionally, the suggestion of an increasingly favorable pressure gradient stabilizing the transition behavior at first blush suggests something other than stationary crossflow vortices as the dominant mechanism. However, it must be considered that a change in angle of attack entails many more effects than a simple changing of the pressure gradient. Of particular note is the movement of the attachment line aft with increasingly negative angles of attack, making the boundary layer thickness smaller

at the step location.

The SWIFTEST experiments also included steps translating normal to the mean chord line, as opposed to normal to the surface. Effectively, this has the effect of ramping the step for forward-facing steps, and creating an "overhang" for the backward-facing steps. This should be noted, since in both cases, forward-facing and backward-facing, the separation-caused recirculation is thought to be a key contributing factor for step excrescence behavior. See the later computations in this paper (e.g. Figure V.3).

II.9.3 A Note on Critical Step Heights

During the SWIFTER and SWIFTEST campaigns, the working definition of 'critical step height' was the step height which resulted in the transition location moving forward to the step location. An alternative definition that could have been used is to define the critical step height as the step height which results in degradation of the laminar flow run. Because this was developed during the SWIFTER experiments, which exhibited almost exclusively binary behavior, there is no material difference between these two definitions. However, during the SWIFTEST campaign it was discovered that SWIFTEST configurations resulted in considerable 'subcritical' behavior where laminar flow runs were degraded, but transition was aft of the step location. It seems that the most appropriate definition to be used when determining a manufacturing tolerance is the latter definition, step height which results in degradation of the laminar flow run. When examining Duncan [35] and Crawford [38] as well as the related works [34, 36, 37] note that they use the first definition.

II.10 Summary of Literature

In unswept experiments, for all cases examined by the author the movement forward of the transition location due to a backward-facing step was gradual. For

unswept forward-facing steps, the movement of transition forward has been reported as both gradual as in Drake et al. [27] and sudden as in Perraud et al. [24] In the studies done by Northrop Grumman Corporation (NGC) it was found that critical step heights increased for favorable pressure gradients.

The SWIFTER experiments exhibited an almost negligible effect due to the local favorable pressure gradient, tested via the changing of angle of attack. This is in contrast to previous experiments and the SWIFTEST experiment which showed a dependence on local pressure gradient. This is hypothesized to be a result of the difference in transition mechanisms in each case.

Hotwire anemometry from the SWIFTER campaign shows that transition associated with forward-facing steps results in a markedly greater increase in steady disturbances and little change in unsteady disturbances. The SWIFTER campaign and Eppink et al. [30] showed that transition associated with backward-facing steps results in increased levels of unsteady disturbances.

Infrared thermography from the SWIFTER and SWIFTEST campaigns shows that the transition front is both spatially fixed to the model and retains the sawtooth pattern characteristic of transition dominated by the stationary crossflow instability. This strongly suggests that the stationary crossflow vortices are playing a role in this breakdown.

When step excrescences are placed near the first neutral point of the crossflow instability, there is evidence of subcritical behavior. Excrescences placed farther downstream of the neutral point do not display subcritical behavior at SWIFTER flight conditions.

III. CALCULATION OF TEST MODEL FLOWFIELDS

III.1 Safety of Flight

The SWIFTER experimental setup, as previously mentioned, was constructed using the same OML as the SWIFT experimental model. However, due to the internal structural changes and the changes in mounting the model to the O-2A aircraft, before commencement of the SWIFTER campaign it was necessary to calculate structural loadings and stresses placed on the model by aerodynamic loading. This was accomplished by creating a three-dimensional CAD model of the aircraft including fuselage, hard points, braces. It was found during extensive studies previously performed within the research group (e.g. Rhodes [39]) that the effects of the aircraft on the test model could be reasonably modeled using a somewhat simplified version of the aircraft fuselage. Removal of the starboard tail boom, tail empennage, pylons, and the propellers greatly simplifies the computational grid, but still allows for the calculation of accurate results. An overview of the resulting model can be seen in Figure III.1. While some benefit is derived from the reduced cell count required to capture this simplified geometry, a much stronger advantage is with the removal of propellers the aircraft may be modeled as a steady-state problem which of course drastically reduces needed computational resources when compared to time-resolved solutions. During a flight safety sortie flown in 2015, the IR cameras were able to take data while the front engine was shut down. It was found that there were not discernible differences in the IR images when the engine was running and IR images from when the engine was shut down. These data further confirm that the simplifications made to the computational model do not significantly alter the results calculated for the test model.

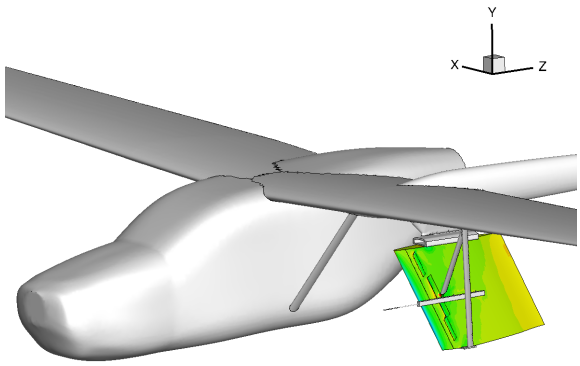

Figure III.1: Simplified Model of Cessna O-2A Aircraft for Safety Calculations (Aft Fairing not Shown)

It was also found during earlier computations of the O-2A, performed as part of the SWIFT experimental campaigns by the author, that the computational model of the flight experiments greatly benefited from the addition of a fairing not present on the actual aircraft. Because the simulation uses a turbulence model for the flow surrounding the fuselage of the aircraft, large scale unsteadiness is captured by introducing artificial viscosity to make the flow steady then correcting for this viscosity using the turbulence model. Therefore in areas likely to experience strong flow separation, a large amount of artificial viscosity must be added in order to stop the unsteadiness associated with this phenomena. In calculating the O-2A, it was found that the area behind the fuselage, near where the rear engine is installed on the aircraft is subject to large amounts of flow separation. This area includes a sharp break to a bluff body in order for the physical aircraft to clear the rear propeller. This typically resulted in the flow solver applying an excessive amount of artificial viscosity to this region, and negatively impacting the convergence of the solution. It was found that by adding a conical "fairing" to this location in the simulation, this flow separation and accompanying artificial viscosity increase could be avoided.

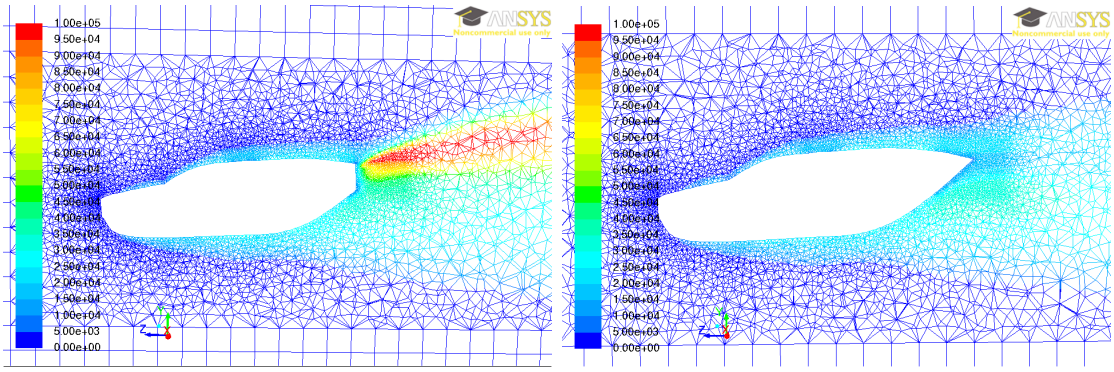

(a) Unmodified (b) Model with Fairing

Figure III.2: Contours of Turbulent Viscosity Ratio

Contours of the artificial viscosity with and without the fairing can be seen in Figure III.2. The addition of the fairing did not affect the results seen on the test model, making the exact shape not important, but did aid in convergence of the solution.

Safety of flight calculations were done using a three-tiered grid; a structured farfield, unstructured region surrounding the fuselage of the aircraft, and a structured grid surrounding the test region and leading edge of the SWIFTER model. For this grid topology due to the inclusion of the Duncan strut, (top bracing strut in Figure III.1)[1] the Martin strut, (bottom bracing strut in Figure III.1)[2] and the five-hole probe this grid was built also using unstructured cells on the pressure side of the test model. The general topology of the unstructured region can also be seen in Figure III.2. The grid was made using ANSYS ICEM, averaging around 27 Million mixed hexahedral and tetrahedral cells for these calculations. An extensive study on the grid resolution [39] was performed by the group examining the grid resolutions required to properly model similar geometries, (i.e. SWIFT) the grids used for the

[1]Named after it's designer Tom Duncan, this strut was put into place during the design of the SWIFTER model to limit deflections

[2]Named after test pilot Roy Martin, who suggested it's inclusion to limit movement of the model during the original SWIFT flights

calculations used in this study consistently used either equal or finer resolution than the grids used in previous studies.

This gridding method proved to be the most efficient way to achieve the resolution necessary for a solution intended to be able to handle boundary layer stability analyses. Although this grid was primarily intended for pressure data, it was built using the same methods as a boundary layer stability grid, and is similar to the grid used in Section III.3. The rule of thumb used within the Computational Stability and Transition Laboratory for subsonic flows such as this one, approximately fifty points are needed to adequately resolve a boundary layer basic state sufficiently to use those data for stability analyses. As is discussed in Rhodes [39] it is not feasible to do this using isotropic cells, such as those used in common tetrahedral meshing. While anisotropic unstructured cell meshing programs such as can be used in Pointwise show promise in getting the correct grid spacing, in the authors experience, attempting to interpolate a boundary layer profile from unstructured cells must be done extremely carefully to avoid incorrect stability results. It is known that stability results are very sensitive particularly to the shape of the boundary layer profile, and small deviations that often occur when interpolating from irregularly spaced and shaped cells can influence one's results. Furthermore, even when the grid is constructed carefully and well, it is known that unstructured cells can cause certain flow phenomena known to be symmetric in reality to be biased to one direction.[3]. As an example of more trivial issues, use of unstructured cells also more makes determination of discretization errors more difficult, as grid refinement ratios are not easily determined.[40] For these reasons, if at all possible unstructured cells were not used in areas where stability of the flow in question was to be examined, leading to the use of the three-tiered method and the complications that it entailed.

[3]Jacob Cooper, personal communication

The solution was calculated using ANSYS Fluent. For safety of flight calculations, the solution assumed laminar flow over the first 65% chord of the test model on the suction side, (back to near the minimum pressure location) and the first 5% chord of the pressure side. The transition from laminar flow to turbulent flow can be seen as a slight dip in the pressure coefficient at these locations. The balance of the test model and the aircraft fuselage were assumed to be turbulent, and modeled with the k-epsilon SST turbulence model. For in-flight tests, the solutions used the density-based formulation in Fluent with calculation of the energy equation. Density was calculated using an ideal gas, and viscosity was found via Sutherland's formula. All boundary conditions were set as farfield, with the temperature, pressure, and density set using the standard atmosphere and reported values for altitude and Reynolds number. With the test article mounted vertically beneath the port wing, the aircraft angle of attack and side-slip angle were adjusted so that the flow data extracted from the location of the five hole probe was equal to that measured experimentally.

Three major cases were calculated prior to the clearance flights of the new model, 1) the test conditions case, calculating the flow at nominal test conditions, 2) the worst case scenario, predicting the maximum loading expected for the model, and 3) the buckling case, calculating the a highly negative angle of attack which would produce the highest buckling forces on the additional struts placed on the model.

Surface pressures on the test model were the primary purpose for these calculations, and were used as the primary flow diagnostic. The surface pressures were used to calculate the effective loading on the airframe and to inform Finite-Element Analysis (FEA) studies performed by Duncan. [35] Using the results of the FEA, loadings throughout the structure of the model, and the corresponding margins of safety, were calculated and found to be acceptable. The overall loading of the model was found to be within the flight-tested conditions used by the USAF during the O-2A's previous

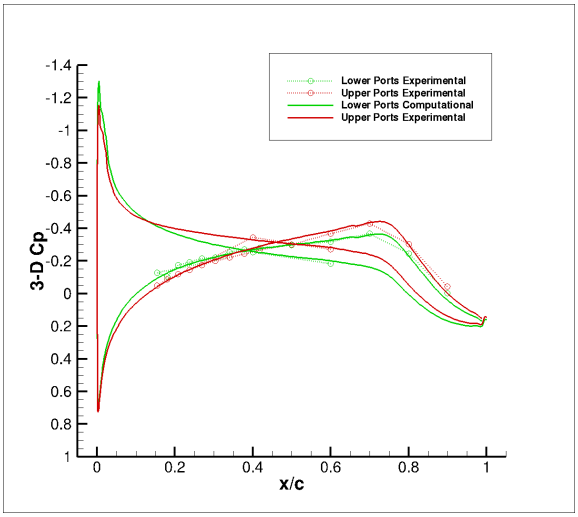

Figure III.3: Coefficient of Pressure - Experimental and Computational -6.5° AoA

usage as a military observation aircraft. Details on the FEA analysis and how the calculated pressures were used can be found in Duncan [35]. Static loading tests were then completed November 11, 2012 using the values found computationally before flight testing was initiated. Envelope clearance flights for the model were completed on January 2, 2013, and showed that the model responded acceptably to accelerometer and strain gauge measurements. Further details on this clearance flight can be found in Duncan. [35] Comparisons between the computationally found values and values later found using in-flight measurements can be seen in Figure III.3.

III.2 Crosswind and Sideslip Calculations

A brief note on the crosswind capabilities of the O2-A while mounting the SWIFTER model. At the beginning of the SWIFTER project, it was decided to revisit the criterion that limited the crosswind capabilities and sideslip angles while testing. Details of the design and safety analysis of the original SWIFT model can be found in McKnight. [41]

There are three potential criteria for determining the limits of crosswind capa-

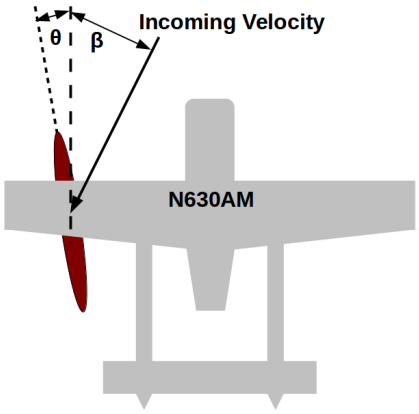

Figure III.4: Sketch of SWIFT/SWIFTER Angles

bilities and sideslip angles of the aircraft. The Pilot's Operating Handbook (POH) for the Cessna O-2A defines crosswind limits based upon rolling moments of the aircraft caused by asymmetric loading of the on-wing pylons. The POH also limits the maximum lateral loading of the pylons at 500 lb._f, based upon the aerodynamic loading produced by the model. Finally there is a hard limit of a 25 kt crosswind, for the aircraft with no external stores.

Asymmetric loading of the pylons restricts the crosswind capabilities of the O-2A to 7 kts according to the POH. During takeoff and landing operations, lateral loading at the most restrictive limits the crosswinds to approximately 15 kts, making the lateral loading less restrictive than the asymmetric loading for these operations. The crosswind capabilities were therefore unchanged from those used during the SWIFT experimental campaign.

During the design of the SWIFTER airfoil it was decided to change the toe-out angle of the model (denoted as θ in Figure III.4) from $-1°$ to $-4°$ in order to facilitate experimental tests. Details of these changes can be found in Duncan. [35] As a consequence of this change, the limit in sideslip angle for the aircraft itself would

be compromised. Due to the lateral loading limits of 500 lb._f on the pylons, during the SWIFT campaign the model was limited to $\pm 7^\circ$ AoA (equal to $(\beta+\theta)$ in Figure III.4). With the 1° toe-out angle, this limits the aircraft angle of side slip (denoted as β in Figure III.4) from $+6^\circ$ to -8° when equipped with the SWIFT model. However, because SWIFTER was designed to be flown with a 4° toe out angle, keeping this same limitation would limit the aircraft sideslip angle from $+3^\circ$ to -11°. While possible to fly the aircraft with these limitations, this situation would be constrictive to a test-pilot and inhibit the ability to perform normal flight operations.[4]

However, it was noted that this limitation on model angle of attack was centered on 0° AoA, despite the SWIFTER model being a cambered airfoil. By performing a number of calculations of the model at differing angles of attack, it was found that the zero-lift angle for the model is approximately -2°. Recall that the limitation on model angle of attack was put in place to limit lateral loading. By changing the limit on model angle of attack from $\pm 7^\circ$, which corresponds to $+500$ lb._f to -250 lb._f to a limit of $+7^\circ$ to -11° which corresponds to ± 500 lb._f of lift, the limit on the aircraft sideslip angle can be changed from the range $+3^\circ$ to -11° to the range $+7^\circ$ to -11°. This change makes the aircraft operations more tractable.

III.3 Stability Calculations

Once the aircraft flight envelope was cleared, the focus of the computations moved from obtaining total pressure loading on the model to satisfy safety concerns, to finding the boundary-layer stability characteristics of the model to aid with the collection of data. The practical effect of this corresponded to further simplifying the CAD model of the aircraft by removing the struts and braces on the pressure side of the airfoil and adjusting the grid to offer further resolution near the excrescence

[4] Aaron Tucker, personal communication

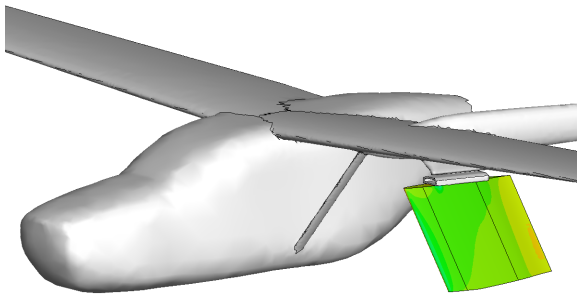

Figure III.5: Simplified Model of Cessna O-2A Aircraft for Stability Calculations

location. Stability simulations were run using the same flow solver settings as the safety of flight calculations.

Grids averaged around 33 million mixed hexahedral and tetrahedral cells. The grid was constructed using the same basic topology as the grid described in III.1, however the removal of the safety struts and five hole probe allowed for structured cells to be used on both the test side and non-test side of the aircraft.

As part of a concurrent separate campaign studying the effectiveness of DRE's on the SWIFTER airfoil [15] a sweep of angles of attack were calculated. From these flowfields, velocity profiles along the test model and their accompanying stability results were also found. These data were used as part of the DRE campaign, and also to inform the SWIFTER and SWIFTEST excrescence experiments in terms of boundary layer thickness, crossflow growth rates, crossflow neutral points etc. These data were also used to inform the boundary conditions of the step-area grids described in Chapter IV, for in-flight conditions.

Overall the model is relatively uniform in the spanwise direction, having slight changes in pressure due to edge effects. However, the model has a total maximum span of 1067 mm, of which only the portion between the two sets of pressure ports, one located 330 mm inboard from the root, and the other located 330 mm from the

tip is considered a valid test area. Within the 407 mm wide test section, the spanwise uniformity is even more favorable given the distance from either of the "wingtips". See Figure III.3 for the very good agreement between the computations and the experimental results of Cp along the two rows of pressure ports.

As part of the condition sweep described above, spanwise variation in the stability behavior was also examined, and it was determined that within the test section, stability results were qualitatively and quantitatively similar enough that no conclusions made using these results would change from root to tip. For this reason, the majority of stability analyses were conducted using only the distribution taken from the direct center of the test section, a region having behavior that fell in between the characteristics of either edge of the test section. This same technique was used successfully during the SWIFT campaign of experiments.

III.4 KSWT Grid

A key part of the design of SWIFTER was a provision to allow the model to be mounted in the KSWT facility at Texas A&M. The SWIFTER was designed to be mounted vertically in the KSWT to allow optical access to the test side of the model in a manner analogous to the in-flight experiments. This was done in order that in addition to the IR images obtained from in-flight experimentation that detailed hotwire anemometry scans could be completed to provide supplemental data and insight.

As part of these campaigns, basic state solutions for the model as installed in the KSWT facility were also needed. Earlier experiments in the KSWT using the ASU(67) airfoil (e.g. Hunt and Saric, [42]) provided experience in calculating models in the tunnel. Previous experiments in the facility had employed contoured wall liners intended to make the flow in the tunnel as spanwise (normal to the leading edge)

invariant as possible. These were made by first calculating the inviscid flowfield for the model as installed in the KSWT test section, but having infinite span. Then streamlines for this flow were calculated in post-processing, and the geometric shapes were extracted. Using a CAD software program, a series of these streamlines were then lofted together to make a surface with a shape corresponding to an undisturbed infinite span flow. Simply then, one side of this surface is used as a "ceiling" and the other is used as a "floor". There are numerous complications with making these wall liners, including the fact that if the angle of attack is not set to the zero lift angle, the streamlines produce a significant change in elevation between the two streamlines converging aft of the trailing edge which makes manufacture more complicated. In addition, creation of the wall-liners requires a non-trivially large CNC router, or a great deal of hot wire foam cutting for a test section the size of the KSWT. Specific to the SWIFTER experiments, the hard foam wall liners also had the possibility of limiting the deflection of the leading edge.

As part of the shakedown tests of the SWIFTER model to test the articulation system, the model was put into the KSWT facility with a 'simple' installation prior to the construction of the wall liners. For this installation, in lieu of the wall liners an extension of the model to enable the SWIFTER to span from ceiling to floor was installed. During this procedure pressure data were acquired along the chord of the model for two spanwise locations. It was discovered that the pressure data were reasonably uniform even without the presence of the contoured wall liners. A calculation performed by Kristin Ehrhardt, modeling the a fully three-dimensional KSWT test section confirmed that the spanwise variation in pressure was acceptable for the tests. A plot of isobar contours for this simulation can be seen in Figure III.6. Note that in this figure, the test region is between the two black horizontal lines, and the image is shown inverted from the actual installation in the wind

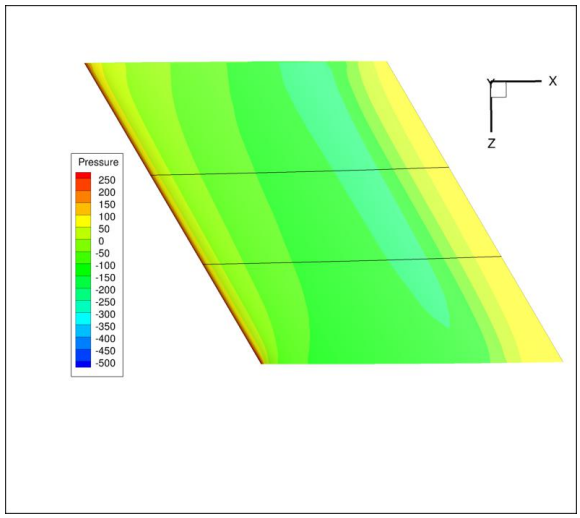

Figure III.6: Gauge Pressure Isobar Contours 3-D Model in KSWT

tunnel. Comparisons with infinite span calculations showed that spanwise infinite calculations produced results falling between the behavior of the root and behavior of the tip. As such, basic states for the KSWT facility were otherwise modeled using a spanwise-invariant assumption, in keeping with previous work in the KSWT.

As might be expected for a subsonic facility with a relatively large model as compared to the test section, it is necessary to model the side walls of the facility. The mounting point for the model was determined from the structural design of the tunnel and the model. Because the grid was modeled as spanwise invariant, the most logical method for creating a computational grid was to set the coordinate system to be parallel/normal to the leading edge, as opposed to parallel/normal to the freestream. The grid can then be made without resolving the spanwise direction as all gradients are zero in that direction.

III.4.1 A Note on Angle of Attack

It should be noted that there are then two separate ways one might denote the angle of attack of the airfoil. An intuitive way to measure angle of attack when

installing an airfoil in a wind tunnel is to measure the deflection of the trailing edge, then using trigonometry and the swept chord length determine the angle of attack. Note however, that this method is essentially using a coordinate system aligned with the freestream direction, and results in a different measure of angle of attack than those measured in the coordinate system aligned with the leading edge, although both correspond to an identical physical situation. For this reason, one may see two angles of attack listed in experimental papers, particularly those in wind tunnels (e.g Hunt and Saric [42] or Duncan [35]).

III.4.2 Grid Topology

Prior to the SWIFTER campaign, a number of angles of attack were modeled computationally and the flowfields examined. It was determined that the angle of $-2.00°$ as measured normal to the leading edge provided both a good match for previous unswept experimental data in terms of pressure gradient and that this angle of attack was near the zero-lift angle for SWIFTER/SWIFTEST geometry. Having a low lift force both reduces the stress on the mounting hardware, and facilitates the installation of contoured wall liners should that be desired.

KSWT solutions were gridded using a completely structured mesh, arranged in a "C" type grid. This topography allowed for a concentration of cells in the boundary layer, and in terms of gridding fitting an airfoil to a standard test section requires fitting a rounded body to a square hole, a C-type grid allows the interfaces and ill-shaped cells to be placed away from the model itself, which is where resolution and grid smoothness is most critical. Additionally an advantage of a C-type grid over something like an H-type grid or O-type grid, is that the attachment line can be smoothly modeled, and simultaneously a clustering of cells to capture the wake behind the airfoil can easily be placed into the grid.

Solutions were calculated by setting a velocity inlet approximately 20 chord lengths upstream to match the freestream data measured in the KSWT facility. Pressure outlets were set approximately 30 chord lengths downstream of the model. Stretching regions were used in both the inlet and outlet regions in an attempt to prevent reflections from the boundary. Unlike the topology in the physical facility, the contraction and expansion regions ahead of and aft of the test section respectively were not modeled. Freestream measurements were taken in the test section of the tunnel, and this is the location where conditions were known. Instead, the tunnel was modeled as a uniformly sized channel with slip walls (skin-frictional force = 0) to prevent the growth of a non-physically sized boundary layer on these walls. Trials were run making the walls viscous and using the no-slip condition along with a "virtual leading-edge" type of approach where the no-slip region was set to begin farther upstream than the test section's size to match experimentally measured boundary layer thicknesses, but it was found that this had a negligible effect on the solution.

Similarly to the in-flight model, the KSWT grid was set to have laminar runs over the attachment line and back to the pressure minimum of the model itself in order to obtain accurate laminar basic states to use for stability analyses. On the aft region of the model, k-ε turbulence modeling was used to prevent separation, and give a more physically representative C_p distribution.

IV. CALCULATION OF STEP-AREA FLOWFIELD

From experimental results, it was known that for the SWIFTER model at in-flight experimental conditions, the critical step heights would be on the order of 100's of microns (0.0001 m) tall. The model itself has a chord length on the order of 1 meter, while the aircraft has a wingspan on the order of 10 meters. Because the flow is subsonic, a farfield must also be modeled, the largest scales of the grid are on the order of 100 meters in size. The necessity of modeling these disparate length scales accurately results in a change of at least 6 orders of magnitude if only one cell is placed in the height of the largest step. From previous experience during the SWIFT campaign, it was known that the approximately 33 million cells were nearing the limits of computational power available. It became apparent that simply integrating step excrescences into the grids used to calculate the flowfield around the aircraft was not tractable computationally, out of necessity an alternative solution was then pursued. Consideration was given to using an overset solver, such as OVERFLOW [43], as these methods are well suited to modeling disparate length scales. However owing to the complexity and time cost of implementing a new flow solver and methodology, it was decided to use a method similar to that used in Rizzetta et al. [44] (albeit without the use of overset grids) in that the flow conditions from the in-flight flowfield would be used as boundary conditions for a smaller calculation.

Velocity and pressure profiles for the undisturbed (no excrescence) SWIFTER airfoil were calculated using the C_p distribution calculated as described in Chapter III. The boundary conditions were created using velocity and pressure data calculated from using the WINGBL2 code written by Pruett [45] using these C_p values

as input. For each profile 3 separate 3-term Fourier series expansions were used to convert the discrete velocity data points into an analytical function. This function was then used as a Dirichlet velocity boundary condition for the inlet of the step-area computational grid. The top surface of this grid used a Dirichlet pressure outlet boundary condition, while the "sides" used a periodic boundary condition. These boundary conditions were then coded into a Fluent User-Defined Function (UDF), which was held constant for each step height.

The coordinate system used selected points the X axis downstream perpendicular to the leading edge and step excrescence. Y is selected to be wall normal, and Z is selected to be the cross product of these two vectors. The resultant Z axis is parallel to the leading edge, and pointed towards the root of the model. These axes can be seen in Figure IV.1. This should be contrasted to the 'prime' axes which are aligned with the freestream flow direction, also seen in Figure IV.1. The diagrams shown correspond to the view one would see looking from the cockpit of the O-2A used in the flight experiments over one's left shoulder towards the port wing.

IV.1 Forward-Facing Grid Topology

The calculation of the step area was done in two stages. The first step was to calculate a gird that was "larger" in a the X and Y dimensions, but only three cells in the Z-direction, making the simulation "quasi 2-D." Calculating the solution in this way allows for the solution be be spanwise invariant, but to calculate all three components of velocity, along with the scalar quantities. This solution used 5 micron uniform spacing in the x and y directions and 25 micron spacing in the z direction. The results from this simulation were found to have negligible spanwise (z-direction) variance, as was expected.

The second step was to calculate a smaller, fully three dimensional grid, with

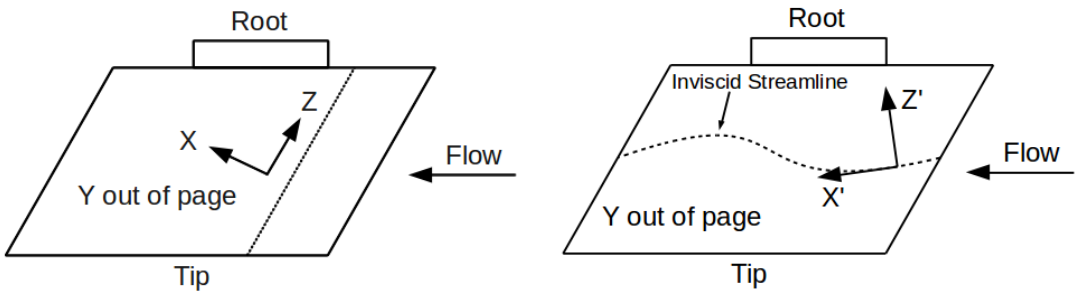

(a) Aligned with Step (b) Aligned With Streamline

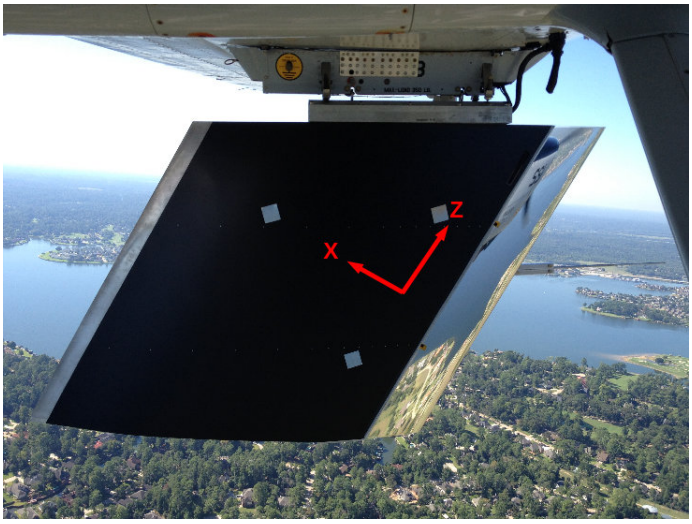

(c) Photo of Model with Coordinate System

Figure IV.1: Coordinate Systems Used for Step-Area Calculations

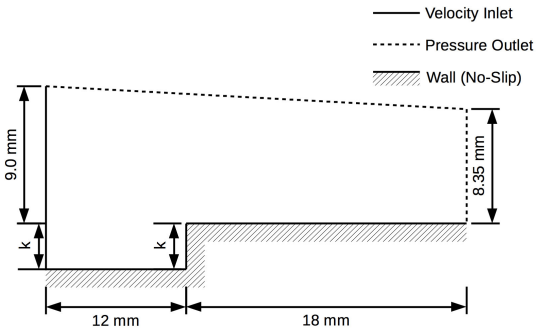

Figure IV.2: Diagram of Forward-Facing 2-D Step Grid Overall Dimensions

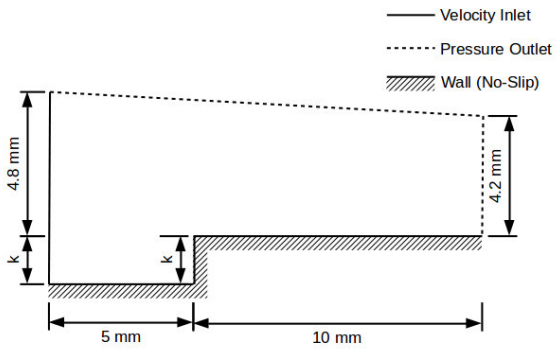

Figure IV.3: Diagram of Forward-Facing 3-D Step Grid Overall Dimensions

increased resolution in the step-corner area. Because the grid was oriented and made in the X-Z coordinate system, instead of the X'-Z' coordinate system, the mean flow is angled with respect to the axes by approximately 30°. Additionally, the details of the flowfield were unknown a priori, the first iteration of grid used uniform 30 micron spacing in the x, y, and z directions. Using a 30 micron spacing in all directions was found to approach the maximum memory available for the Texas A&M University Eos computer cluster using 8 nodes. When grid convergence studies on the uniformly spaced grids suggested additional grid resolution was needed, a second set of grids were produced using the topology seen in Figure IV.4. Numbers in Figure IV.4 represent the length of the line segment, note that the diagram is not to scale, but rather shown with lengths labeled for clarity.

This grid is separated into three distinct regions; A, B, and C, listed in order of increasing grid spacing, which are reported in Table IV.1. It was found that this grid topology used approximately the same number of cells but resulted in better grid convergence, as might be expected from clustering cells near regions of high velocity gradient.

In addition to the velocity data calculated from the larger step-area grid, an

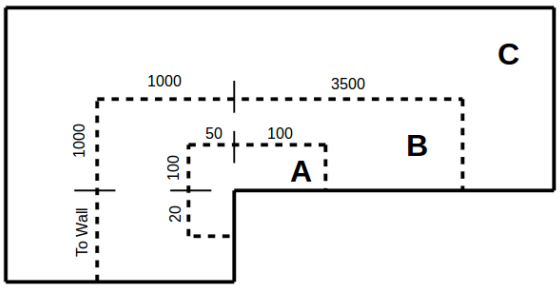

Figure IV.4: Diagram of Forward-Facing Step 3-D Grid Refinement

	Max Spacing	Growth Rate
Region A	1	N/A
Region B	10	1.05
Region C	40	1.05

Table IV.1: Grid Spacing (Grid 1)

additional input was used for these fully three-dimensional simulations. From the basic-state profiles calculated as described in Chapter III, Linear Stability Theory calculations were performed using LASTRAC with the settings found in Appendix A. Then by extracting the eigenmode for a given crossflow wavelength, then reconstructing the physical flow field (as in Appendix B) one can use the crossflow instability as an inflow condition. Because the disturbance profile was calculated from linear stability theory, and is therefore an eigenmode, the amplitude of the disturbance is arbitrary in the stability theory equations. In order to implement this disturbance as a physical flowfield, an amplitude was estimated by assuming an initial disturbance amplitude (A_0) of $10^{-4} \cdot U_e$ then using the the calculated LST N-Factor of the particular disturbance to find the amplitude as would be found at the inlet. For an example, the 4.5 mm crossflow vortex has an N-Factor of approximately 4 at 15%

chord, therefore the amplitude of the vortex according to LST at 15% is

$$A = e^N(A_0) \tag{IV.1}$$

$$= e^N(10^{-4} \cdot U_e) \tag{IV.2}$$

$$= e^4(10^{-4} \cdot 93.83 \text{ m/s}) \tag{IV.3}$$

$$A = 0.512 \text{ m/s} \tag{IV.4}$$

Note that this value is an estimate, since the receptivity process has not been fully characterized, and hotwire data for in-flight conditions is not available, thus A_0 is not known exactly for these conditions. Larger amplitudes were also used, and it was found that the amplitude of the disturbances downstream simply scaled with the initial amplitude, as one would expect from a disturbance with an amplitude in the linear regime.

IV.2 Forward-Facing Grid Convergence

The grid chosen to study grid convergence was the 300 micron forward facing step at 15% chord. This was chosen because it was near the experimentally reported critical step height, and the flowfield is complex. The Grid Convergence Index (GCI) method as described in Roache [40] was used to determine grid convergence. This method is essentially a Richardson Error Estimation, but with a Factor of Safety implemented to account for uncertainties e.g. observed order of convergence. Because a grid triad was used, and was able to confirm that the grids used were in the asymptotic region of convergence, the factor of safety used was 1.25 as recommended by Roache.

The solution functional of perturbation amplitude was chosen for grid convergence studies, given this quantity was the main object of the simulations. Reported in Table

	Finest X-Y Spacing (Microns)	Z-Spacing (Microns)	U Perturbation Station 36	U Perturbation Station 51	U Perturbation Station 101
Grid 1	1	50	1.0316	0.84716	0.70939
Grid 2	2	50	1.0396	0.84292	0.67967
Grid 3	4	50	1.0625	0.82893	0.61878

Table IV.2: 2.25 mm Wavelength Perturbation Amplitudes Used for GCI Study

	GCI Station 36	GCI Station 51	GCI Station 101
Grid 1	0.52%	0.27%	4.99%
Grid 2	1.48%	0.90%	10.68%
Grid 3	4.23%	2.97%	21.88%

Table IV.3: GCI Values Using $F_s = 1.25$ (2σ Error Bound Estimate)

IV.2 are the values of the 2.25 mm wavelength U-Component of the perturbation quantity at three different chordwise locations. Station 36 is just aft of the step location, Station 101 is located very close to the outlet boundary, and Station 51 is an intermediate location. Reported in Table IV.3 are the resulting error estimations in U-Perturbation amplitude at these stations.

While the observed order of convergence was less than the expected theoretical value, as reported in Table IV.4, the values appear to be in the asymptotic range. The degree of error increases downstream near the outlet, but remains small enough that the resulting perturbation amplitudes are well separated from the error estimates, as seen in Figure IV.5. This indicates that the differences in U-Perturbation amplitude are not due simply to discretization error, but must be attributable to other sources.

	Observed Order Station 36	Observed Order Station 51	Observed Order Station 101
Triad 1 (1-2-3)	1.52	1.72	1.03

Table IV.4: Observed Orders of Convergence

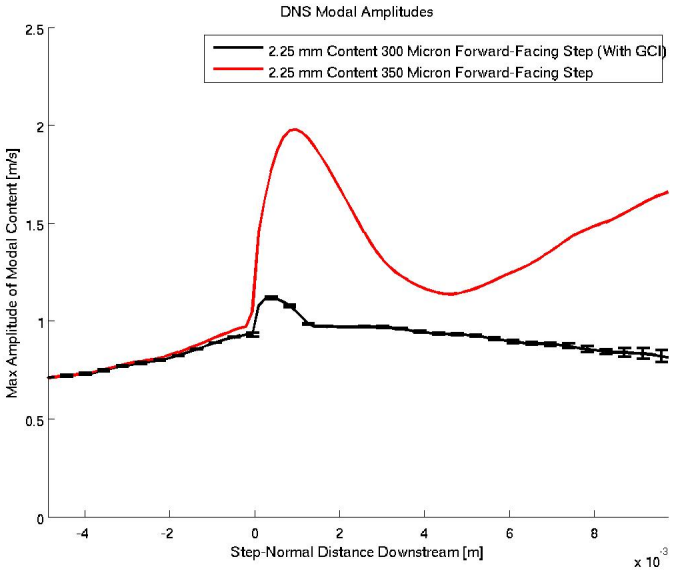

Figure IV.5: Perturbation Amplitudes with GCI Error Estimates (Grid 1)

IV.3 Backward-Facing Grid Topology

The backward-facing steps were analyzed using a topology very similar to the forward-facing steps. As seen in Figure IV.6 the grid was roughly the same shape, but the obvious change that had to be made was now the extended region of the grid is behind the step location. The reference datum of the coordinate system was set such that the corner of the step has Y = 0. Similar to the forward-facing steps, the grid was refined in three steps using the spacings given in Table IV.1 but using a modified topology seen in Figure IV.7.

IV.4 Analysis Methodology - DNS

After calculation of the flow field on the smallest step-area grid as described in Chapter IV, velocity data were usually extracted using Tecplot 360 for data analysis. It must be noted that when using Tecplot to perform data analysis for Fluent-calculated solutions that Fluent natively stores its data in a cell-centered format.

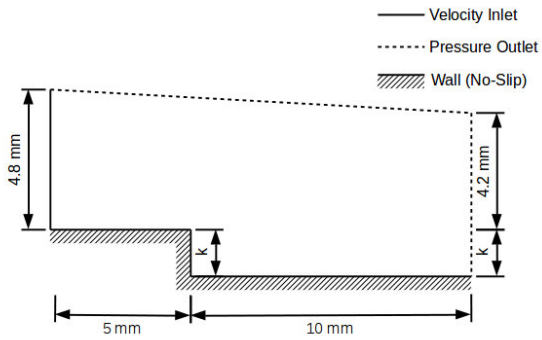

Figure IV.6: Diagram of Backward-Facing Step 3-D Grid Overall Dimensions

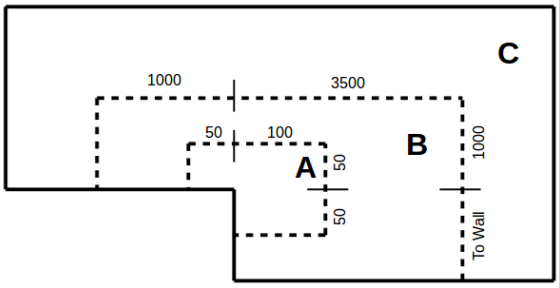

Figure IV.7: Diagram of Backward-Facing 3-D Step Grid Refinement

For this reason, if one uses the Fluent native data loader to import the solution file into Tecplot, the data may display artifacts of this storage which are not desirable for stability analyses. An example of these artifacts are that the velocity at no-slip walls will often be reported as non-zero, due to the interpolation scheme used internally by Tecplot. For data analyses where stability calculations were not involved, the data was loaded into Tecplot and manipulated by Tecplot or output into ASCII data and manipulated in Matlab. For applications where the artifacts of cell-centered storage would be detrimental to the solution, data was directly output by Fluent in an ASCII node-valued data format. Output of the data directly from Fluent however, is more expensive in terms of storage space, as the data must be stored in an uncompressed,

non-binary format, making manipulation via Matlab the preferred method.

After loading the data into Tecplot, slices of constant X were extracted for 100 stations along the solution area (giving a spacing of 150 microns). Using an in-house Matlab script, a Fast-Fourier Transform (FFT) was taken of each wall-normal location across the span of the computational domain, allowing for the calculation of spatially coherent disturbances. The growth of these disturbances was then tracked along the downstream dimension, and the wall-normal disturbance profiles were then examined. This method is similar to that found in Rizzetta et al. [44]

V. FORWARD-FACING RESULTS

V.1 General Flow Topography

For all forward-facing step sizes, there exist two regions of recirculating flow; one is located in the concave corner in front of the step and the second on top of the step's plateau. Unlike channel flows, and unswept wings, these recirculation regions are not areas of closed flow, but become open flows due to a spanwise velocity component. Examination of the two recirculation regions reveals that both are helical flows with a mean velocity in the root to tip direction. It is worth noting that the spanwise component within the recirculation is in the opposite direction of the 'normal' crossflow direction which flows tip to root. Both the crossflow and this helical motion are driven by a spanwise (normal to the inviscid stream direction) pressure gradient, caused by the combination of sweep and chordwise pressure gradient, which is present even in spanwise-invariant flows. However, unlike the favorable gradient present on the majority of the wing, approaching the step, there exists a local region of adverse pressure gradient. Passing over the step itself, there is a very short region of favorable pressure gradient, followed by a second region of adverse gradient as seen in Figure V.2 causing both helical flows to move root to tip. Note in the figure that

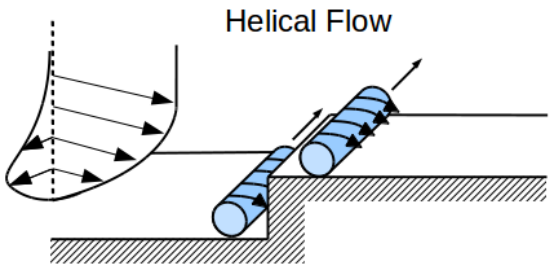

Figure V.1: Cartoon of Forward-Facing Swept Steps

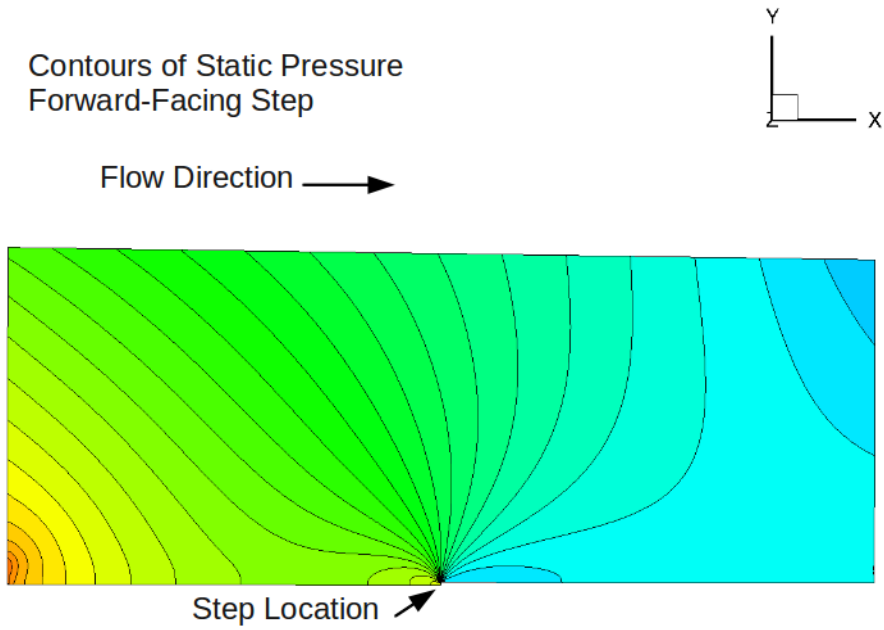

Figure V.2: Pressure Contours for Forward-Facing Step

high pressure is red, while low pressure is blue, meaning the edge gradient is favorable. These pressure-gradient features were also seen experimentally for SWIFTER, (Figures 89 and 90 in Duncan. [35]) Local pressures were not measured during the SWIFTEST experiments, due to the excrescence being located on the leading edge, where pressure ports could not be fitted.

As would be expected, the size of both recirculation regions increases with larger step sizes. The front recirculation region has a height equal to approximately one quarter step height for small steps to approximately one half the step height for larger steps. This region typically has a length 2-3 times its height. The top recirculation region also scales with step height, but tends to have a higher aspect ratio than the lower recirculation region. The length of the bubble can vary greatly from approximately 2-5 times the step height, but the height of the region is much smaller, being a small fraction of the step height. As an example the top recirculation region was

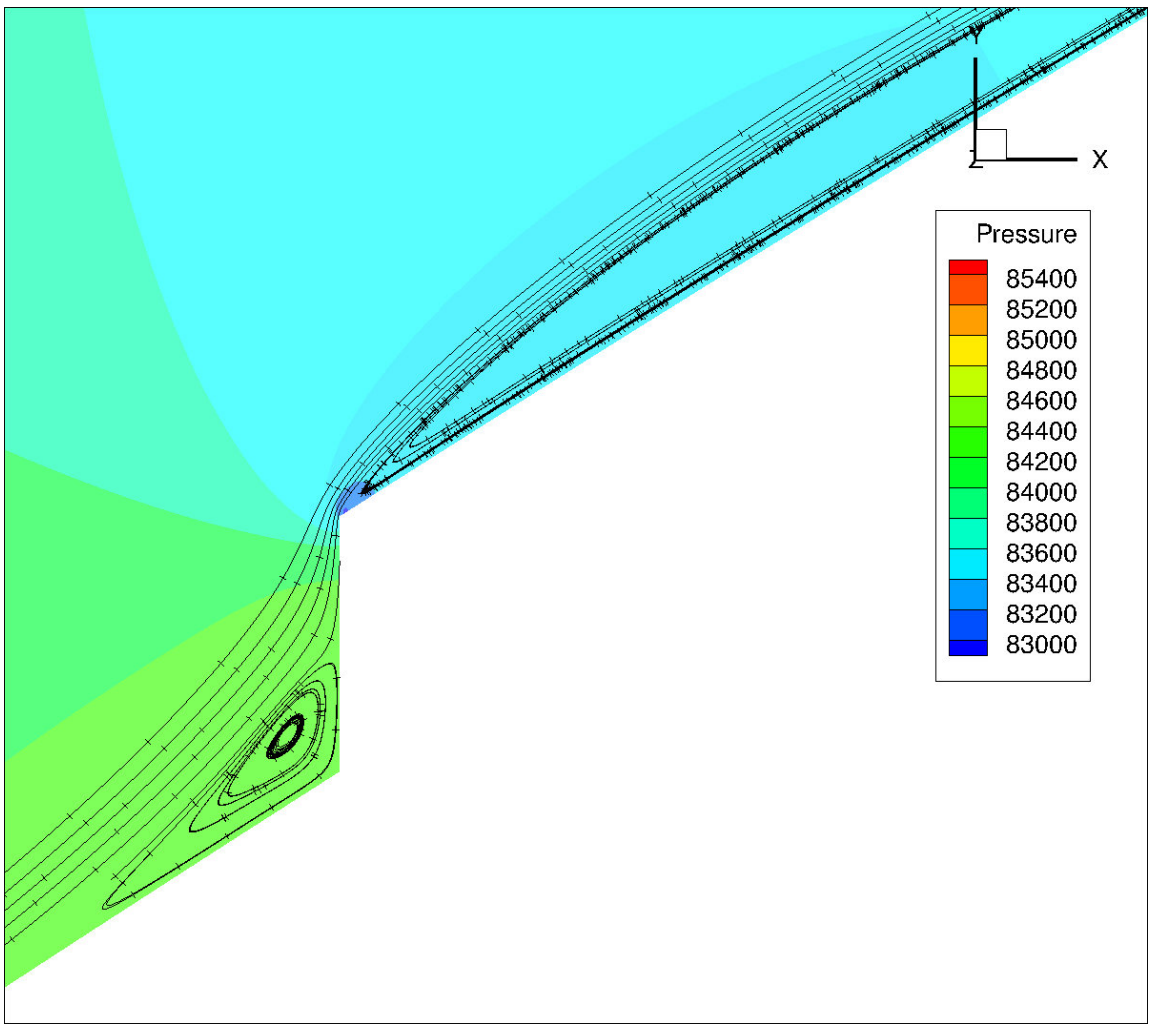

Figure V.3: Streamlines for Forward-Facing Step (Case at 1% x/c)

measured to be 50 microns high for a 350 micron tall step. See Figure V.3 showing streamlines in the vicinity of a step for SWIFTEST.

The size of this top recirculation region varied greatly with step height, making it hard to give a general rule of thumb for this region. At the same dividing line as the change in character of eigenmode discussed in Section V.2 the helical flow "bubble" present on the top of the step increases greatly in size. This increase in size is present whether or not a crossflow disturbance is present in the flow, with the only difference being that in the case of a crossflow disturbance this bubble will appear distorted, with a wavelength in the distortion pattern equaling that of the crossflow perturbation. It is believed that this bubble size plays a key role in the development of disturbances, so this is an important observation.

V.2 DNS Modal Disturbance Growth

The behavior of the forward-facing step described below was captured using completely steady (time-invariant) calculations. Also note that the figures discussed in this section are found in Appendix C.

In order to examine the growth of disturbance modes using DNS studies, it was necessary to select an incoming disturbance. It is known from IR thermography images such as that seen in Figure V.4b that the SWIFTER and SWIFTEST airfoils when operated at in-flight conditions are dominated by the stationary crossflow instability. Furthermore, the images also show that this is still true when transition is caused by a critical step.

For this reason, the logical choice for an incoming disturbance mode is that of a stationary crossflow wave. The initial focus was for nominal in-flight conditions of the SWIFTER experiment (excrescence at 15% chord, -6.5° angle of attack, Re' = 5.5 10^6 /m). Linear stability theory analyses reveal that locally at 15% x/c, the wave

with the highest level of growth (highest N-factor) is one with a spanwise wavelength of approximately 2.25 mm (parallel to the leading edge.) Overall (up to the pressure minimum) the crossflow wave experiencing the highest level of growth is one with a spanwise wavelength of approximately 4.50 mm. See Figure V.4a.

Initial analyses focused on the 4.50 mm wavelength, as this wavelength was thought to be the modal disturbance most responsible for transition. However, as the computational campaign continued, it was discovered that the response of the disturbances depended on the wavelength. A step which strongly amplified the 2.25 mm wave might have little effect on the 4.50 mm wave, for example. It was found that in general, the smaller wavelengths began to respond at step heights lower than the larger wavelengths did for forward-facing steps and that these heights seemed to correspond more closely to the experimentally observed data. For this reason, later analyses began to focus on the 2.25 mm wavelength. This makes physical sense as the 2.25 mm wave dominates at this particular step location.

V.2.1 Note on Wavelength Notation

Note that as is customary within the stability community, all crossflow wavelengths are denoted by the measurements taken parallel to the leading edge (in the Z direction). By doing this, one ensures that the measurement of crossflow wavelength does not vary with the local effective sweep angle, as it would if taken normal to the inviscid streamline (in the Z' Direction).

V.2.2 U and W Perturbations

For all step sizes, approaching the location of the step, the U (step-normal) and W (step-parallel) disturbance profiles retain much of the character that is present in the disturbances seen in a zero step case. See the full progression of disturbance modes in Appendix C. Here the location indications are as in Table V.1.

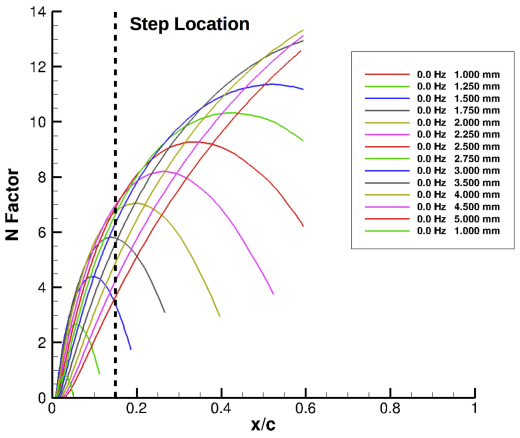

(a) N-Factors In-Flight Conditions

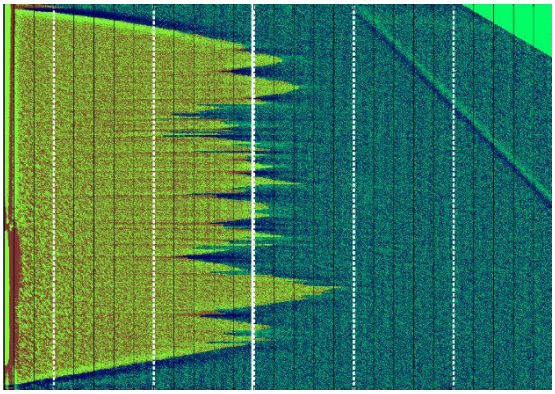

(b) Sample IR Image (subcritical) (Courtesy Glen Duncan & Brian Crawford, December 2014)

Figure V.4: In-Flight Stationary Crossflow Transition

Figure	Station	Location Relative to Step
C/D-1	1	5 mm Upstream
C/D-2	11	3.5 mm Upstream
C/D-3	21	2.0 mm Upstream
C/D-4	31	0.5 mm Upstream
C/D-5	41	1.0 mm Downstream
C/D-6	51	2.5 mm Downstream
C/D-7	61	4.0 mm Downstream
C/D-8	71	5.5 mm Downstream
C/D-9	81	7.0 mm Downstream
C/D-10	91	8.5 mm Downstream
C/D-11	101	10 mm Downstream

Table V.1: Locations of Figures in Appendices C & D

These profiles are familiar with a large single peak, approximately 400 microns from the wall, and returning to zero at the edge of the boundary layer. However, the peak of the disturbance seems to be "lifted" from the wall slightly as one approaches the location of the step. This "lifting" is not equal to the step height, but is somewhat less than what would be expected with a one-to-one correlation. The cases with a larger step, also show a second lobe form near the wall, apparently as a result of interaction with the helical flow existing before the step location.

Just after passing over the step location, again all disturbance profiles are somewhat similar to one another. There appears, however, a large secondary lobe near the wall. This second lobe appears to be due to the interaction with the helical flow present on top of the step. As evidence when examining images of the modes one can see that the second lobe is the same height from the wall as the recirculation regions. The secondary lobe is larger, and has a higher amplitude with increasing step heights. At this point there is no obvious demarcation between a 'critical' and a 'non-critical' step height as the modes appear very similar to one another with the only difference being the amplitude of the disturbance in the secondary lobe. For example see Figure C.5 in Appendix C.

Downstream the dividing line between critical and subcritical becomes apparent between 300 and 350 microns for these conditions. See Figure C.11 in Appendix C. Cases with larger step heights larger diverge from those that are smaller than the dividing line. In cases with small steps, the secondary lobe disappears and merges back into the original shape, leaving a mode shape very similar to that of the case with a zero height step. However, for cases with a larger step size, this secondary lobe continues to increase in size, and appears to "swallow" the original lobe and becomes a larger more strongly amplified peak. This new eigenfunction appears to grow more strongly than the original crossflow vortex. A series of modes can be seen

in Appendix C.

A test was run using a 350 micron tall step, but with a bubble on top artificially made smaller. This was done by running a grid containing a 350 micron tall step, but using the boundary conditions found for a 300 micron tall step. It was noted that the development of the eigenvalue amplitudes and shape followed that of the 'sub-critical' step heights, when the step height should have produced 'critical' behavior. This suggests that the change in character and growth rate of the disturbances is related more closely to the properties of the second bubble related to the step than to any physical properties of the step itself. These data support the observation that the interaction between the second recirculation helix and the incoming instability are key to this reaction. This conclusion is also supported by Holmes et al. [28] who found that 'ramping' of the step resulted in larger excrescence tolerances, presumably due to the decrease in bubble size affected by the change in geometry, once again noting that Holmes et al. did not have crossflow present.

V.2.3 V Perturbations

The V (wall normal) perturbation also tends to change character at this point. For a sub-critical step height, after passing over the excrescence the V perturbation appears as two separate vortices, rotating in opposite directions, as seen in Figure V.5a. For critical step height and above, there appears a stronger, single vortex, as seen in Figure V.5b.

V.3 Additional Instabilities

In addition to the increased growth and change of shape of the original stationary disturbance, by examining the stability of the helical flow calculated in the step-area grid, it was found that there exists a traveling mode with similar wavelengths to the stationary mode, but with a much higher local growth rate. This mode appears

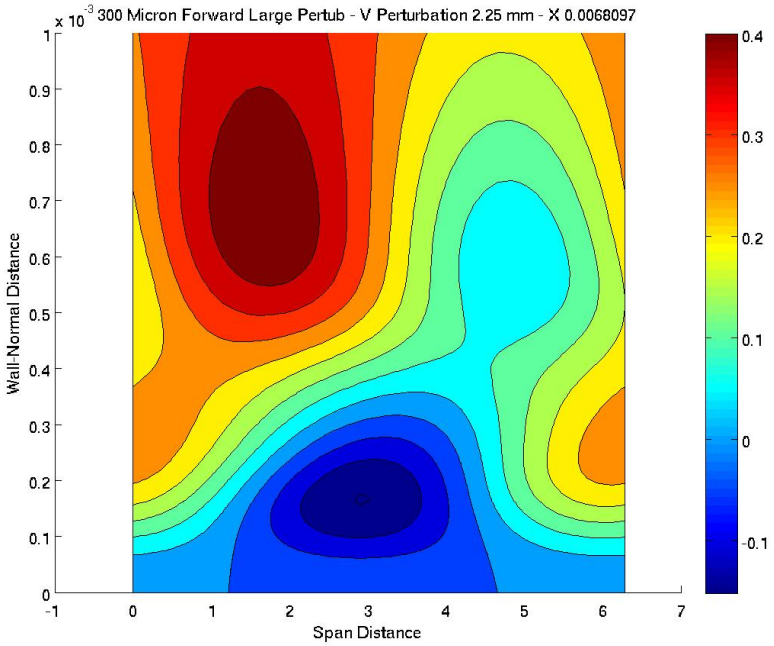

(a) Sub-Critical

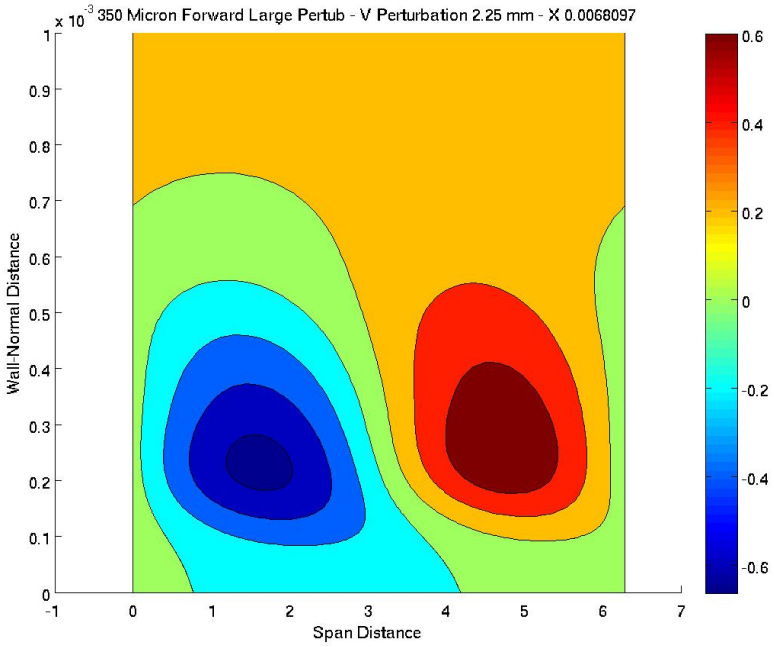

(b) Critical

Figure V.5: Y-Velocity Disturbances Critical vs Sub-Critical

only in the areas of recirculation, where the helical flow features are present, but appears for both critical and subcritical modes. This mode may be related to the sudden movement of transition forward to the step location, as the mode appears to only exist in the recirculation region, and this region dramatically increases in size around the experimentally observed critical step height. This mode is similar to the traveling mode described as part of the backward-facing steps and seen in Figure E.2. Experimental data shows that once the step height has become "critical", meaning the excrescence causes transition at a location very close to the step location, the unsteady fluctuations increase. This could be due to an effect similar to the secondary instabilities typically associated with breakdown due to stationary crossflow, or due to a newly destabilized mechanism.

V.4 Physical Interpretation and Correlation

A number of methods were investigated to find a method to correlate the experimentally observed change in transition location to flow data able to be computed without performing direct simulations of the step-area flows.

V.4.1 Crossflow Eigenmode V-Max

During the course of calculations, it was noticed that the interaction between the crossflow vortex and the helical structure found on top of the step appears to amplify the disturbance. This was supported by examining the eigenvalues for these cases, a description of which is found in Section V.2. For this reason, a physical explanation involving these two factors was sought. It is known that the bulk flow direction of the helical flow is toward the tip of the wing (Negative Z). If one looks along the positive X axis where X is into the page (where Positive Y is "up" and Positive Z is "to the right" in the field of view) from this vantage the helical flow on the top of the step will be to the left and the crossflow vortices will be rotating counter-clockwise,

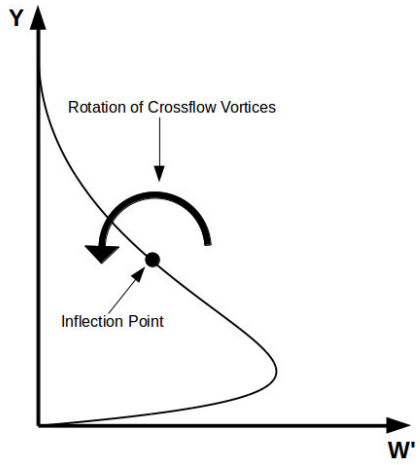

Figure V.6: Rotational Direction of Crossflow Vortices

as seen in Figure V.6.

At low step heights, any interference between the crossflow vortices and the helical flow on top of the step will be destructive, as the helical flow and the lower half of the crossflow vortex oppose one another in terms of direction, as in Figure V.7a However, once the step height is increased to be higher than the center of the crossflow vortex, it appears that interference between the helical flow and crossflow vortex are now *constructive* as the two flow features are moving in the same direction.

During calculations of the crossflow vortices, it was found however that crossflow eigenmodes are neither identical nor are the eigenmodes self-similar scaled to the wavelength of the disturbance. This is to say that the height of the center of the crossflow vortex neither remains constant as one changes wavelengths, as it would be if every crossflow vortex was directly centered on the stationary inflection point in the W' direction, nor does this height also does not simply scale with the wavelength examined, as it would be if the eigenmodes were scaled self-similar disturbances as for example Blasius velocity profiles are. For this reason, it was found that a correlation

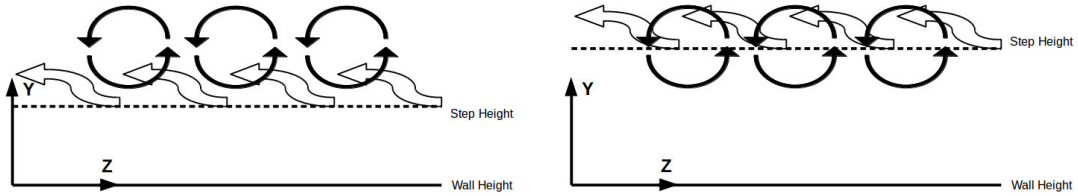

(a) Sub-Critical (b) Critical

Figure V.7: Cartoon of Sub-Critical vs Critical Steps

using the inflection point of the basic state did not provide satisfactory results.

It was then reasoned that the center of the vortex would roughly correspond to the maximum value of the V-Perturbation, since the top and bottom of the vortex must necessarily have zero Y-Velocity. For the same reasons the inflection point proved to be an ineffective method to predict the critical step height, the height of the maximum V-perturbation appears to change with the wavelength of crossflow disturbance.

By examining the shape of V-velocity perturbations, as seen in Figure V.8, the velocity profile for each wavelength is a unique shape. However, taken as a whole it becomes apparent that the collection of perturbation profiles has a common wall-normal distance where the maximum can exist. For the smaller wavelengths up to approximately that of the local most amplified wave (maximum local N-Factor), this location corresponds to a clearly defined maximum. However, for larger wavelengths, which appear to plateau, the maximum is less well defined. During experimental studies [35, 38] it was found that the step heights that trigger movement forward of the transition front correspond to the height at which the first (lower) 'elbow' in the collection of profiles occurs. For example in Duncan [35] it was found that the

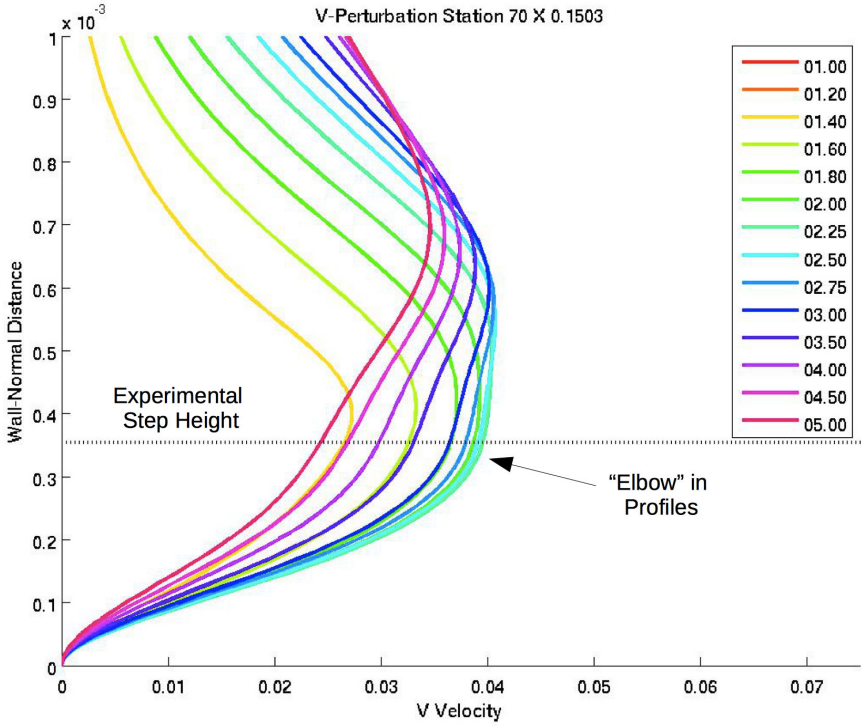

Figure V.8: Comparison of LST Y-Velocity Perturbation for Stationary Crossflow Wavelengths

critical step height for the conditions shown in Figure V.8 is a height of 354 microns. Computationally the shift in behavior occurs between step heights of 300 and 350 microns, details of which can be seen in Appendix C.

In order to capture this effect, a correlation is proposed. For each stationary-crossflow wavelength, find the distance from the wall of the maximum amplitude of the V-perturbation shape function from LST. This is done by finding the mathematical maximum of the shape profile, then finding all points within a certain tolerance of this value to account for the plateau shapes. The lowest point within this tolerance is chosen as the correlation height for that particular crossflow wavelength. Then to select the single manufacturing tolerance for the wing, the critical height for the crossflow wavelength with the highest local N-Factor at the step location is used.

It was found that the value that provided the best results for this particular geometry was to set the value at 97% of the V-maximum. There are a number of adjustments that may be made to this correlation to make the resulting value more conservative if desired. For example, the shape of the perturbation profiles is necessarily zero at the wall and also zero at infinity. By choosing a smaller percentage of the maximum velocity (e.g. 90% of V-maximum), the critical step height returned by the correlation will become more conservative (smaller). A second alternative is to choose the wavelength that gives the smallest tolerance as opposed to the wavelength with the largest local N-Factor. A summary of this correlation applied to the SWIFTER/SWIFTEST geometry can be found in Tables V.2 and V.3.

For excrescences located at 1% x/c for KSWT test conditions, the first neutral point of all stationary crossflow wavelengths are downstream of 1% chord when calculated using LASTRAC with settings found in Appendix A. Because the correlation is based upon amplification of stationary crossflow wavelengths, it was not applicable to chordwise stations forward of the first crossflow neutral points.

Re' /m (x 10^6)	Duncan Experimental Fit (microns)	Tufts-Reed Criterion Minimum Height (microns)	Tufts-Reed Criterion Highest N-Factor Height (microns)
1.00 (Tunnel)	1526	1111	1393
1.45 (Tunnel)	1110	1013	1068
4.80 (6.50° AoA)	398	361	392
5.00 (6.50° AoA)	384	354	391
5.50 (6.50° AoA)	354	331	339
5.50 (7.50° AoA)	354	349	349

Table V.2: SWIFTER Critical Step Height Correlation 15% x/c (Using 97% VMax Limit)

Re' /m (x 10^6)	Crawford Smallest Step w/ Degraded Laminar Run (microns)	Tufts-Reed Criterion Minimum Height (microns)	Tufts-Reed Criterion Highest N-Factor Height (microns)
1.45 (Tunnel)	1323	N/A	N/A
4.80 (6.50° AoA)	192	151	184
5.00 (6.50° AoA)	192	148	172
5.50 (6.50° AoA)	192	146	168
5.50 (7.50° AoA)	192	163	192

Table V.3: SWIFTEST Critical Step Height Correlation 1% x/c (Using 97% VMax Limit)

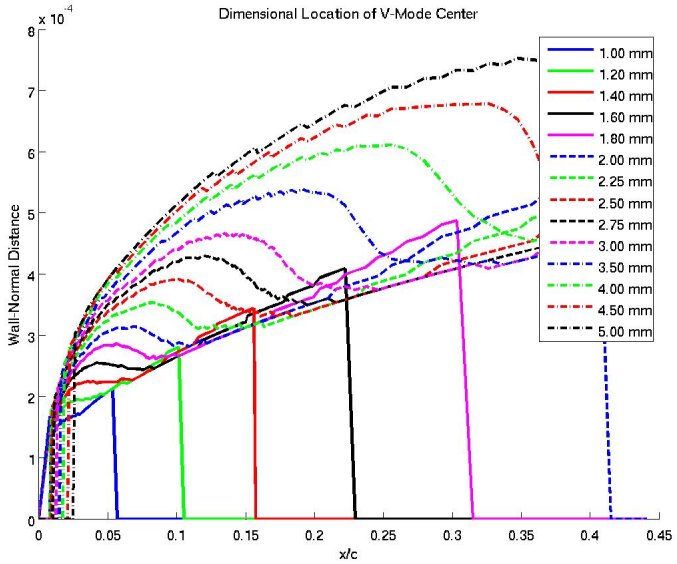

Figure V.9: Critical Step Heights 6.5° AoA 5.5M/m Re'

This correlation is particularly appealing because inherent in calculating stability behavior, one has necessarily taken into account the upstream development of the boundary layer including all Reynolds number, sweep, and pressure gradient effects. In other words, because one is calculating the stability of eigenmodes in the boundary layer as it exists on the airfoil, there is no need for corrective factors. The cost for performing this analysis when designing a laminar-flow airfoil is relatively low, as it seems imperative that one would at a minimum perform linear stability analyses as part of the design process anyway. In addition, the correlation can easily be modified to become more or less conservative as the situation warrants by choosing different percentages of this maximum, e.g. choosing 50% of the Vmax height would result in a significantly more conservative value than the 97% value presented here.

V.4.2 Notes on Non-Dimensionalization

That the disturbance profiles all seem to have related features (e.g. the "elbow" in the profiles at 350 Microns in Figure V.8) seems to suggest that they are driven by the same feature of the baseflow, (e.g. an inflection point in the crossflow velocity profile). Some attempts were made to non-dimensionalize this correlation with a characteristic length scale. A seemingly obvious choice is the Blasius Length Scale

$$\eta = \sqrt{\frac{\nu_e x}{U_e}} \tag{V.1}$$

While individual plots at a given unit Reynolds number appear to collapse somewhat to a constant value of Blasius length scale once the crossflow is sufficiently developed (see Figure V.10), when comparing plots from different flow conditions the collapse is not always as clean, nor is it to the same value. For comparison the plot in Figure V.11a does not seem to collapse. In addition the Blasius non-dimensionalization only seems to collapse once sufficiently downstream. Near the leading edge is an area where the effective sweep angle and boundary-layer edge values change rapidly. This corresponds to the area where the Blasius collapse is least effective, suggesting a length scale that accounts for differences in sweep and pressure gradient, perhaps based on Falkner-Skan-Cooke type boundary layers.

V.5 Effect of Incoming Disturbances on Transition Movement

The correlation is designed to predict the step height at which the presence of a step will begin to affect the location of transition to turbulence, specifically the start of a sudden and strong amplification. One can expect that this may happen in one of two different ways, depending on the amplitude of the disturbance coming into 'contact' with the step excrescence.

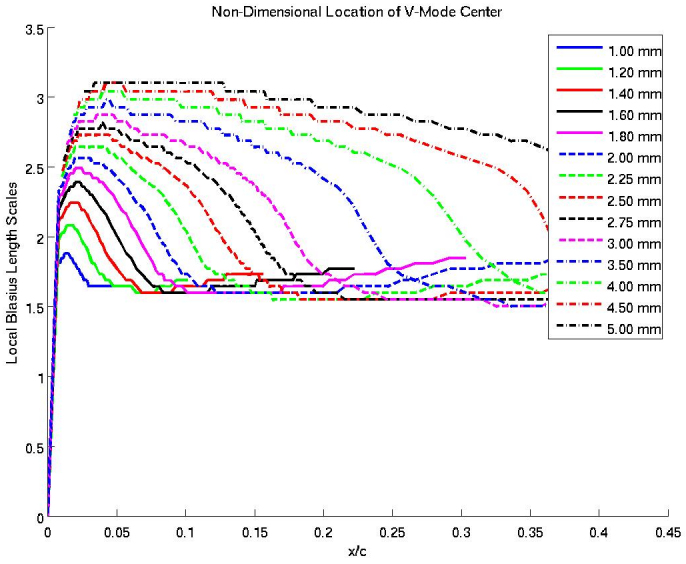

Figure V.10: Non-Dimensional Critical Step Heights 6.5° AoA 5.5M/m Re'

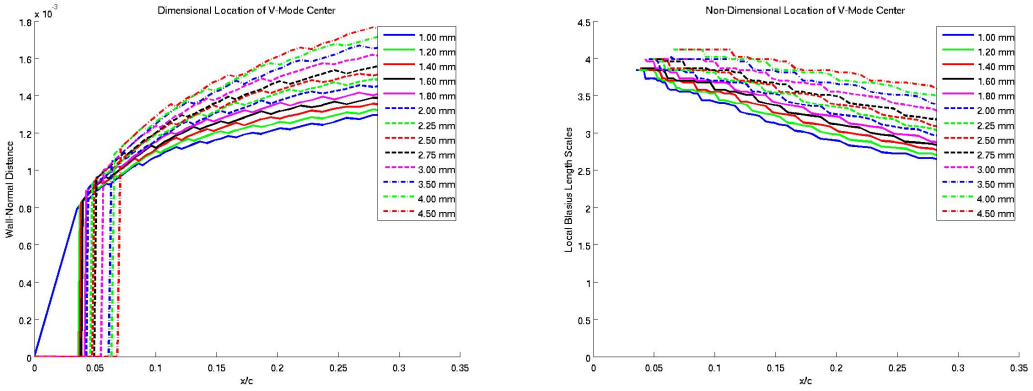

(a) Dimensional (b) Non-Dimensional

Figure V.11: Critical Step Heights KSWT Geometry 1.45M/m Re'

V.5.1 High Amplitude Crossflow

For high amplitudes, as could be expected for the in-flight model, a sudden amplification of the instability could result in quick breakdown to turbulence. Even though the disturbances reach a large amplitude, it is known that breakdown from stationary crossflow waves occurs via secondary instability mechanisms. If the incoming disturbance is already approaching levels conducive to secondary instabilities, and is hit with a sudden and drastic amplification breakdown to turbulence may quickly follow.

V.5.2 Low Amplitude Crossflow

If the incoming crossflow disturbances are of a low amplitude, even a sudden and strong amplification of the instabilities may not result in sudden breakdown to turbulence. As described above, if the amplitudes of the disturbances are small and not large enough to approach the onset of secondary instabilities, the amplification seen from interaction with a critical step will not necessarily result in transition to turbulence right away. This phenomena would appear as a movement forward of the transition location. It is believed that the phenomena seen with the 1% cases are a case of a small amplitude perturbation being amplified by the forward-facing step.

V.5.3 Choice of Wavelength

As was previously mentioned, the behavior of the disturbances when interacting with a forward-facing step depended strongly on the wavelength of the disturbance. It was found that steps which produced the distinct change of eigenmode for 2.25 mm as seen in Appendix C did not produce the same effect for the eigenmodes of a 4.50 mm wave until a larger step height. This is in keeping with the findings and reasoning of the correlation proposed, which shows that the vortex core of a 4.50 mm

wave tends to exist at a larger wall-normal distance than the 2.25 mm wave does. It follows from this that the reaction to the step is highly dependent on which crossflow modes are present in the flow.

VI. BACKWARD-FACING RESULTS

VI.1 Basic Flow Topology

In the region of a backward-facing step on a swept wing, for all step sizes the most prominent flow feature is a region of recirculation downstream of the step location. See Figure VI.1 The size of the recirculation region is driven by the size of the step excrescence, making the region as tall as the step height. See the streamline pattern in Figure VI.2. Similar to a forward facing step, note that the recirculation region is no longer a closed flow, but rather open, owing to the combination of sweep and pressure gradient which causes spanwise flow. Like the helical flow associated with the forward-facing steps, the bulk motion of this helix is also against the 'normal' crossflow direction, that is, the helix flows root to tip while the crossflow velocity profile is tip to root. Similarly, this is due to the local reversal of the normally favorable pressure gradient to an adverse one in the region of the step excrescence. The length of the recirculation region extends approximately 12 step heights downstream for small steps, and up to approximately 15 step heights as the size increases. The recirculation helix is somewhat larger than either recirculation region found in the

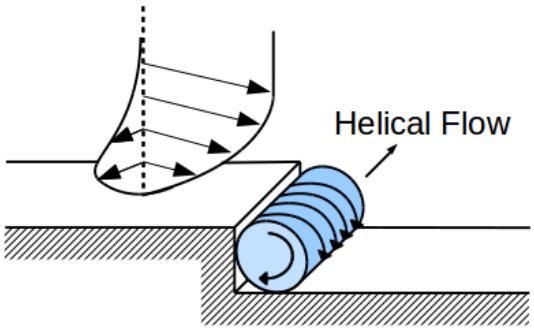

Figure VI.1: Cartoon of Backward-Facing Swept Steps

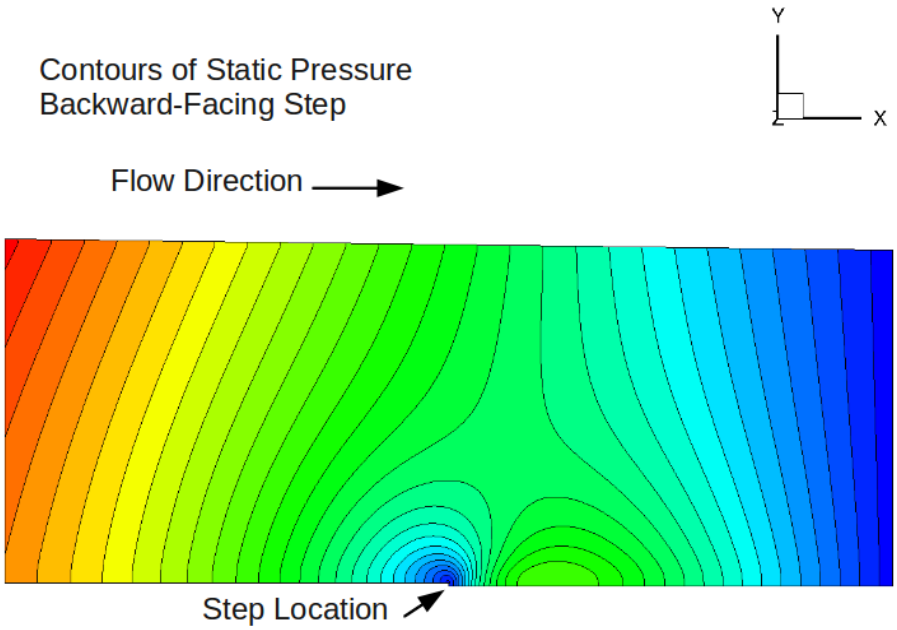

Figure VI.2: Pressure Contours for Backward-Facing Step

forward-facing cases, however because of its position aft of "under" the step, the interaction of the flow with this recirculation region appears somewhat less than for forward-facing steps.

If one examines the pressure field related to a backward-facing step, approaching the step there exists a small region of increased favorable pressure gradient. Immediately following the step location, there is then a region of adverse pressure gradient, eventually recovering to the edge conditions present if there is no step present. This can be seen in Figure VI.2.

It is also interesting to note that for a backward facing step, if one measures the velocity profile at a given location downstream of the step (e.g. 1.5 mm downstream of excrescence) the velocity profiles above the step location are largely the same. There is some movement downward of the velocity profile with increasing step heights, but it is well less than the amount the step is increased e.g. a 50 micron

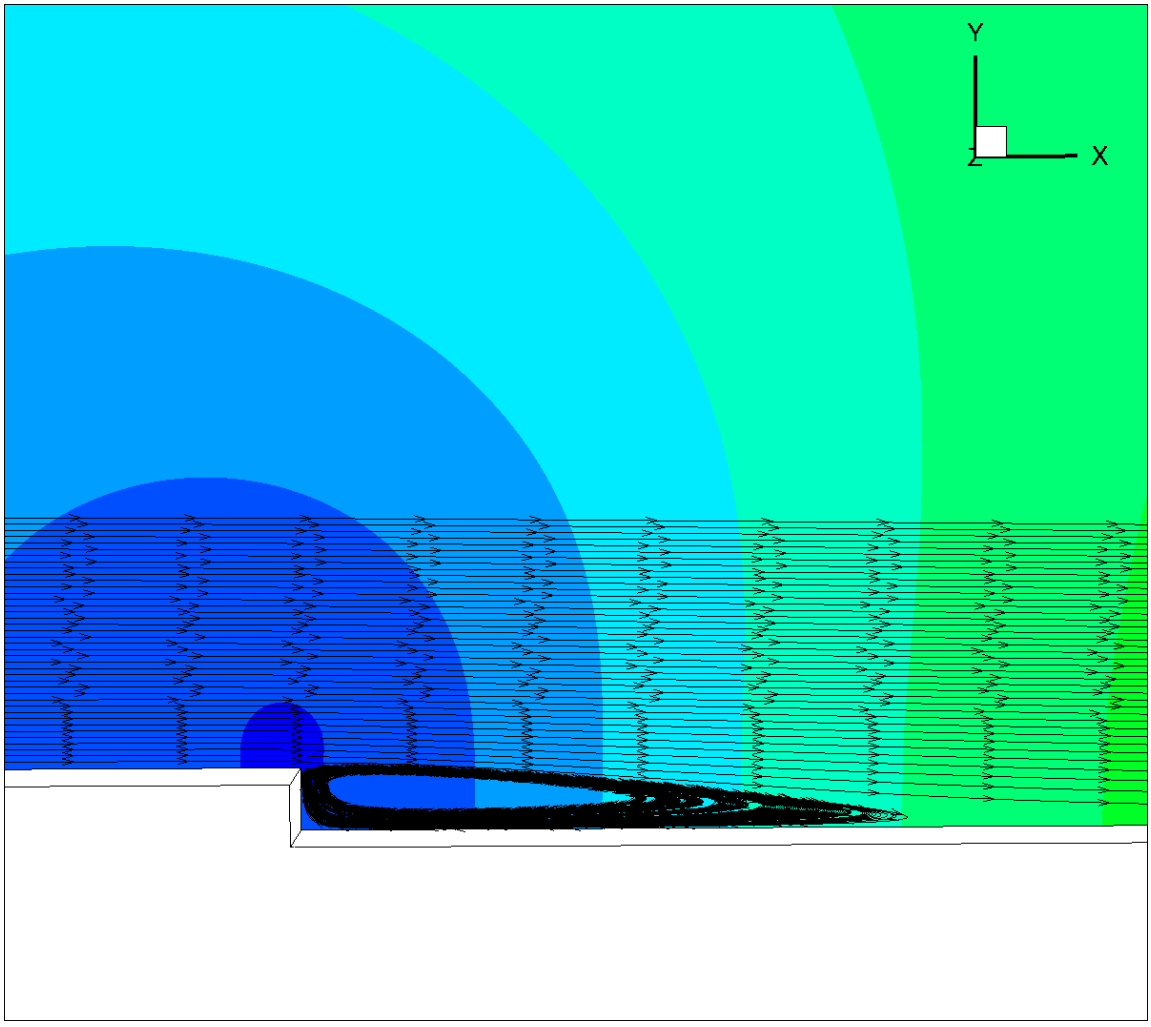

Figure VI.3: Streamlines for Backward-Facing Step

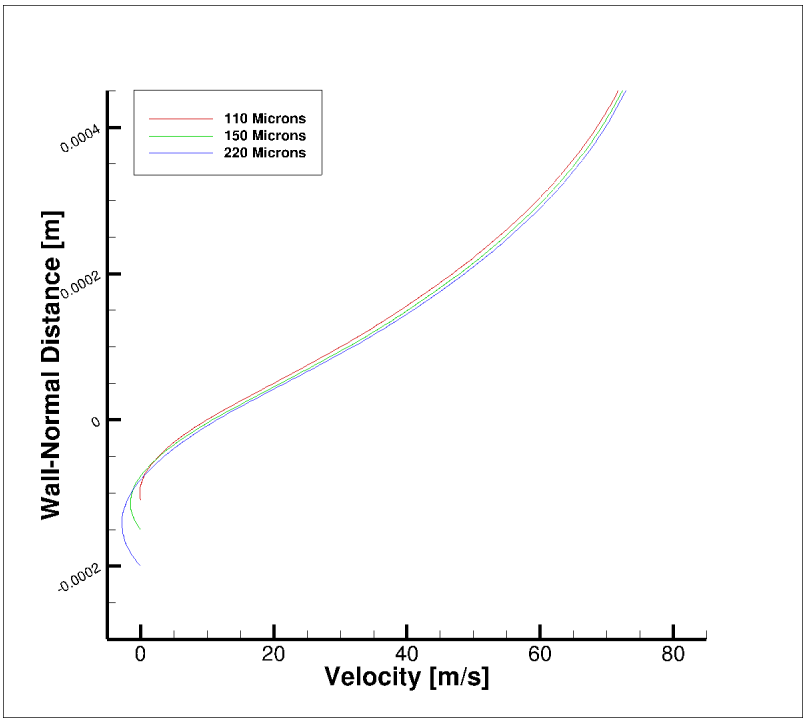

Figure VI.4: Velocity Profiles 1.5 mm Downstream of Step, Various Heights

step increase may translate the velocity profile downward by 5 microns. An example of this can be seen in Figure VI.4.

VI.2 Absolute Instabilities

Due to the nature of the experimental results given by the SWIFTER experiment, [35, 34] as well as the results reported in Perraud et al. [24] both of which showed backward-facing steps exhibiting a "binary" type of response, having either little effect on the transition location or causing transition to progress forward to the location of the step, early effort into investigating this problem put effort into examining the existence or non-existence of absolute instabilities. An absolute instability appeared to be an ideal candidate for explanation of the behavior seen with these excrescences, as an absolute instability if observed experimentally would behave as

described in the literature, being either no effect if subcritical then rapidly causing transition once critical.

Effort was put into writing a stability analysis code using linear "biglobal" formulations. By assuming a basic state that is dependent on two dimensions (as opposed to one dimension as in Linear Stability Theory, or one strongly and one weakly as in the Parabolized Stability Equations) biglobal analysis allows examination of a basic state that is varying rapidly in the streamwise direction for instabilities that extend over a large region of this variation, i.e. are not local. For an example of this in practice see Rodriguez and Theofilis. [46] The code written in house was formulated using hard coded fifth-order finite differencing methods, and a multi-domain setup formulated specifically for a step flow. Substituting an disturbance of the form $q'(x, y, z, t) = q(y, z)e^{i(\alpha x - \omega t)} + \text{C.C.}$ into the Navier-Stokes equations separated into a form containing a non-varying basic state and a small disturbance allows one to solve the resulting equations as an eigenvalue problem similar to linear stability theory. The obvious difference is now that the the eigenmode shape is a two dimensional one, as opposed to a simple velocity profile.

The in-house code was unable to determine the existence of an unstable absolute instability for step heights even well above the experimentally determined critical step height. Because the code was unverified, and the problem at hand was a new geometry for which there is little to no computational data available a second code was used to investigate this problem. The Mafalda biglobal stability code, used with permission of Pedro Paredes also did not find the existence of a temporally growing absolute instability for step heights of 250 microns for in-flight conditions at 5.5 M/m unit Reynolds number for excrescences at 15% x/c. For reference, the experimentally determined critical step height for these flow conditions and excrescence location is approximately 138 microns.

VI.3 DNS Disturbance Growth

VI.3.1 Stationary Crossflow

When examining the perturbation profiles as calculated for the backward-facing steps, there exists a change in the behavior of the perturbations. Despite this difference, which is largely manifested in the mode shape, the change in amplification rates is not as dramatic or as straight forward as the case for forward-facing steps. These eigenmodes can be seen in Appendix D.

As step height is increased, the disturbance profile will become increasingly bifurcated, as seen in the forward-facing steps. However for many cases this bifurcated profile has a smaller amplification rate than the case for k = 0 (no step). In addition, unlike the case for forward facing steps, this change in character happens gradually as step height is increased instead of suddenly at a certain step height. Note that in the Figures of Appendix D, the highest step shown (220 microns) is well above the experimentally observed critical height (138 microns) for an in-flight condition at 15 % x/c. When examined in context of the known experimental data for swept open-flow backward-facing steps [35, 38, 47] this suggests that the breakdown due to backward-facing steps is not solely due to amplification of incoming steady crossflow vortices.

VI.3.2 Traveling Crossflow-Like Modes

Using the BiGlobal formulation Mafalda as used in Paredes et al. [48] and Paredes et al. [49] local traveling instabilities were examined within the recirculation region of the backward-facing steps for step heights larger than the experimentally determined critical height. The velocity profiles used were in the Y-Z plane using the coordinate system seen in Figure IV.1.

If one uses the biglobal formulation in this plane and inputs a spanwise invariant

	Mafalda 2.25 mm	LASTRAC 2.25 mm	Mafalda 4.50 mm	LASTRAC 4.50 mm
α_R	0.2839	0.2850	0.1411	0.1415
α_I	$-3.693 \cdot 10^{-3}$	$-3.678 \cdot 10^{-3}$	$-5.191 \cdot 10^{-3}$	$-5.205 \cdot 10^{-3}$

Table VI.1: Complex Alpha, Stationary Crossflow, In-Flight Conditions, 15% x/c

basic state, the result is equivalent to doing linear stability theory as is commonly understood. In order to verify that the code produced equivalent results, a velocity profile was extruded into a spanwise invariant basic state. This was then compared to the output from LASTRAC running the same velocity profile. The comparison for a stationary crossflow wave is shown in Table VI.1. Given the favorable comparison between them, Mafalda was used to examine local stability with the knowledge that this could be extended to a distorted base flow for future studies.

For in-flight conditions using the SWIFTER excrescence location (15% x/c), instabilities were found in the range from approximately 500 Hz - 1500 Hz with the most unstable being around 1000 Hz. These modes appear to exist for a range of wavelengths as well, including the unstable range of stationary crossflow wavelengths. The examination of these modes focused on the range of wavelengths surrounding the most unstable crossflow wavelength, as the probability of interaction with the stationary modes seemed the highest. This range and peak amplification however, depended strongly on the size and strength of the recirculation region at the location used for the stability analyses. Both the frequency of the most unstable wave and amplification rate of the instabilities found using this method were highest near the step, decreasing as the location moved downstream. An example can be seen in Figure VI.5 for KSWT conditions for a 1400 micron tall backward-facing step. Here "Alpha I" is the growth rate with more negative being more unstable. Out-

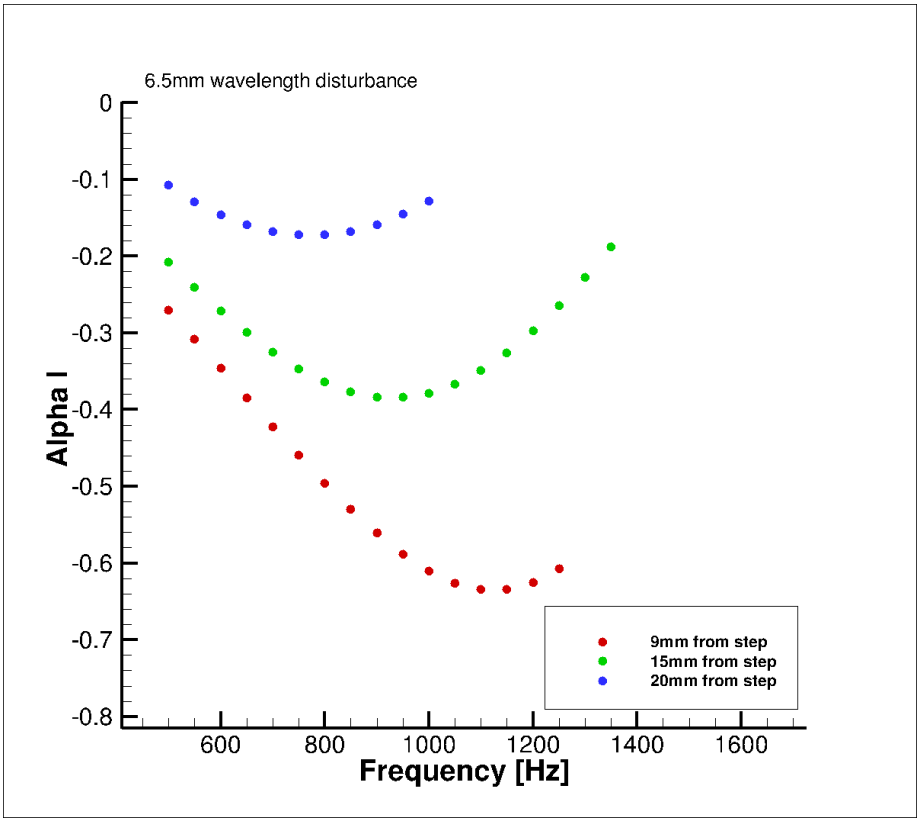

Figure VI.5: Mode Growth Rates for Various Downstream Locations

side of the recirculation helix, this disturbance mode was not able to be found using the BiGlobal formulation. Experimentally, an increased level of disturbances was observed in the 400-900 Hz range for similar steps as seen in Figure VI.7.

As can be seen in Figure E.2, the U-perturbation quantities in particular are divided into two lobes. The character of the disturbance changes as the frequency increases, for lower frequencies the disturbance was strongest above the recirculation region. It should be noted that the lower lobe is inside the recirculation region, while the upper lobe is outside it, extending upward to the location of the incoming stationary crossflow vortex. However, as frequency continues to increase, the bottom lobe which is located inside the recirculation region becomes comparatively stronger

and eventually dominates the disturbance profile.

This instability exists for both subcritical steps, albeit at a lower amplification rate, and for cases where the step height is above the experimentally determined critical value. Unlike the forward-facing steps which seem to have a binary behavior in the amplification of stationary waves, from these data, it seems likely that this instability is present even for subcritical steps.

This mode was calculated for both the undistorted basic state and for a basic state that had been distorted using a stationary crossflow mode. It was found that the distorted basic state did not significantly increase or decrease the calculated growth rate for a given mode. The mode shapes also appeared to have a very similar character between the two basic states. This was unexpected, and this examination was in fact a driving force behind using the biglobal formulation for this study, instead of simply using local stability theory.

These modes were also able to be found for conditions as in the KSWT facility. Again, the frequency of these modes was found to be in the 1000 Hz range, with a growth rate much larger than the related stationary crossflow disturbance. The character of the modes found for KSWT conditions is slightly different than those found for the in-flight modes. The KSWT modes have less of a presence in the recirculation region than do the in-flight modes, and seem to be more focused on the region above the bubble. This can be seen in Figure VI.6. Note that these, despite being found in a flow with a large recirculation region appear similar to the modes in-flight found for small recirculation regions, such as Figure E.1.

Comparing the mode in Figure VI.6 to the PSDs taken in the KSWT as in Figure VI.7, one can see that the frequency range and approximate location of the disturbances matches well with the region of increased disturbance seen in the upper boundary layer from 400Hz - 1000Hz.

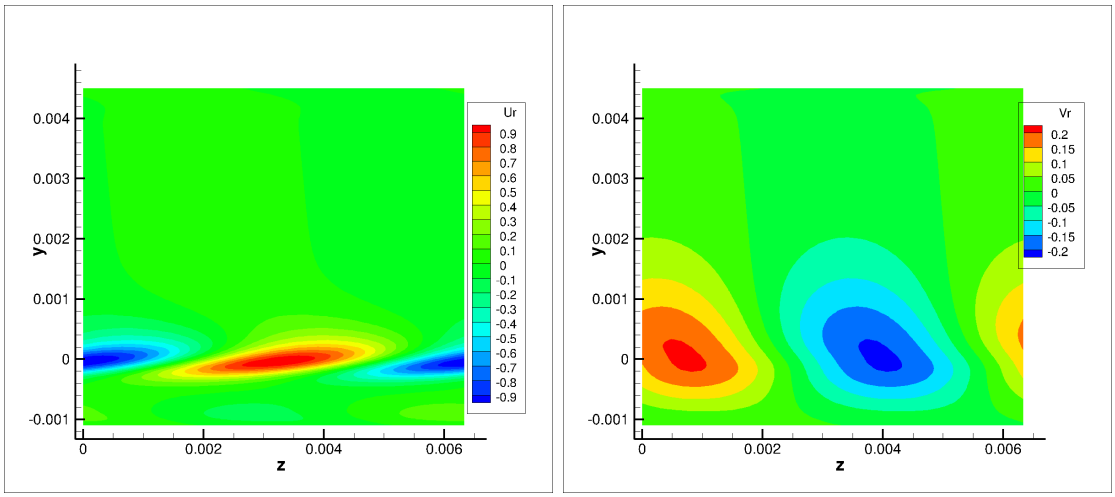

(a) U Perturbation

(b) V Perturbation

(c) W Perturbation

Figure VI.6: BiGlobal Traveling Mode - KSWT - 1100 Micron Backward-Facing - 9 mm Downstream - 950Hz - 6.50 mm Wavelength

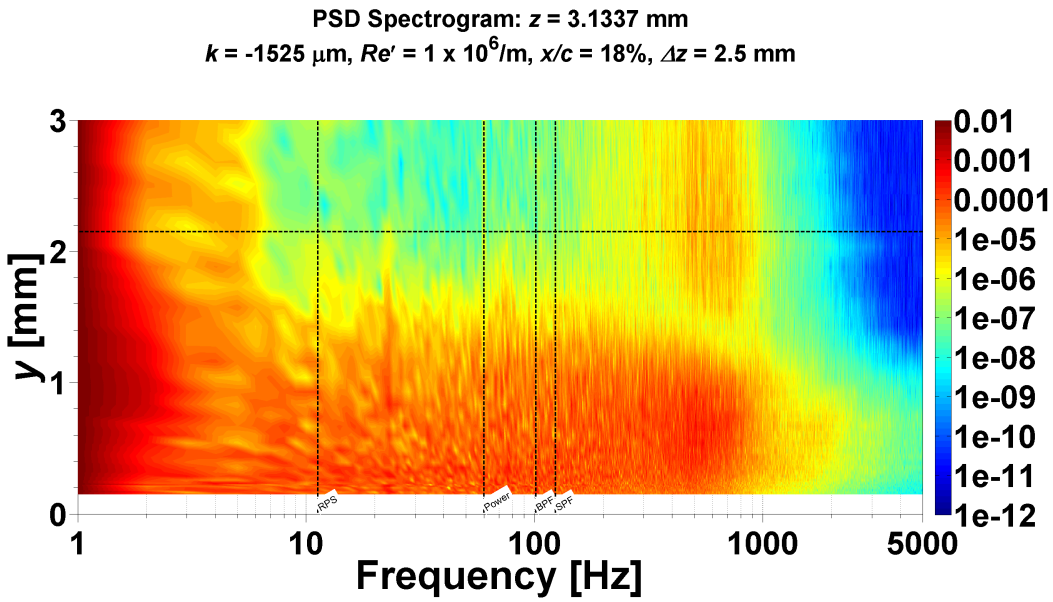

Figure VI.7: Power Spectral Density - Unsteady Disturbances KSWT Facility (Courtesy Glen Duncan & Brian Crawford, December 2014)

VI.4 Time Dependence of Solutions

It was found that at certain step heights, the backward-facing step solutions would not converge to a steady state solution, but rather appeared to take on a time-dependent character. It has to be noted that the solutions being discussed were calculated assuming a time-independence, i.e. that the solutions would converge to a steady state. The result is that the solutions are not temporally resolved, i.e. a single solution can not be seen as a 'snapshot' of any given time as each cell advances according to the set Courant number and not according to a fixed time step. With these cautions in mind, it seems that when solving grids using the same methods as was done here, some information may be gleaned from examining at what step heights solutions become time-dependent.

VI.4.1 In-Flight Conditions

For the model as installed on the O-2A aircraft, two sets of solutions were found as discussed in Chapter IV, a spanwise invariant solution, and a fully three-dimensional solution. The step height at which the solutions became time dependent were different for the two solution methods as the spanwise invariant solutions remained time-independent for larger step heights. For spanwise invariant calculations, time independent solutions were able to be calculated even up to a step height of 300 microns, well beyond the experimentally observed critical step height. However, when the solutions were calculated resolving all three dimensions, the solutions became time-dependent with a step height as low as 250 microns, but remained time-independent with a step height of 220 microns. For reference, the experimentally determined critical step height is 138 microns for these conditions. By looking at the rotational velocities, it can be seen that there are largely two-dimensional vortices shedding of the convex corner of the aft-facing step.

The three-dimensional solutions were tried for both an undisturbed inflow condition and also for inflow conditions containing a stationary crossflow vortex. Changing this parameter did not change the time-dependencies of any solution tested, nor did increasing the strength of the incoming crossflow vortex i.e. those that were time-dependent without crossflow remain time-dependent with crossflow and the same pattern was true for time-independence. Examining the stationary crossflow vortex magnitudes also showed that this time independence did not appear to affect the development of stationary modes significantly, meaning that the shedding of the vortices did not significantly enhance or degrade the amplitude of these vortices.

Local stability was calculated using LASTRAC on velocity profiles in the recirculation regions of these flowfields. A traveling 2-D wave similar to a T-S wave was

found to be unstable only in the recirculation region, meaning the instability was not present outside the recirculation helix. This wave was found to have very high growth rates, on the order of 10 times larger than the stationary crossflow waves at this same location. These waves, similar to the crossflow like modes, however were found using local stability theory which as previously discussed may not maintain good assumptions for the flowfield being analyzed.

VI.4.2 KSWT Conditions

For the model as installed in the KSWT facility, the solutions were calculated using only spanwise invariant solutions. As the boundary-layer length scales were increased due to the lower unit Reynolds number compared to flight, and the relevant step heights also increased as found in the experimental work, it was necessary to create spatially larger grid sizes for the KSWT computations as compared to those used for in-flight conditions. These solutions were gridded using a uniform 10 micron spacing in the wall-normal and streamwise directions, placing on the order of 100 cells in the wall-normal recirculation region. The inlet was increased from 12 to 24 mm long, and the outlet was increased from 18 mm to 36 mm long, but maintained the same topology as the previous 2-D grids.

For the KSWT computations it was found that the solutions became time-dependent at a value much closer to the experimentally determined critical value. When calculating the KSWT flowfield, the solutions were found to be time-independent at a 1400 micron tall step size, but time-dependent at 1525 microns tall. For reference, the experimentally determined critical step height for these conditions is listed at 1262 microns. However, it should be noted that the demarcation between a critical step and a subcritical step was less clear in the KSWT set of experiments than for the in-flight conditions. For the KSWT experimental cases, the critical step height

was defined as the highest step height for which there were no signs of intermittent turbulent wedges. However, the experimental notes show that the case with a 1400 micron tall backward facing step showed mixed intermittent turbulence and laminar flow, while the 1525 micron tall backward facing step shows fully turbulent flow.

VI.5 Physical Interperatations of Observed Breakdown

If breakdown of the shear-layer as described in Section VI.4 is able to cause transition to turbulence "on it's own" so to speak and does so via two-dimensional T-S like waves this could help explain the observed behavior. Based on experimental observations, it is thought that T-S waves and the stationary crossflow vortex do not interact strongly to enhance one another. For this reason, if the breakdown to turbulence is dominated by the growth of and eventual secondary instabilities related to a stationary crossflow wave this shear layer breakdown would presumably do little to enhance or inhibit the growth of the existing crossflow instabilities. This assumption is in keeping with the observed behavior of the stationary modal disturbances in Section VI.4. Therefore, if this shear layer breakdown causes transition to turbulence directly, it would appear as a 'critical' step, creating turbulent flow very close to the step location. However, if the shear layer does not cause transition there would be little effect on the pre-existing stationary crossflow waves. This situation would appear experimentally as a subcritical step, having no effect on the crossflow vortices themselves. This same reasoning applies to the T-S like instability related to the recirculation region.

This explanation is somewhat problematic in that the transition front retains the sawtooth and spatially fixed character seen in transition dominated by the stationary crossflow instability. This can clearly be seen in Figure II.10. In addition, tests within the KSWT were able to show that acoustic disturbances at a high level (110 dB) did

not affect the character of transition on the model, suggesting that two dimensional disturbances were not a large factor for both forward- nor for backward-facing steps. [38]

It is hypothesized that the cause of breakdown is the traveling crossflow-like waves like the ones seen in Figure E.2. Because this instability has a wavelength and character similar to the incoming stationary crossflow vortices, it is possible that this instability can interact with the stationary wave, and trigger secondary instabilities. As is noted in White, [50] "superposition of the stationary and traveling [crossflow] waves can produce sufficient distortion to destabilize the secondary instability." Further discussion of the potential of traveling waves to incite secondary instabilities when combined with a stationary wave can be found in Wassermann and Kloker [51], Lerche and Bippes [52] and Lerche. [53]

When examining the eigenmode of the disturbances as seen in Figure E.2, the lower lobe is located inside the recirculation region, but the upper lobe is located up in the boundary layer. Note that for these figures, $Y = 0$ denotes the location where the wall is located upstream of the step location. This top lobe could nonlinearly interact with the standing stationary crossflow wave and through this interaction push the flow into turbulence. If a nonlinear interaction between modes is the cause of breakdown to turbulence, it could explain why the transition front maintains a pattern related to stationary crossflow while simultaneously incrementally increasing unsteady disturbance levels with increased step height as seen in the hotwire anemometry campaign. In addition a nonlinear interaction between stationary and this traveling mode is consistent with the experimental observations of Duncan et al., [34] Crawford et al., [37] and Eppink et al. [30] This also is consistent with the findings of these computations as well as Balakumar [29] which both showed that the backward-facing step tended to somewhat attenuate the amplitude of sta-

tionary waves. Experimental and computational results suggest that there must be some interaction between steady and unsteady disturbances, making this explanation particularly attractive. Again, since this disturbance can be found only along the recirculation region, it seems that if this interaction causes transition the effect would be transition near the step location, and if the stationary crossflow vortices are able to pass through the region without transitioning to turbulence, the instability related to the bubble ceases to exist, and there is little or no effect.

VII. CONCLUSIONS

An encouraging result from both the current set of computational and experimental results and from literature review is that the manufacturing tolerance related to forward-facing steps is in all cases except those at very small Reynolds number (< 1.0 10^6 /m) less restrictive than the tolerance related to backward-facing steps when put into terms of practical use, i.e. maximum allowable dimensional step size. For implementation 'today', the best practice is to ensure step excrescences manufactured into swept laminar-flow surfaces are manufactured to be forward-facing.

A correlation has been proposed for determining the manufacturing tolerance for forward-facing steps under conditions where transition is dominated by stationary crossflow, which is the case for many swept wing laminar flow designs. One calculates the LST eigenmodes for stationary crossflow, and examines the Y-Velocity perturbation profile. Find the maximum of the Y-Velocity perturbation, then find the lower of the two points where the profile crosses some tolerance of the maximum (e.g. 97% of the maximum). The wall normal distance found this way is the forward-facing step height tolerance for a given wavelength of crossflow. For a conservative value, use all crossflow wavelengths with a first neutral point forward of the excrescence, and for a more aggressive value use the wavelength with highest local N-Factor to that point. This correlation may be made more conservative by changing the parameter used to select the tolerance defining the maximum of V-Perturbation. While the correlation appears to work well for the two Reynolds number ranges examined at 15% chord, and the Reynolds number range which produces stationary crossflow at 1% chord, further experiments using different geometries need to be tried to validate this correlation.

Indications both in literature and from our computational results indicate that decreasing the size of the "upper" recirculation region may diminish the impact of a forward-facing step. An intuitive way to accomplish this would be to either ramp or round the forward-facing step face. This needs to be confirmed with a more extensive study on steps, but there are currently no indications that this practice would be detrimental to performance. For immediate implementation, the best practice would be to ensure when possible that forward-facing steps include a rounded or ramped face.

The effects seen by backward-facing steps were unable to be captured using solely examination of the stationary perturbation development. While a difference in the shape of the modal disturbance was observed as step height increased, the amplitude of the disturbances was not drastically affected by these step heights. This result appears to be in keeping with experimentally observed data, which showed that the backward-facing step produced a significantly higher increase in unsteady disturbances than steady disturbances.

The observed transitional behavior of a backward-facing step in a crossflow dominated environment is consistent with the expected behavior of a non-linear interaction between stationary crossflow modes, and a computationally observed traveling mode present within the recirculation bubble. Complete investigation of this mode will require either time-resolved DNS studies or possibly a non-linear BiGlobal stability formulation.

VIII. FUTURE WORK

VIII.1 Validation of Forward-Facing Correlation

The correlation for determining the critical step height for forward-facing steps for cases where transition is dominated by the stationary crossflow instability appears to work for the experimental cases presented. However, there do not appear to be any other well controlled experiments on a geometry dominated by the stationary crossflow instability with step excrescences. In order to prove this rule, and potentially correct it, further geometries need to be explored.

VIII.2 Development of a Canonical Excrescence Case

Given the relative recentness of the interest in the interaction between stationary crossflow and surface excrescences, a so-called canonical problem has not yet been developed for study of excrescences. In some sense, the minimal working example for truly studying excrescences is not known. The results from Saric, West, Tufts, & Reed [15] suggest that while modeling simplified cases for stability problems can result in insight and useful work, in order to examine all the potentially relevant flow physics one may need to model actual flight geometries at actual flight Reynolds numbers.

However, in order to examine a robust correlation, one should examine the entirety of the parameter space. This can not be easily done with varying a full flight geometry, as was experienced with the current experiments in the case of backward-facing steps. The SWIFTER (15% x/c) campaign exhibited a binary response to step height (steps either produced no effect or a very large effect with no intermediate steps) which was unexpected for backward-facing steps. However, when the SWIFTEST (1% x/c) experiments resulted in a gradual movement forward of the

transition front, the question of what was the cause of this change was not easily answered. Many differences existed between the conditions of SWIFTER excrescences and SWIFTEST excrescences including a different pressure gradient, different levels of stationary crossflow development, the angle of the step excrescence, effective sweep angle, among others. Furthermore, it is intractable to completely separate these effects on a practical flight geometry due to structural constraints etc. In order to separate these effects, it seems necessary to set out a canonical case which allows for the variation of these parameters, and thorough examination of the effects of each.

A list of parameters to be potentially included in a thorough computational study includes:

1. Height of step
2. Unit Reynolds number
3. Distance from leading edge
4. Edge pressure gradient
5. Local sweep angle
6. Angle of contact between step excrescence and surface
7. Shape of excrescence
8. Surface curvature
9. Level/type of incoming modal disturbances
10. Level/type of freestream disturbances

A seemingly obvious starting point is a flat surface with a square step with an incoming Falkner-Skan-Cooke boundary layer profile and a nominal stationary crossflow vortex.

VIII.3 Time-Resolved Calculations

A further step in investigating the backward-facing steps would be to introduce time-resolved calculations along with time-varying boundary conditions. Because the mode investigated is a traveling mode, time-resolved DNS computational studies would be required to investigate this mode if using a manner similar to the study of forward-facing steps. However, the receptivity of this instability is not at all known, and because the mode exists only within the recirculation region, and does not appear to be convected "into" the domain, the manner in which this mode may be seeded is not clear.

VIII.4 Aspect Ratio of Crossflow Vortices

During the course of this study it was observed that the crossflow perturbations were neither self-similar nor the same height. A rule of thumb in the boundary-layer stability community is that the most unstable stationary crossflow wave is four times the local boundary layer height. While examining eigenfunctions calculated during the course of this research, there appeared to be a minimum wall-normal distance where the vortex cores are for unstable modes. As an example, see Figure V.8. There is also an obvious maximum where this vortex core can be located, due to the boundary layer edge. It is also known that the stationary crossflow vortex must rotate around the inflection point in the crossflow velocity profile. It may be therefore that there is a preferred 'aspect ratio' for the crossflow vortex, corresponding to the locally most unstable wavelength. Exploration of this idea may lead to increased understanding of the physics of the stationary crossflow vortex.

REFERENCES

[1] International Air Transport Association, "Economic Performance of the Airline Industry," Tech. rep., December 2014, http://www.iata.org/whatwedo/Documents/economics/IATA-Economic-Performance-of-the-Industry-mid-year-2014-report.pdf, Accessed May 2015.

[2] Arcara Jr., P. C., Bartlett, D., and McCullers, L. A., "Analysis for the Application of Hybrid Laminar Flow Control to a Long-Range Subsonic Transport Aircraft," *SAE Paper 91-2113*, September 1991.

[3] United States Department of Transportation Bureau of Transportation Statistics, "Airline Fuel Cost and Consumption (U.S. Carriers - Scheduled)," Tech. rep., 2014, http://www.transtats.bts.gov/fuel.asp, Accessed May 2015.

[4] Saric, W. S., Reed, H. L., and White, E. B., "Stability and Transition of Three-Dimensional Boundary Layers," *Annual Review of Fluid Mechanics*, Vol. 35, No. 1, 2003, pp. 413–440.

[5] Saric, W. S. and Reed, H. L., "Toward Practical Laminar Flow Control-Remaining Challenges," *AIAA-2004-2311*, 2004.

[6] Arnal, D., Perraud, J., and Séraudie, A., "Attachment Line and Surface Imperfection Problems," *VKI course "Advances in Laminar-Turbulent Transition Modeling", Brussels, EN-AVT-09*, June 2008.

[7] Rayleigh, L., "On the Stability, or Instability, of certain Fluid Motions," *Proceedings of the London Mathematical Society*, Vol. 1, No. 1, 1880, pp. 57–72.

[8] Morkovin, M. V., Reshotko, E., and Herbert, T., "Transition in open flow systems-a reassessment," *Bull. Am. Phys. Soc*, Vol. 39, No. 9, 1994, pp. 1882.

[9] Reshotko, E., "Transient growth: A factor in bypass transition," *Physics of Fluids*, Vol. 13, No. 5, May 2001, pp. 1067–1075.

[10] Arnal, D. and Archambaud, J., "Laminar-Turbulent Transition Control: NLF, LFC, HLFC," *VKI course "Advances in Laminar-Turbulent Transition Modeling", Brussels, EN-AVT-09*, June 2008.

[11] Garzon, G. A. and Matisheck, J. R., "Supersonic Testing of Natural Laminar Flow on Sharp Leading Edge Airfoils. Recent Experiments by Aerion Corporation." *AIAA-2012-3258*, 2012.

[12] Pfenninger, W., "Laminar Flow Control - Laminarization," *AGARD Report No. 654*, 1977.

[13] Saric, W. S., Carrillo, R. B., and Reibert, M. S., "Leading Edge Roughness as a Transition Control Mechanism," *AIAA-1998-0781*, 1998.

[14] Saric, W. S., Carpenter, A. L., and Reed, H. L., "Passive Control of Transition with Roughness in Three-Dimensional Boundary Layers," *Philosophical Transactions of the Royal Society A*, Vol. 369, No. 1940, April 2011, pp. 1352–1364.

[15] Saric, W. S., West, D. E., Tufts, M. W., and Reed, H. L., "Flight Test Experiments on Discrete Roughness Element Technology for Laminar Flow Control," *AIAA-2015-0539*, 2015.

[16] Bilstein, R. E., "Orders of Magnitude: A History of the NACA and NASA, 1915-1900," *NASA-SP-4406*, 1989.

[17] Blackburn, H. M., Barkley, D., and Sherwin, S. J., "Convective Instability and Transient Growth in Flow over a Backward-Facing Step," *Journal of Fluid Mechanics*, Vol. 603, 2008, pp. 271–304.

[18] Armaly, B. F., Durst, F., Pereira, J. C. F., and Schönung, B., "Experimental and Theoretical Investigation of Backward-Facing Step Flow," *Journal of Fluid Mechanics*, Vol. 127, 1983, pp. 473–496.

[19] Kaiktsis, L., Karniadakis, G. E., and Orszag, S. A., "Onset of three-dimensionality, equilibria, and early transition in flow over a backward-facing step," *Journal of Fluid Mechanics*, Vol. 231, 1991, pp. 501–528.

[20] Gresho, P. M., Gartling, D. K., Torczynski, J. R., Cliffe, K. A., Winters, K. H., Garratt, T. J., Spence, A., and Goodrich, J. W., "Is the Steady Viscous Incompressible Two-Dimensional Flow Over a Backward-Facing Step at Re=800 Stable?" *International Journal for Numerical Methods in Fluids*, Vol. 17, 1993, pp. 501–541.

[21] Kaiktsis, L., Karniadakis, G. E., and Orszag, S. A., "Unsteadiness and Convective Instabilites in Two-Dimensional Flow Over a Backward-Facing Step," *Journal of Fluid Mechanics*, Vol. 321, 1996, pp. 157–187.

[22] Barkley, D., Gomes, M. G. M., and Henderson, R. D., "Three-dimensional instability in flow over a backward-facing step," *Journal of Fluid Mechanics*, Vol. 473, 2002, pp. 167–190.

[23] Beaudoin, J. F., Cadot, O., Aider, J.-L., and Wesfreid, J. E., "Three-Dimensional Stationary Flow Over a Backward-Facing Step," *European Journal of Mechanics B/Fluids*, Vol. 14, No. 11, 2004, pp. 147–155.

[24] Perraud, J., Arnal, D., Séraudie, A., and Tran, D., "Laminar-Turbulent Transition on Aerodynamic Surfaces with Imperfections," *RTO-AVT-111 Symposium, Prague*, 2004.

[25] Drake, A., Bender, A. M., and Westphal, R. V., "Transition Due to Surface Steps in the Presence of Favorable Pressure Gradients," *AIAA-2008-7334*, 2008.

[26] Drake, A. and Bender, A. M., "Surface Excrescence Transition Study," Tech. Rep., AFRL-RB-WP-TR-2009-3109, 2009.

[27] Drake, A., Bender, A. M., Korntheuer, A. J., Westphal, R. V., McKeon, B. J., Geraschenko, S., Rohe, W., and Dale, G., "Step Excrescence Effects for Manufacturing Tolerances on Laminar Flow Wings," *AIAA-2010-375*, January 2010.

[28] Holmes, B. J., Obara, C. J., Martin, G. L., and Domack, C. S., "Manufacturing Tolerances for Natural Laminar Flow Airframe Surfaces," *SAE Paper 85-0863*, 1985.

[29] Balakumar, P., King, R. A., and Eppink, J. L., "Effects of Forward- and Backward-Facing Steps on the Crossflow Receptivity and Stability in Supersonic Boundary Layers," *AIAA-2014-2639*, 2014.

[30] Eppink, J. L., Wlezien, R. W., King, R. A., and Choudhari, M., "The Interaction of a Backward-facing Step and Crossflow Instabilities in Boundary-Layer Transition," *AIAA-2015-0273*, January 2015.

[31] Carpenter, A. L., Saric, W. S., and Reed, H. L., "Roughness Receptivity in Swept-Wing Boundary Layers : Experiments," *International Journal of Engineering Systems Modeling and Simulation*, Vol. 2, No. 1/2, 2010, pp. 128–138.

[32] Carpenter, A. L., *In-Flight Receptivity Experiments on a 30-Degree Swept-Wing Using Micron-Sized Discrete Roughness Elements*, Ph.D. thesis, Texas A&M University, May 2009.

[33] Rhodes, R. G., Reed, H. L., Saric, W. S., Carpenter, A. L., and Neale, T. P., "Roughness Receptivity in Swept-Wing Boundary Layers – Computations," *In-*

ternational Journal of Engineering Systems Modeling and Simulation, Vol. 2, No. 1/2, March 2010, pp. 139–148.

[34] Duncan Jr., G. T., Crawford, B. K., Tufts, M. W., Saric, W. S., and Reed, H. L., "Effects of Step Excrescences on a Swept-Wing in a Low-Disturbance Wind Tunnel," *AIAA-2014-0910*, January 2014.

[35] Duncan Jr., G. T., *The Effects of Step Excrescences on Swept-Wing Boundary-Layer Transition*, Ph.D. thesis, Texas A&M University, August 2014.

[36] Tufts, M. W., Duncan Jr., G. T., Crawford, B. K., Reed, H. L., and Saric, W. S., "Computational Design of a Test Article to Investigate 2-D Surface Excrescences on a Swept Laminar-Flow Wing," *International Journal of Engineering Systems Modeling and Simulation*, Vol. 6, No. 3/4, 2014, pp. 181–190.

[37] Crawford, B. K., Duncan Jr., G. T., Tufts, M. W., Saric, W. S., and Reed, H. L., "Effects of Step-Excrescence Location on Swept-Wing Transition," *AIAA-2015-1233*, January 2015.

[38] Crawford, B. K., *Laminar-Turbulent Transition due to 2-D Excrescences at 1% Chord on a Swept Wing*, Ph.D. thesis, Texas A&M University, May 2015.

[39] Rhodes, R. G., *Computations of Laminar Flow Control on Swept Wings as a Companion to Flight Test Research*, Master's thesis, Texas A&M University, December 2008.

[40] Roache, P. J., *Verification and Validation in Computational Science and Engineering*, Hermosa Publishers, PO Box 9110 Albuquerque, New Mexico, 1998.

[41] McKnight, C. W., *Design and Safety Analysis of an In-Flight, Test Airfoil*, Master's thesis, Texas A&M University, August 2006.

[42] Hunt, L. E. and Saric, W. S., "Boundary-Layer Receptivity of Three-Dimensional Roughness Arrays on a Swept-Wing," *AIAA-2011-3881*, 2011.

[43] Jespersen, D., Pulliam, T., and Buning, P. G., "Recent Enhancements to OVERFLOW," *AIAA-97-0644*, 1997.

[44] Rizzetta, D. P., Visbal, M. R., Reed, H. L., and Saric, W. S., "Direct Numerical Simulation of Discrete Roughness on a Swept Wing Leading Edge," *AIAA Journal*, Vol. 48, No. 11, 2010, pp. 2660–2673.

[45] Pruett, C. D., "A Spectrally Accurate Boundary-Layer Code for Infinite Swept Wings," *NASA Contractor Report 195014*, 1994.

[46] Rodriguez, D. and Theofilis, V., "Massively Parallel Solution of the BiGlobal Eigenvalue Problem Using Dense Linear Algebra," *AIAA Journal*, Vol. 47, No. 10, 2009, pp. 2449–2459.

[47] Eppink, J. L., *The Interaction of a Backward Facing Step and Crossflow Instabilities in Swept Boundary Layer Transition*, Ph.D. thesis, Tufts University, Medford, MA, 2014.

[48] Paredes, P. and Theofilis, V., "Spatial Linear Global Instability Analysis of the HIFiRE-5 Elliptic Cone Model Flow," *AIAA-2013-2880*, June 2013.

[49] Paredes, P., Perez, E., Reed, H. L., and Theofilis, V., "High-Frequency Instabilities Along the Windward Face of a Hypersonic Yawed Circular Cone," *AIAA-2014-2774*, June 2014.

[50] White, E. B., *Breakdown of Crossflow Vortices*, Ph.D. thesis, Arizona State University, August 2000.

[51] Wassermann, P. and Kloker, M., "Transition Mechanisms Induced by Travelling Crossflow Vortices in a Three-Dimensional Boundary Layer," *Journal of Fluid Mechanics*, 2003, pp. 67–89.

[52] Lerche, T. and Bippes, H., "Experimental Investigation of Cross-Flow Instability under the Influence of Controlled Disturbance Excitation," *Transitional Boundary Layers in Aeronautics*, 1997.

[53] Lerche, T., "Experimental Investigation of Nonlinear Wave Interactions and Secondary Instability in Three-Dimensional Boundary-Layer Flow," *6th European Turbulence Conf., Lausanne, Switzerland*, 1996, pp. 357–360.

APPENDIX A

COMPUTATIONAL SETTINGS

A.1 LASTRAC Settings for Stationary Crossflow

```
grid_type           = dual_cluster
relax_type          = wall_temp
num_normal_pts      = 122
use_extrap_mprof    = true
strm_order          = second_order
wall_normal_order   = fourth_order
solution_type       = local_eig_solution
nonl_pse_calc       = false
strm_curvt          = false
qp_approx           = true
pns_approx          = true

wave_ang_min        = 65.
wave_ang_max        = 99.
np_growth_rate_min  = -1.e-2
alpha_i_max         = 0.05
lod_max             = 60
wall_dpdy_ratio_min = 1.e-4
```

All other settings can be assumed to be default, or particular to the basic state used e.g. number of stations.

APPENDIX B

RECONSTRUCTION OF EIGENMODES

B.1 Euler's Formula

B.1.1 Euler's Formula

$$e^{ix} = \cos(x) + i\sin(x) \tag{B.1}$$

B.1.2 Cosine Corrollary

$$e^{ix} + e^{-ix} = \cos(x) + i\sin(x) + \cos(-x) + i\sin(-x) \tag{B.2}$$

$$e^{ix} + e^{-ix} = \cos(x) + i\sin(x) + \cos(x) - i\sin(x) \tag{B.3}$$

$$e^{ix} + e^{-ix} = 2\cos(x) \tag{B.4}$$

B.1.3 Sine Corrollary

$$e^{ix} - e^{-ix} = \cos(x) + i\sin(x) - \cos(-x) - i\sin(-x) \tag{B.5}$$

$$e^{ix} - e^{-ix} = \cos(x) + i\sin(x) - \cos(x) + i\sin(x) \tag{B.6}$$

$$e^{ix} - e^{-ix} = 2i\sin(x) \tag{B.7}$$

$$q'(x,y,z,t) = q(y)e^{i(\alpha x+\beta z-\omega t)} + \text{C.C.} \tag{B.8}$$

$$= (q_r + iq_i)\ e^{i(\alpha_r x+i\alpha_i x+\beta_r z+i\beta_i z-\omega_r t-i\omega_i t)} + \text{C.C.} \tag{B.9}$$

$$= (q_r + iq_i)\ e^{i(\alpha_r x+i\alpha_i x+\beta_r z+i\beta_i z-\omega_r t-i\omega_i t)} ... +$$

$$... + (q_r - iq_i)\ e^{i(-\alpha_r x+i\alpha_i x-\beta_r z+i\beta_i z+\omega_r t-i\omega_i t)} \tag{B.10}$$

$$= (q_r + iq_i)\ e^{-\alpha_i x}e^{-\beta_i z}e^{\omega_i t}\left(e^{i(\alpha_r x+\beta_r z-\omega_r t)}\right) + ...$$

$$... + (q_r - iq_i)\ e^{-\alpha_i x}e^{-\beta_i z}e^{\omega_i t}\left(e^{i(-\alpha_r x-\beta_r z+\omega_r t)}\right) \tag{B.11}$$

$$= q_r\ e^{-\alpha_i x}e^{-\beta_i z}e^{\omega_i t}\left(e^{i(\alpha_r x+\beta_r z-\omega_r t)} + e^{-i(\alpha_r x+\beta_r z-\omega_r t)}\right) + ...$$

$$... + iq_i\ e^{-\alpha_i x}e^{-\beta_i z}e^{\omega_i t}\left(e^{i(\alpha_r x+\beta_r z-\omega_r t)} - e^{-i(\alpha_r x+\beta_r z-\omega_r t)}\right) \tag{B.12}$$

$$= q_r\ e^{-\alpha_i x}e^{-\beta_i z}e^{\omega_i t}\ 2\cos(\alpha_r x + \beta_r z - \omega_r t) - +...$$

$$... + q_i\ e^{-\alpha_i x}e^{-\beta_i z}e^{\omega_i t}\ 2\sin(\alpha_r x + \beta_r z - \omega_r t) \tag{B.13}$$

$$= e^{-\alpha_i x}e^{-\beta_i z}e^{\omega_i t}\left[2q_r(y)\cos(\alpha_r x + \beta_r z - \omega_r t) - 2q_i(y)\sin(\alpha_r x + \beta_r z - \omega_r t)\right] \tag{B.14}$$

$$q'(x,y,z,t) = q(y,z)e^{i(\alpha x-\omega t)} + \text{C.C.} \tag{B.15}$$

$$= (q_r + iq_i)\ e^{i(\alpha_r x+i\alpha_i x-\omega_r t-i\omega_i t)} + \text{C.C.} \tag{B.16}$$

$$= (q_r + iq_i)\ e^{i(\alpha_r x+i\alpha_i x-\omega_r t-i\omega_i t)} + (q_r - iq_i)\ e^{i(-\alpha_r x+i\alpha_i x+\omega_r t-i\omega_i t)} \tag{B.17}$$

$$= (q_r + iq_i)\ e^{-\alpha_i x}e^{\omega_i t}\left(e^{i(\alpha_r x-\omega_r t)}\right) + (q_r - iq_i)\ e^{-\alpha_i x}e^{\omega_i t}\left(e^{i(-\alpha_r x+\omega_r t)}\right) \tag{B.18}$$

$$= q_r\ e^{-\alpha_i x}e^{\omega_i t}\left(e^{i(\alpha_r x-\omega_r t)} + e^{-i(\alpha_r x-\omega_r t)}\right) + ...$$

$$... + iq_i\ e^{-\alpha_i x}e^{\omega_i t}\left(e^{i(\alpha_r x-\omega_r t)} - e^{-i(\alpha_r x-\omega_r t)}\right) \tag{B.19}$$

$$= q_r\ e^{-\alpha_i x}e^{\omega_i t}\ 2\cos(\alpha_r x - \omega_r t) - q_i\ e^{-\alpha_i x}e^{\omega_i t}\ 2\sin(\alpha_r x - \omega_r t) \tag{B.20}$$

$$= e^{-\alpha_i x}e^{\omega_i t}\left[2q_r(y,z)\cos(\alpha_r x - \omega_r t) - 2q_i(y,z)\sin(\alpha_r x - \omega_r t)\right] \tag{B.21}$$

APPENDIX C

FORWARD-FACING EIGENMODE PLOTS

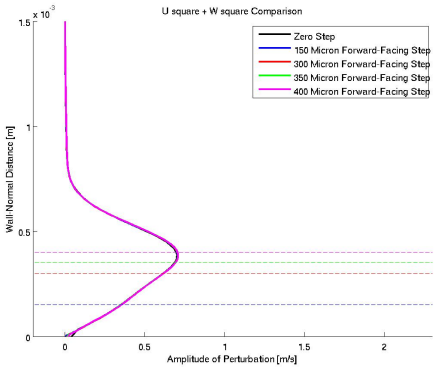

(a) U+W Perturbation

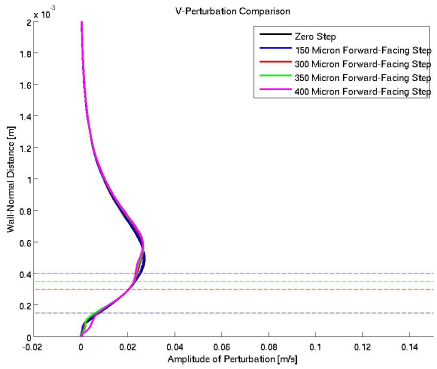

(b) V Perturbation

Figure C.1: 2.25 mm Stationary Disturbance Profiles - Forward Facing - Station 1

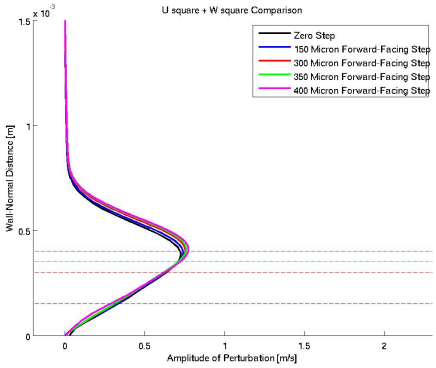

(a) U+W Perturbation

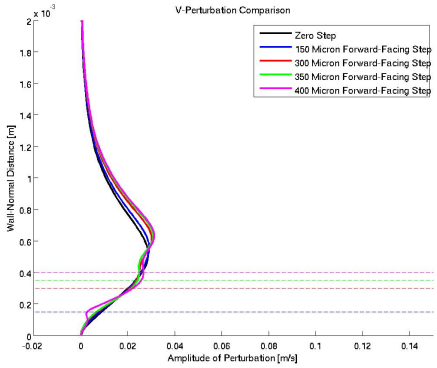

(b) V Perturbation

Figure C.2: 2.25 mm Stationary Disturbance Profiles - Forward Facing - Station 11

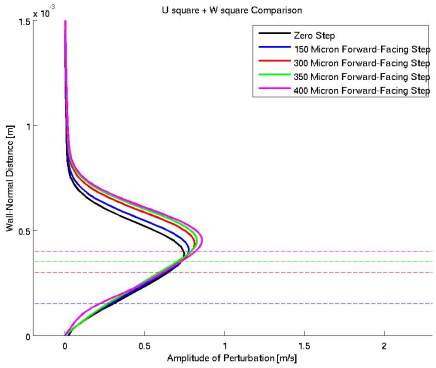

(a) U+W Perturbation

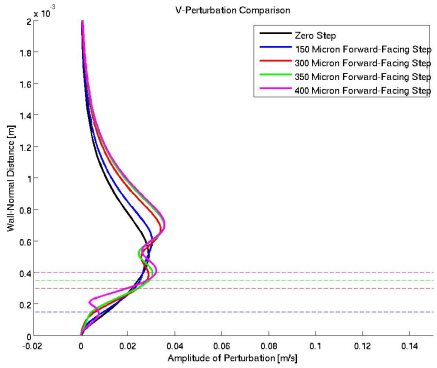

(b) V Perturbation

Figure C.3: 2.25 mm Stationary Disturbance Profiles - Forward Facing - Station 21

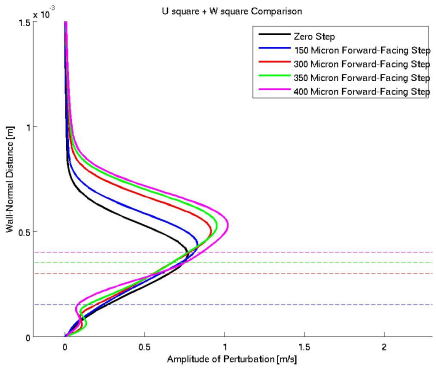

(a) U+W Perturbation

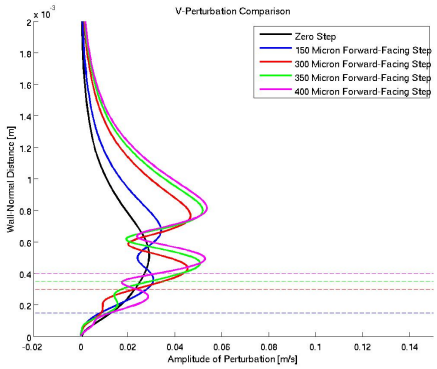

(b) V Perturbation

Figure C.4: 2.25 mm Stationary Disturbance Profiles - Forward Facing - Station 31

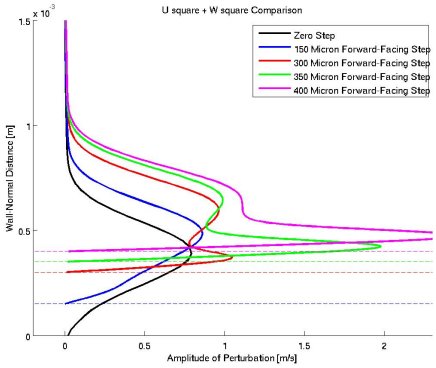

(a) U+W Perturbation

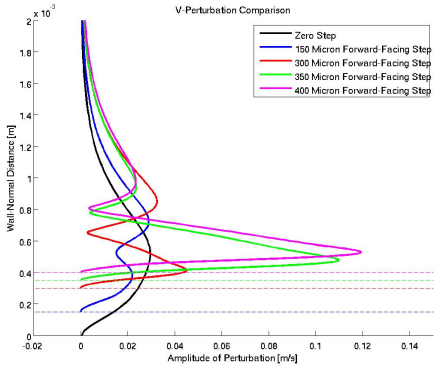

(b) V Perturbation

Figure C.5: 2.25 mm Stationary Disturbance Profiles - Forward Facing - Station 41

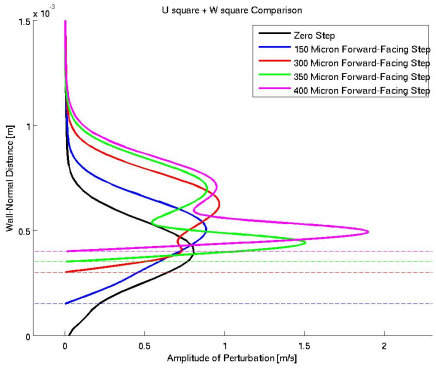

(a) U+W Perturbation

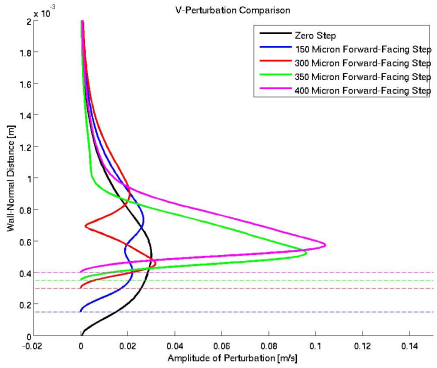

(b) V Perturbation

Figure C.6: 2.25 mm Stationary Disturbance Profiles - Forward Facing - Station 51

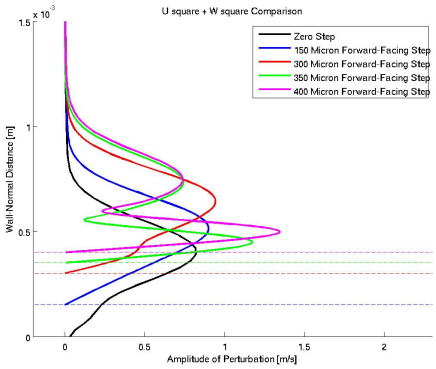

(a) U+W Perturbation

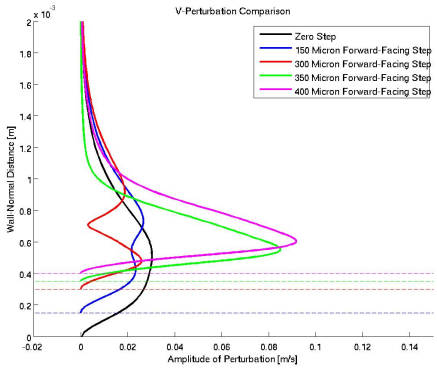

(b) V Perturbation

Figure C.7: 2.25 mm Stationary Disturbance Profiles - Forward Facing - Station 61

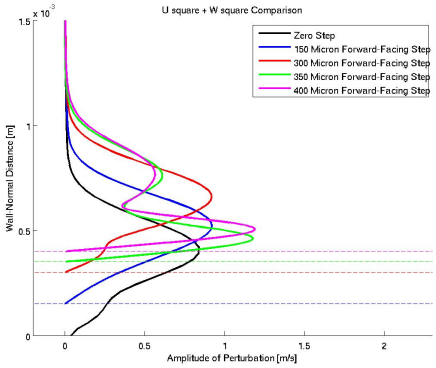

(a) U+W Perturbation

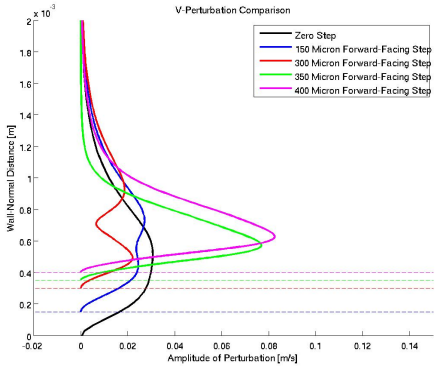

(b) V Perturbation

Figure C.8: 2.25 mm Stationary Disturbance Profiles - Forward Facing - Station 71

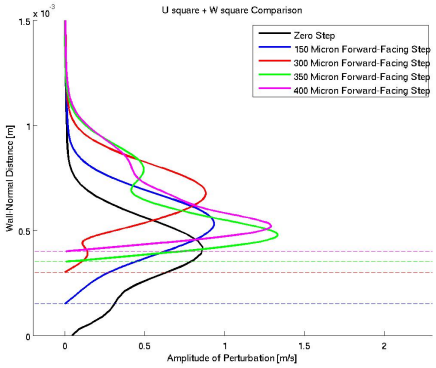

(a) U+W Perturbation

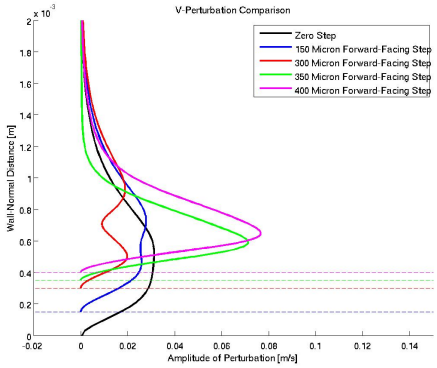

(b) V Perturbation

Figure C.9: 2.25 mm Stationary Disturbance Profiles - Forward Facing - Station 81

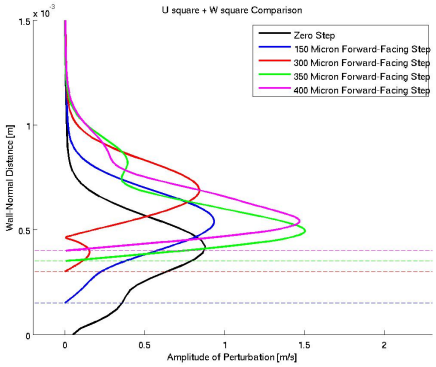

(a) U+W Perturbation

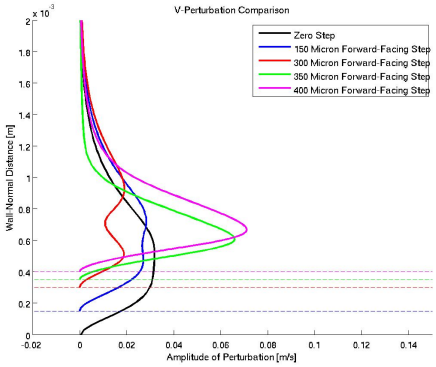

(b) V Perturbation

Figure C.10: 2.25 mm Stationary Disturbance Profiles - Forward Facing - Station 91

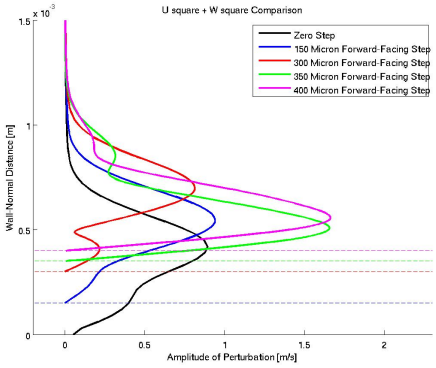

(a) U+W Perturbation

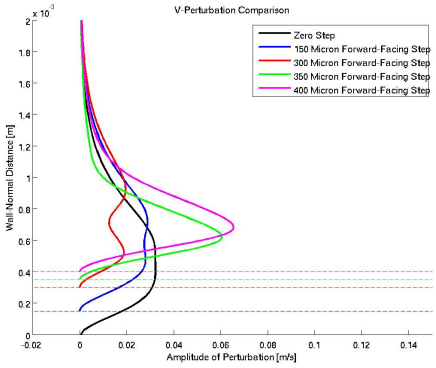

(b) V Perturbation

Figure C.11: 2.25 mm Stationary Disturbance Profiles - Forward Facing - Station 101

APPENDIX D

BACKWARD-FACING EIGENMODE PLOTS

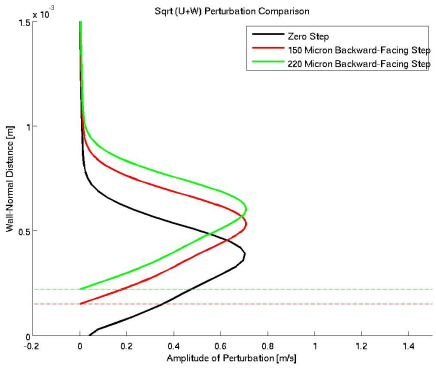

(a) U+W Perturbation

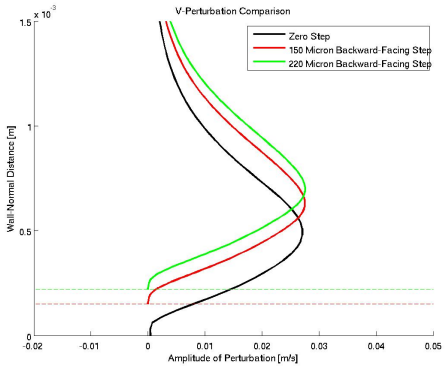

(b) V Perturbation

Figure D.1: 2.25 mm Stationary Disturbance Profiles - Backward Facing - Station 1

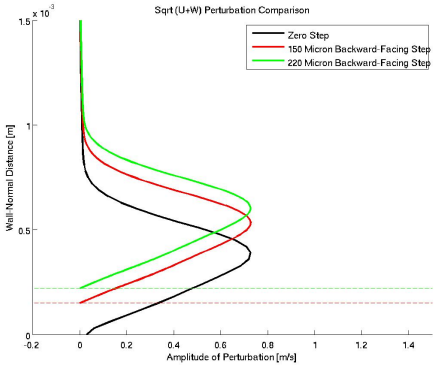

(a) U+W Perturbation

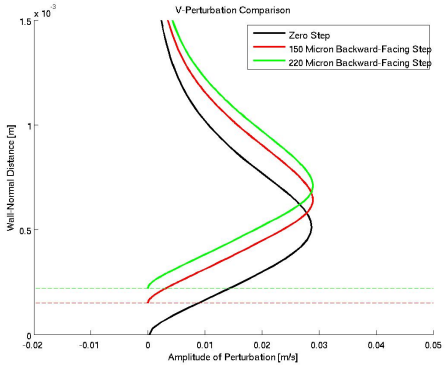

(b) V Perturbation

Figure D.2: 2.25 mm Stationary Disturbance Profiles - Backward Facing - Station 11

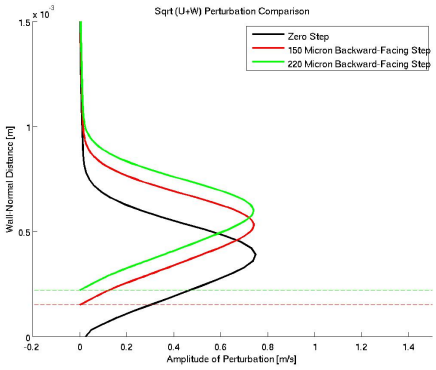

(a) U+W Perturbation

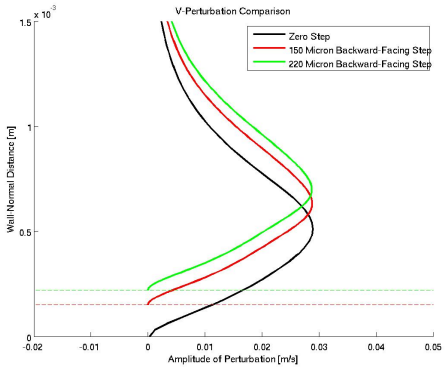

(b) V Perturbation

Figure D.3: 2.25 mm Stationary Disturbance Profiles - Backward Facing - Station 21

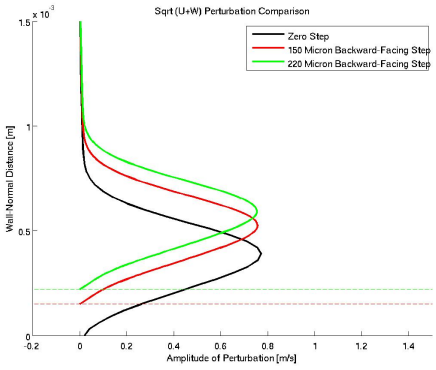

(a) U+W Perturbation

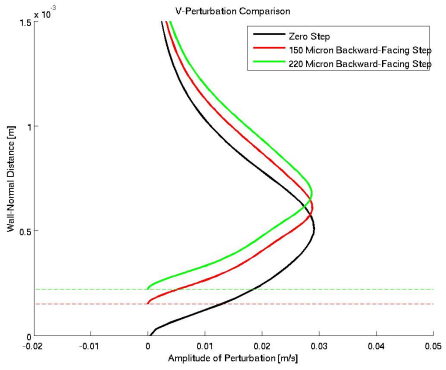

(b) V Perturbation

Figure D.4: 2.25 mm Stationary Disturbance Profiles - Backward Facing - Station 31

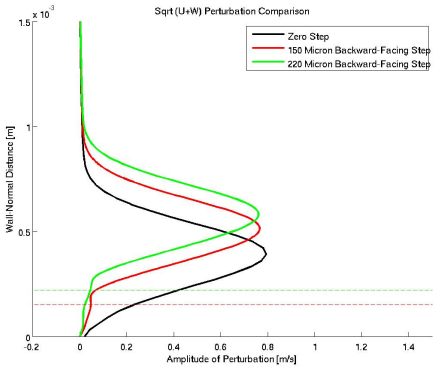

(a) U+W Perturbation

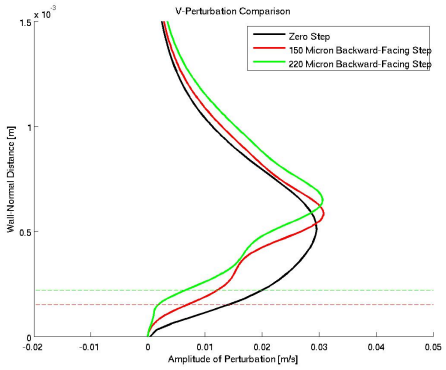

(b) V Perturbation

Figure D.5: 2.25 mm Stationary Disturbance Profiles - Backward Facing - Station 41

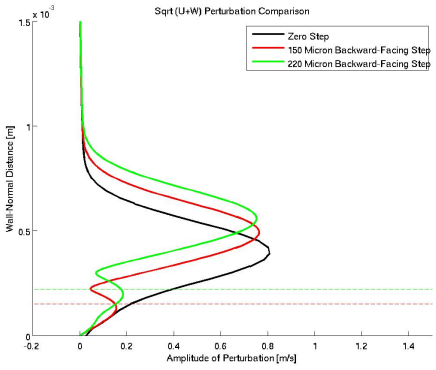

(a) U+W Perturbation

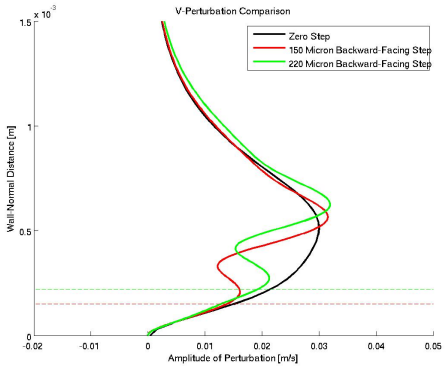

(b) V Perturbation

Figure D.6: 2.25 mm Stationary Disturbance Profiles - Backward Facing - Station 51

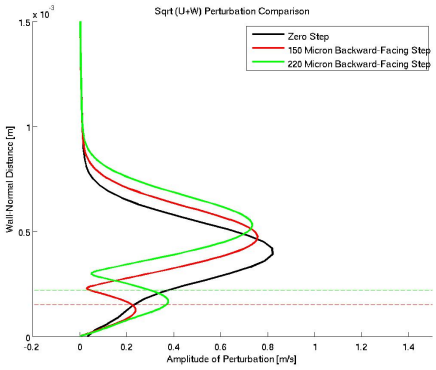

(a) U+W Perturbation

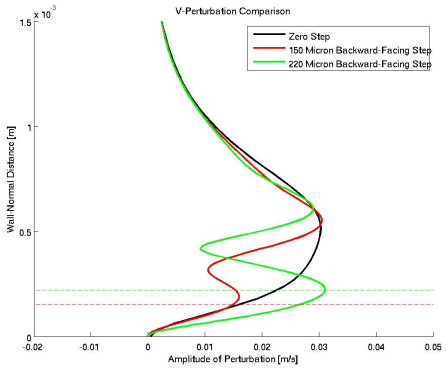

(b) V Perturbation

Figure D.7: 2.25 mm Stationary Disturbance Profiles - Backward Facing - Station 61

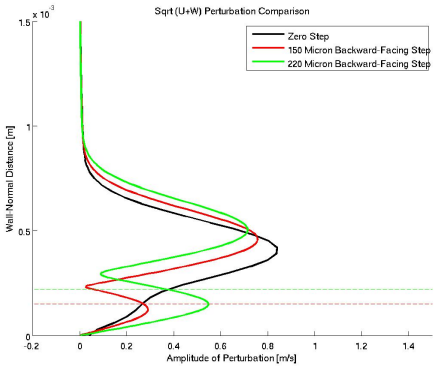

(a) U+W Perturbation

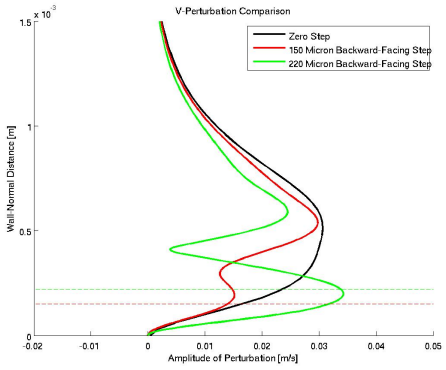

(b) V Perturbation

Figure D.8: 2.25 mm Stationary Disturbance Profiles - Backward Facing - Station 71

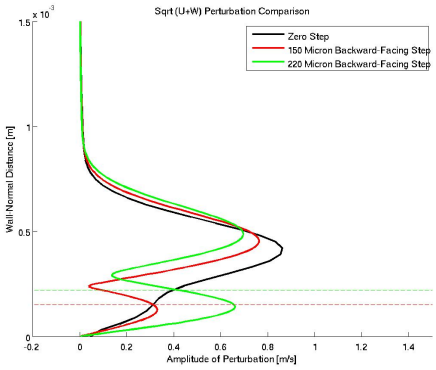

(a) U+W Perturbation

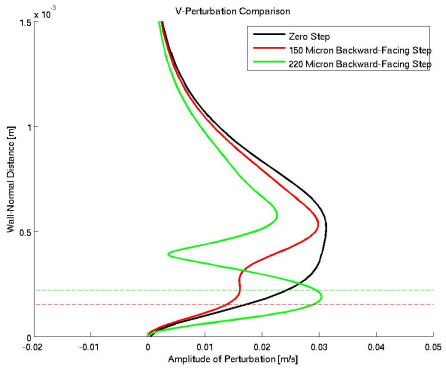

(b) V Perturbation

Figure D.9: 2.25 mm Stationary Disturbance Profiles - Backward Facing - Station 81

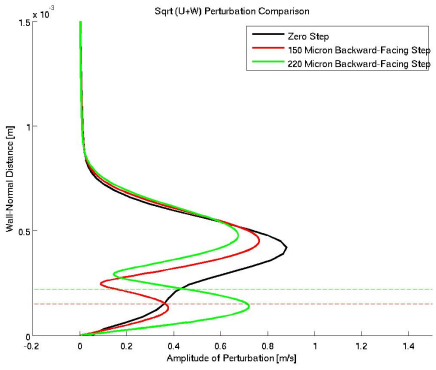

(a) U+W Perturbation

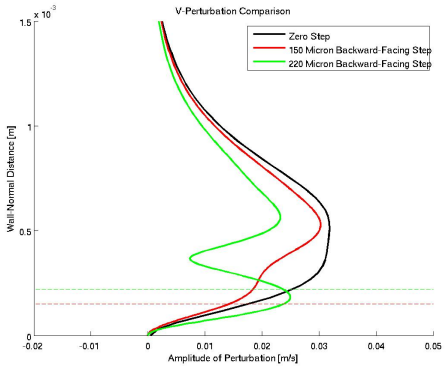

(b) V Perturbation

Figure D.10: 2.25 mm Stationary Disturbance Profiles - Backward Facing - Station 91

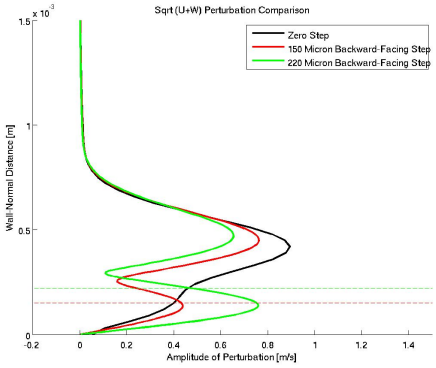

(a) U+W Perturbation

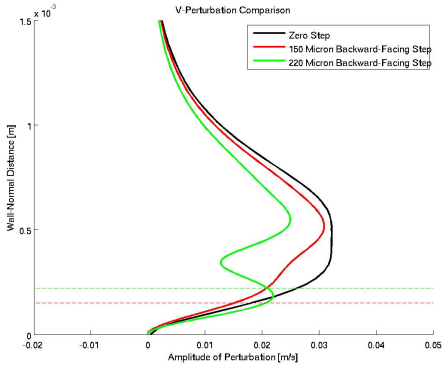

(b) V Perturbation

Figure D.11: 2.25 mm Stationary Disturbance Profiles - Backward Facing - Station 101

APPENDIX E

BACKWARD-FACING TRAVELING MODES

	Figure E.1	Figure E.2	Figure E.3
Step Height	110 Microns	150 Microns	220 Microns
δ_{99}	0.85 mm	0.85 mm	0.85 mm
L_{Ref}	$1.95 \cdot 10^{-4}$ m	$1.95 \cdot 10^{-4}$ m	$1.95 \cdot 10^{-4}$ m
α_R	0.11906	0.2414	0.4056
α_I	-0.0428	-0.09917	-0.1631
β_R	0.2723	0.2723	0.2723
Most Unstable Frequency	550 Hz	750 Hz	1100 Hz

Table E.1: Values for Traveling Bubble Modes (Most Unstable 1.5 mm Downstream)

	Mode 1	Mode 2	Mode 3
Step Height	110 Microns	150 Microns	220 Microns
α_R	0.1508	0.1466	0.1398
α_I	-0.0433	-0.0938	-0.1397
β_R	0.2723	0.2723	0.2723
Frequency	600 Hz	600 Hz	650 Hz

Table E.2: Values for Traveling Bubble Modes (Aligned with Stationary Wave)

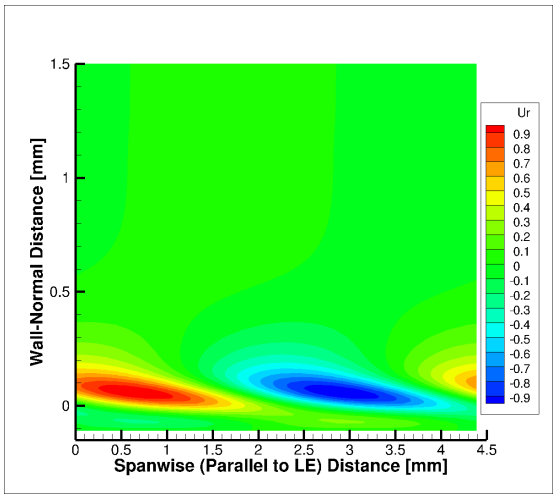

(a) U Perturbation

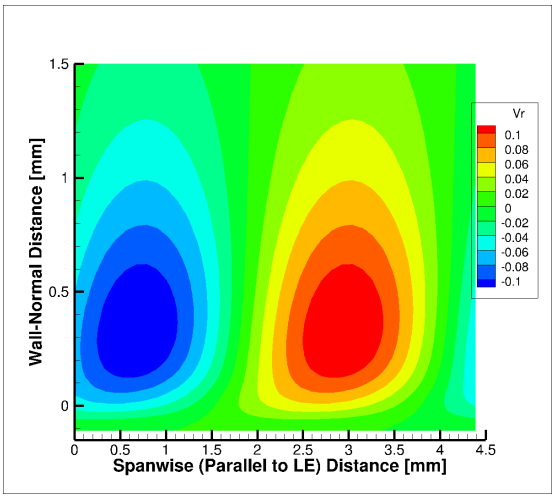

(b) V Perturbation

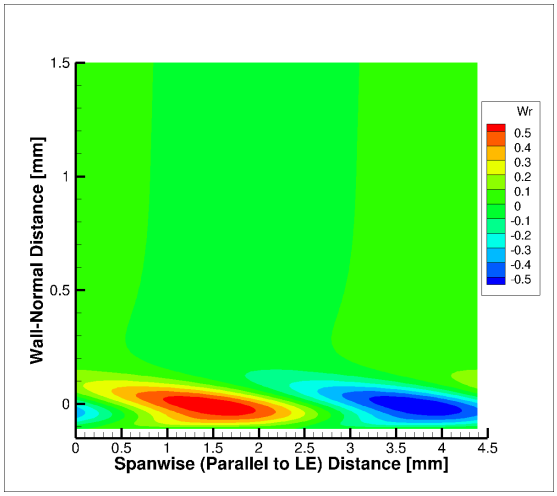

(c) W Perturbation

Figure E.1: BiGlobal Traveling "Bubble" Mode - In-Flight - 110 Micron Backward-Facing - 1.5 mm downstream - 550 Hz - 4.50 mm Wavelength

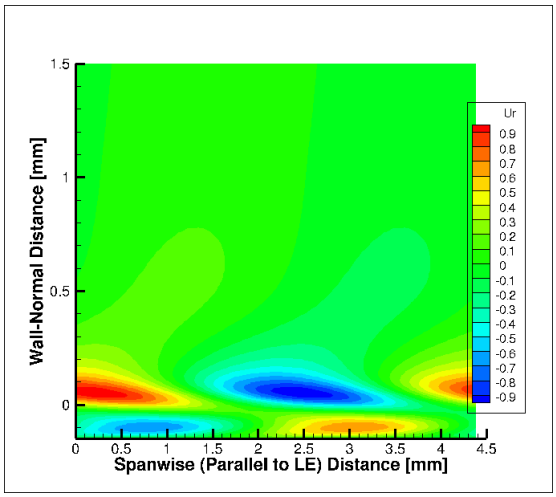

(a) U Perturbation

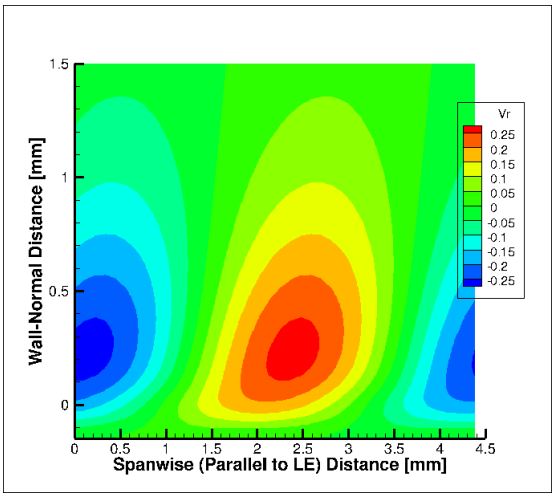

(b) V Perturbation

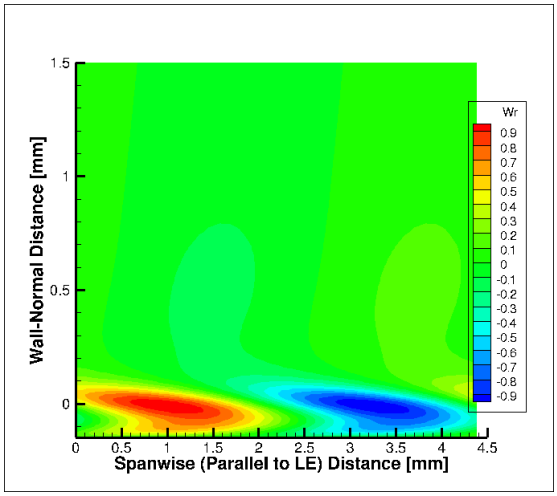

(c) W Perturbation

Figure E.2: BiGlobal Traveling "Bubble" Mode - In-Flight - 150 Micron Backward-Facing - 1.5 mm downstream - 750 Hz - 4.50 mm Wavelength

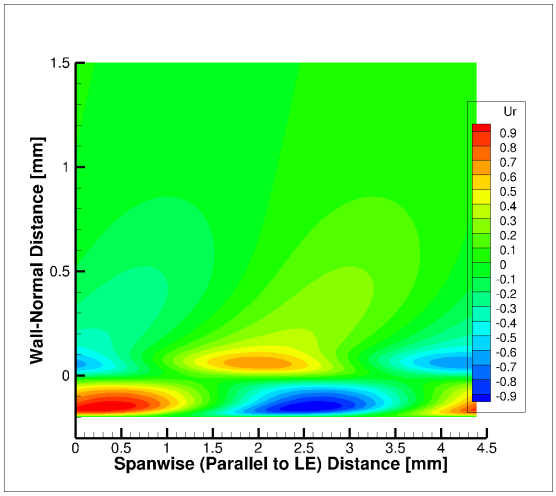

(a) U Perturbation

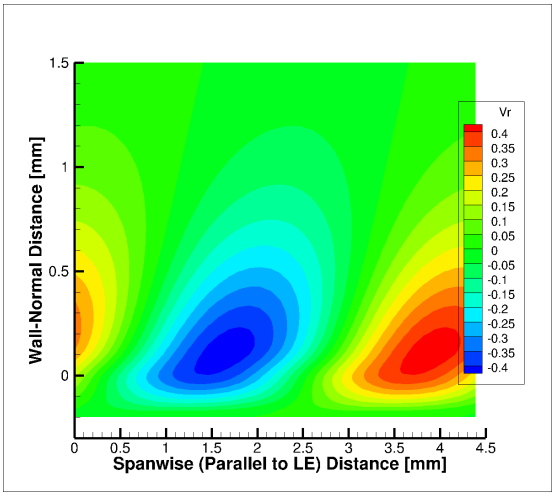

(b) V Perturbation

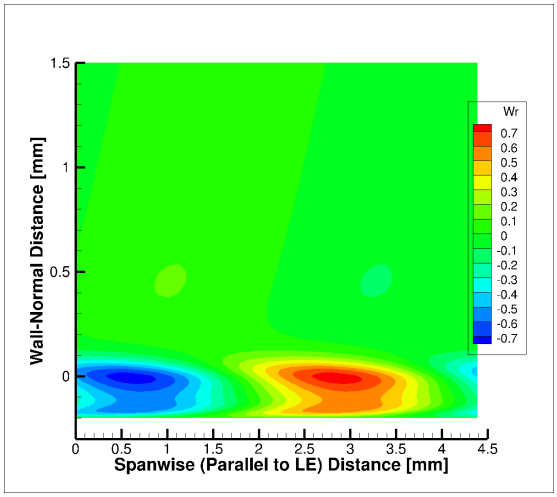

(c) W Perturbation

Figure E.3: BiGlobal Traveling "Bubble" Mode - In-Flight - 200 Micron Backward-Facing - 1.5 mm downstream - 1100 Hz - 4.50 mm Wavelength